

Charging of Small Two-Dimensional Electron Puddles

by

Misha Brodsky

M.S. Physics

St.Petersburg Technical University, Russia, 1992

Submitted to the Department of Physics
in partial fulfillment of the requirements for the degree of

Doctor of Philosophy

at the

MASSACHUSETTS INSTITUTE OF TECHNOLOGY

September 2000

© Massachusetts Institute of Technology 2000. All rights reserved.

Author

Department of Physics
August 31, 2000

Certified by

Raymond C. Ashoori
Associate Professor
Thesis Supervisor

Accepted by

Thomas J. Greytak
Professor, Associate Department Head for Education

Charging of Small Two-Dimensional Electron Puddles

by

Misha Brodsky

Submitted to the Department of Physics
on August 31, 2000, in partial fulfillment of the
requirements for the degree of
Doctor of Philosophy

Abstract

We study electron additions in 2D quantum dots of varying sizes and over a wide range of electron densities using Single Electron Capacitance Spectroscopy. For high electron densities in dots of any size, we observe a conventional pattern of nearly periodic Coulomb blockade. However, the addition spectra of electron droplets larger than $0.2 \mu m$ in diameter and below a critical electron density ($n_0 = 1 \times 10^{11} cm^{-2}$ in all of our dots) are highly nonperiodic and contain pairs and bunches: two or more successive electrons can enter the dot at nearly the same energy; they show almost no sign of repelling each other. Application of high perpendicular magnetic field increases n_0 , creating a sharp boundary between periodic and “paired” parts of the addition spectrum. Previously, we hypothesized that disorder and electron interactions within the low-density dot split it into two spatially separate droplets, and pairing arises once this localization occurs. We have produced experiments to study this transition in a controlled fashion.

One probes the spatial extent of electronic wavefunctions by investigating the dependence of these energies on changes in the dot confining potential. We find that for low electron densities, electrons occupy distinct spatial sites localized within the dot. At higher densities, the electrons become delocalized, and all wavefunctions are spread over the full dot area. The transition occurs around the critical electron density $n_0 = 1 \times 10^{11} cm^{-2}$. For densities just below the critical density our data establish the existence of electronic states localized at the dot’s periphery.

We also create a dot with a potential profile containing two minima separated by a barrier. Our studies conclusively demonstrate that under precisely the same conditions for observation of the paired electron additions, a low-density electron droplet inside the dot indeed splits up into smaller fragments, each residing in a disorder minimum. We find that the two electrons added as a pair actually enter into spatially distinct regions within a dot, and we measure the remnant residual interaction between the fragments. Surprisingly, it displays nearly complete independence on the strength of the applied field for fields larger than required for the localization transition.

Thesis Supervisor: Raymond C. Ashoori
Title: Associate Professor

Acknowledgments

Throughout the time I spent at MIT, there have been many people who helped me in this adventure.

My thesis advisor, Ray Ashoori, is an extraordinary person. His energy and excitement never seem to end. He is daring and adventurous. His desire and courage to take on very technically challenging experiments has always inspired me. Ray gave me an opportunity to share the remarkable experience of setting up a new lab. It took us a lot of hard work but boosted my self-confidence.

I am deeply grateful to Nikolai Zhitenev, a former postdoc in our group. In essence, Nikolai was my second advisor. I learned a lot during the countless hours we spent in the lab together. Rather than simply answering my frequent questions, Nikolai always guided my thoughts in the right direction.

I have benefited a lot in learning from theorists. First, I would like to thank Lenya Levitov, who showed a great deal of patience while explaining a variety of physical problems, even though some of my questions were asked at least twice. Kostya Matveev possesses a wonderful talent of explaining any theoretical issue to an experimentalist. I appreciate his help.

Numerous people contributed to the success of this thesis project. It would not be possible without wafers grown by Loren Pfeiffer and Ken West. David Berman not only shared his e-beam fabrication tricks, but he selflessly spent many hours in the clean room and at the microscope with me. Other members of our group: Ho Bun Chan, Paul Glicofridis, Sven Heemeyer, Dima Pouchine, Omar Saleh and Stuart Tessmer were always willing to help and did so. Also I thank Ho Bun for putting up with me as his office-mate for all these years. Discussions with Gleb Finkelstein are greatly appreciated. My special thanks to Darius Torchinsky for proof-reading this thesis.

Our neighbours in building 13 - the spin polarized hydrogen group - Dale Fried, Tom Killian, David Landhuis, Steve Moss and Lorenz Willmann were always letting me borrow their tools and equipment. I particularly thankful to Steve for helping me

with latex and english grammar while I was writing this thesis.

It was a privilege to have another quantum dot group just down the hall from us. I had many illuminating discussions with David Abusch-Magder, David Goldhaber-Gordon, Yuri Khavin, Olivier Klein and Marc Kastner. I would like to thank Marc for his willingness to discuss physics and for his enthusiasm for new results. His intuitive approach to difficult problems inspires me. Nicole Morgan was always there to explain peculiarities of English language.

I spent the summer of 1997 at Bell Labs. It was a very exciting experience that certainly influenced my career choice. I am grateful to Peter Wolff who pushed for the internship program at our department, to Cherry Murray who hired me and to Rafi Kleiman who was my mentor at Bell.

My friends made sure that I was aware of other side of the life besides physics. It is impossible to name everybody, but I would like to mention Natalia Levin, Misha Boroditsky, Mitya Chklovskii, and Gleb Shtengel.

Finally I would like to thank my parents for their constant understanding, love and support.

This work was supported by Office of Naval Research, National Science Foundation, DMR; Center for Materials Science, the Joint Services Electronics Program, and the Packard Foundation.

To my parents.

Contents

1	Introduction	12
1.1	Two-Dimensional Electron Systems in GaAs	13
1.2	Localization in Two-Dimensional Systems	14
1.3	Coulomb Blockade	15
1.4	Thesis Overview	20
2	Single Electron Capacitance Spectroscopy	22
2.1	MBE Wafer	23
2.2	Fabrication of Vertical Dots	26
2.2.1	Electron Beam Lithography	27
2.2.2	Individual Circular Dot	28
2.2.3	Dot with Adjustable Confinement: Putting an Additional Gate Around a Dot	31
2.2.4	Dot with Artificial Disorder Potential	32
2.3	Capacitive Measurements	35
2.3.1	Sample Impedance	38
2.3.2	Measurement Apparatus Design: Pitfalls and Solutions	39
2.3.3	Data Acquisition	44
2.4	Advantages of Vertical Structures	45
3	Detailed Study of Single Vertical Quantum Dots.	47
3.1	Early Observations	47

3.2	Periodic and Aperiodic Bunching in the Addition Spectra of Quantum Dots	50
3.2.1	Large Dot Spectra in Zero Magnetic Field	52
3.2.2	Evolution of the Spectra in Magnetic Field	55
3.2.3	Tunneling Rates	59
3.2.4	Universality of the Bunching Phenomena	60
3.3	Why is it that the Pairing is Related to Localization?	63
3.4	Theories Proposed	65
3.5	Summary	68
4	Localization-Delocalization Transition in Quantum Dots	69
4.1	Added Electron: Where Does It Go?	70
4.2	Probing Localization: Experimental Results	72
4.2.1	Localization in Zero Field	72
4.2.2	Effects of High Magnetic Fields	76
4.2.3	Interaction Between Localized and Delocalized States	77
4.3	Localization Results from Electron Correlations	79
4.4	Possible Physical Mechanisms for Localization	80
4.5	Summary	82
5	Localization in Artificial Disorder: Two Coupled Quantum Dots	83
5.1	How to Model a Disorder Potential	85
5.2	Addition spectrum of a small symmetric dot	88
5.2.1	Constant Interaction Model for Single Particle States	89
5.2.2	Single Particle States in Magnetic Field: Darwin-Fock spectrum	91
5.2.3	Even-Odd Asymmetry in Coulomb Blockade Spectra	92
5.2.4	Our Data from a Small Dot	94
5.2.5	Limitations of the Model	97
5.2.6	Conclusions	98
5.3	Double Dot System	98
5.3.1	Two Potential Minima: Two Electron Puddles	98

5.3.2	High-Density Electron Puddles Merge	102
5.3.3	Low-Density Electron Puddles Merge and Break up	103
5.4	Summary	111
6	Summary and Directions for Future Research	115
6.1	Further Study of Localization	117
6.2	Spectroscopy of Excited States and Study of Tunneling Rates	118
6.3	Spin in Small Dots	119
6.3.1	How and Why Coulomb Interactions Could Modify Darwin-Fock Spectrum	119
6.3.2	Beyond Darwin-Fock: Data	121
A	Fabrication Recipes	125
A.1	Sample Cleaning	125
A.2	Mesa Definition	126
A.3	Ohmic Contacts: Positive Resist	127
A.4	Ohmic Contacts: Negative Resist	128
A.5	Lead Deposition	129
A.6	Dot Formation	129
A.7	Side Gate Deposition	130
A.8	Patches Deposition	131
B	JEOL 6400 Scanning-Electron Microscope: getting the best litho- graphical resolution	133

List of Figures

1-1	Small metallic island	16
1-2	Charge on the island	19
2-1	Sample structure	24
2-2	Photograph of prefabricated samples	25
2-3	Resist profiles	29
2-4	Fabrication schematics	30
2-5	Micrograph of our sample with the sidegate	33
2-6	Top view micrograph of double dot system	34
2-7	Setup schematic	36
2-8	Dot's charge and lockin signal	37
2-9	Equivalent circuit diagram of the sample	40
2-10	Diagram of the two stage cold amplifier	41
2-11	Capacitance trace	45
3-1	Single sample schematic	49
3-2	Paired electron additions	51
3-3	Periodic paired addition	53
3-4	Fourier transform	54
3-5	Grayscale image of the measured capacitance I	57
3-6	Grayscale image of the measured capacitance II	58
3-7	High field data	61
3-8	Phase diagram	62
3-9	Electron tunneling in the 2D system	64

4-1	Side gated sample schematic	71
4-2	Localization in zero field	74
4-3	Localization in magnetic field	75
4-4	Interaction between localized and delocalized states	78
5-1	Double dot sample schematic	86
5-2	Capacitance trace	87
5-3	Darwin-Fock spectrum	90
5-4	Magnetic field evolution of four consecutive peaks	95
5-5	Single-particle spectrum for elliptical dots	96
5-6	Two small symmetric dots	100
5-7	Interaction between two high-density dots	101
5-8	Interaction between two high-density dots	105
5-9	The spectrum expanded to the right of the boundary: data	108
5-10	The spectrum expanded to the right of the boundary: schematic	109
5-11	Reconstruction of the hybrid states	112
5-12	Schematic field dependence of the tunneling matrix element U	113
6-1	Addition spectrum of a small quantum dot	122
6-2	Collapsed addition spectrum	123

Chapter 1

Introduction

A steadfast drive to build faster and more powerful computers has led to a revolution in the semiconductor industry. Tremendous technological advances over the past few decades have made possible fabrication of semiconductor structures of unprecedented purity and crystalline perfection. In addition, the newfound ability to confine electrons to short length scales has furnished physicists with new model structures and has enabled them to explore new effects.

As a result, a new field of physics has emerged - mesoscopics. Mesoscopic physics deals with systems whose length scales are large compared with the size of atoms but are short compared with those of macroscopic samples. Because of the properties of materials the quantum mechanical phase coherence can be maintained over distances of a few microns at low temperatures (below 1K). Since modern fabrication techniques allows us to scale down the device dimensions, quantum effects can be studied. These include various manifestations of the electron-electron interaction.

Physicists are particularly interested in systems of reduced dimensionality. Experimentalists can design and fabricate a device to address specific theoretical issues. Two-dimensional systems in strong perpendicular magnetic fields have the remarkable properties of a quantized Hall conductance, which results from quantization of the energy in a series of Landau levels [1, 2] . Modifications of Fermi liquid theory to account for the role of electron-electron interaction and the possibility of the existence of a 2D conducting phase at low temperature remain subjects of strong current

interest [3, 4, 5, 6]. The studies of conductance of one dimensional channels led to the discovery of a formal relation between conduction and transmission, known as the Landauer formula [7, 8]. More recent experiments probe the Luttinger liquid [9, 10], which describes the interactions of electrons in one dimension. The physics of zero dimensional structures, known as quantum dots or artificial atoms [11, 12, 13, 14] have produced a number of novel results, such as the recently observed Kondo effect [15, 16]. The real advantage of artificial atoms in experiment is that their size, shape and electron occupancy can be adjusted, even *in situ*, thus enabling experimentalists to tailor their systems to specific needs.

While it is not possible to name every area of present-day interest, we point the reader to good reviews of the field, which can be found in references [17, 7, 18, 19]. Still several topics, which are the most relevant to the research described in this thesis deserve individual introduction. We present them in the following sections.

1.1 Two-Dimensional Electron Systems in GaAs

Among novel modern structures, GaAs/AlGaAs heterostructures have emerged as the most popular material for confining electrons. In these structures electrons are confined at the interface of GaAs and AlGaAs, forming a thin layer of highly mobile electrons. [20]. Motion perpendicular to the layer is frozen out, and these electron compose what is referred to as a two-dimensional electron gas (2DEG). Chapter 2 provides more details on the exact structure of such systems.

In addition to the reduced dimensionality, GaAs/AlGaAs heterostructures combine a number of desirable properties. A large screening length facilitates variation of the electron density by moderate electric fields. The low electron density implies a large Fermi wavelength (typically 100 nm), which is comparable to the dimensions of features that can be fabricated with standard semiconductor processing techniques. The mean free path can be quite large (exceeding $10\mu m$). A circular Fermi surface simplifies analysis. Finally, the low effective mass of $m^* = 0.067m_0$ generally increases the magnitude of quantum effects.

1.2 Localization in Two-Dimensional Systems

For half a century physicists have worked to understand localization of strongly interacting electrons in a disorder potential. The two basic mechanisms that cause localization of charge carriers are the electron interaction [21] and disorder [22].

Anderson pointed out that if the disorder is made progressively stronger, one should expect a qualitative change in the nature of electron wavefunctions in three dimensional samples. Based upon the scaling hypothesis introduced by Thouless [23, 24], a second major advance in the Anderson localization problem appeared in publication of seminal paper by the “gang of four” [25]. The most remarkable conclusion was that in the limit of zero temperature and infinite sample, electrons are always localized in low dimensional systems. This discovery led to a series of remarkable phenomena which go under the name of both “weak” and “strong localization”. These theories describes single particles and did not consider the electron interaction phenomena. On the other hand, Mott demonstrated that localization can occur in a perfectly periodic lattice with no disorder if sufficiently strong repulsion is introduced between two electrons occupying the same lattice site.

Both disorder and electron interaction exist in real physical systems. Though their interplay in two-dimensional systems has been a subject of intense experimental and theoretical studies [17, 26, 27, 3, 4], no theory exists which fully describes the effects of both disorder and interaction.

The problem is especially difficult when the electron interactions are strong. This was demonstrated once more by recent experiments, which suggested the existence of a conducting phase in dilute two dimensional electron systems in total disagreement with the predictions of the scaling theory [25] of noninteracting electrons. Strong electron electron interactions may thus be a central feature that allows the existence of a conducting phase in two dimensions. However, the nature of this phase remains unclear.

Up to now, the localization of electrons has been studied in transport and optical experiments in two dimensional bulk samples. The principal drawback of these tech-

niques is that the measured conductivity is a *macroscopic* quantity averaged over the entire sample.

Quantum dots provide convenient systems to study electron localization on a *microscopic* scale. In essence, quantum dots are tiny puddles of two dimensional electrons. By measuring how the energy to add individual electrons to a quantum dot changes in response to an external parameter (such as magnetic field or the dot's confinement), we directly assess the spread of electron wavefunctions within a puddle and the position of a particular electron if it is localized.

However, conventional lateral dots do not function well for localization studies. The traditional transport spectroscopy techniques for studying lateral quantum dots [11] sense primarily delocalized electronic states. A possible exception is transport studies in vertical structures [28, 13], but these do not permit variation of electron density, a critically important parameter that changes the effective strength of electron interactions. We note that since the Fermi energy $E_F \propto n$ in two dimensions and the electron interaction energy $E_{ee} \propto n^{1/2}$, the ration $E_F/E_{ee} \propto n^{-1/2}$. Therefore, the lower the electron density, the greater the role of electron-electron interactions.

We thus have developed a novel experimental technique: Single Electron Capacitance Spectroscopy (SECS) [29, 30], which is described in Chapter 2. It has demonstrated the capability of probing both *localized* and delocalized states of electrons. Furthermore, this method allows us to study two dimensional dots of various geometries and sizes over a broad range of electron densities [29, 31, 32, 33, 34].

1.3 Coulomb Blockade

In this section we introduce the Coulomb blockade - a vital notion for any quantum dot experiment. We briefly review the conditions under which Coulomb charging effects are important. In other words, the conditions under which the addition/subtraction of an individual electron to/from the system has a measurable effect.

Let us consider the electronic properties of the system depicted on the Figure 1-1. It consists of a small metallic island coupled to two terminals: an infinite reservoir of

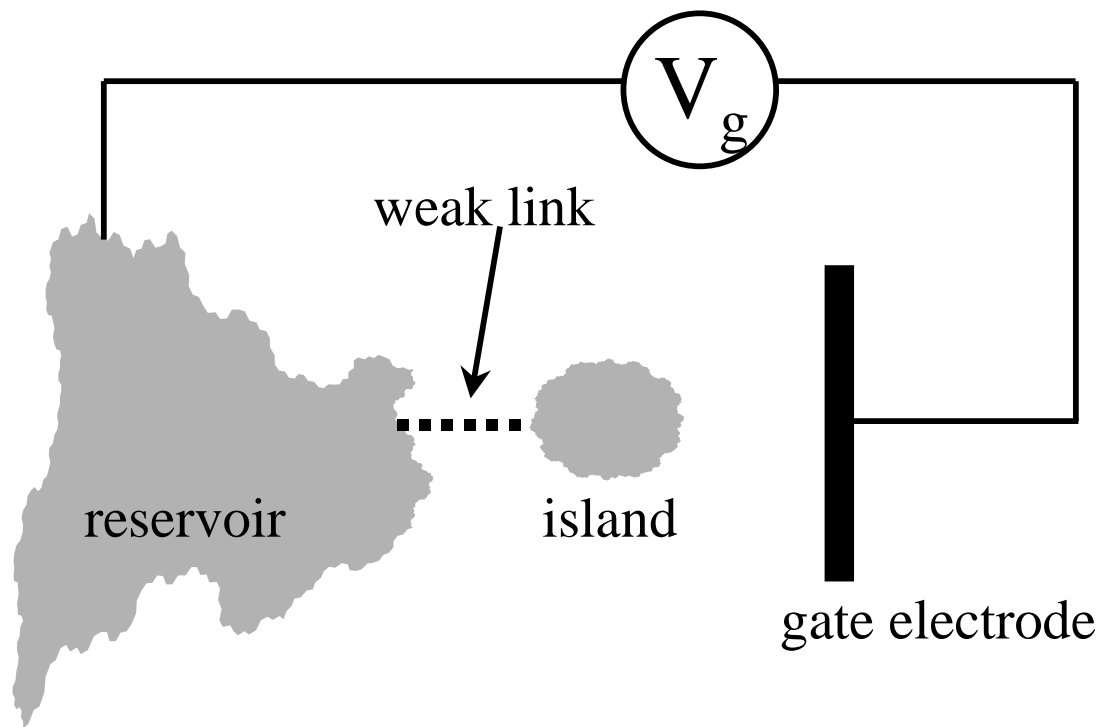


Figure 1-1: A small metallic island is coupled to an infinite a reservoir of electrons and a gate electrode. Electron transfer can occur only between the island and the reservoir as indicated by the dashed line. Gate electrode is coupled capacitively and is used to adjust the electrostatic potential of the island. The capacitance between the island and the gate is C_g .

electrons and a gate. Particle exchange can occur only by tunneling through a barrier between the island and the reservoir, as indicated by the dashed line. The gate is coupled to the island only electrostatically or capacitively, and can be used to adjust the potential of the island. If we first assume that the coupling of the island to the reservoir is absent, then the number of electrons on the island is an integer N , i.e. the charge on the island is quantized and equal to Ne . Now if we allow a weak tunneling between the island and the reservoir, then the number of electrons N adjusts itself until the energy of the whole circuit is minimized. We will discuss below what this “weak coupling” means.

Consider an electron tunneling event from the reservoir onto the island. The charge on the island is suddenly changes by the quantized amount e . The associated increase in the Coulomb energy can be conveniently expressed in terms of the total capacitance C of the island. An extra charge e changes the electrostatic potential by the charging energy $E_c = e^2/C$. This charging energy becomes important when it exceeds the temperature in the reservoir $k_B T$. If this is the case, the second electron cannot be transferred from reservoir onto the island, because the reservoir simply does not have electrons with sufficiently high energy. This suppression of charge transfer is called Coulomb blockade [14, 19].

The second condition for the Coulomb blockade is that the barrier is opaque enough so that electrons are localized either in the reservoir or on the island. This means that the quantum fluctuation in the number N due to tunneling through the barrier is much less than one over the time scale of the measurement. This requirement translates to a lower bound for the tunnel resistance R_t of the barrier. The fluctuation of the island’s charge was calculated for the first time by Matveev and Glazman [35, 36]. They showed that for values of $R_t \gg h/e^2$ the charge on the island is quantized in units of the electron charge.

Intuitively, this estimate can also be obtained by the following line of arguments, first proposed by Thouless who considered a similar problem when he examined the conductance of thin metallic wires [37]. He argued that electrons are localized on a metal particle if the average energy level spacing $\Delta\epsilon$ is larger than the lifetime

broadening Γ of the levels:

$$\Delta\epsilon \gg \Gamma \quad (1.1)$$

In our situation the lifetime broadening $\Gamma = h/\tau$ arises because electrons escape from the island to the reservoir by tunneling across the barrier during the time τ . Consider a voltage V applied between the island the reservoir. The resulting current will flow by means of the $eV/\Delta\epsilon$ levels, and each level on the average carries a current of order of e/τ . Then the barrier resistance is:

$$R = \frac{V}{I} = \frac{h}{e^2} \frac{\Delta\epsilon}{\Gamma} \gg \frac{h}{e^2} \quad (1.2)$$

In summary, the two requirements for observing effects due to single electron charging are:

$$R_t \gg h/e^2 \quad (1.3)$$

$$e^2/C \gg k_B T \quad (1.4)$$

The first one can be met by weakly coupling the island to the reservoir. The second one can be met by making the dot smaller, thus minimizing its capacitance; and by cooling the entire system to low temperatures.

A capacitively coupled gate electrode with the capacitance C_g (see Figure 1-1) can be used to lift the Coulomb blockade and to facilitate electron transfers. Application of a gate bias voltage V_g to the gate electrode placed nearby changes the electrostatic potential of the island in a continuous manner. In terms of charge, while tunneling changes the island charge by an integer, the gate voltage induces an effective continuous charge $Q = C_g V_g$. This charge represents the charge that the island would like to have. If we sweep the bias V_g , the build up of the induced charge will be compensated in periodic intervals by the tunneling of discrete charges onto the island. Figure 1-2 illustrate this idea by plotting both the charge on the dot and the continuous charge Q as a function of the bias voltage V_g . The charge on the island can then be measured by capacitive technique as we describe in Chapter 2.

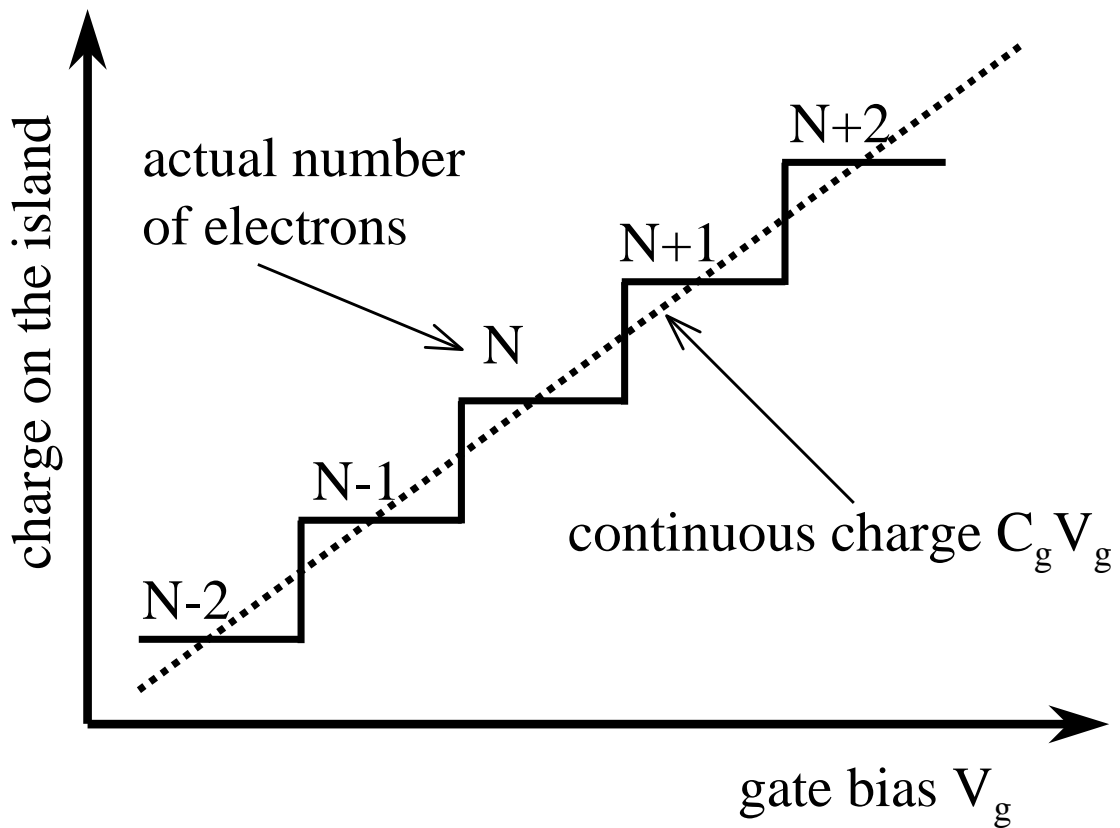


Figure 1-2: Schematic comparison, as a function of gate voltage, between actual and continuous charge (see text). The actual charge on the island changes by integer number of electrons. The continuous charge $Q = C_g V_g$ represent the charge that the island would like to have to minimize its energy.

Finally, we would like to refer the reader to the several review articles in the field for more detailed description of the underlying physics [14, 13]. Physicists from building 13 can find an excellent and very clear discussion of Coulomb blockade in Ethan Foxman’s thesis [38].

The simple classical reasoning we have presented shows that electron addition onto the island or the dot, as we call it, are periodic in the gate voltage. However, physical phenomena inside the dot with a characteristic energy scale compared to the charging energy E_c disrupts this periodicity. In fact, the addition spectrum, i.e. a set of the gate bias V_g values at which electron additions occur, provide us with insight into the physics of the dot. The amount of energy required to add an electron to a dot depends on electron interactions *within* a dot. By making our island out of the two dimensional electron gas (see Chapter 2), we are able to study localization phenomena in two dimensional electron puddles.

1.4 Thesis Overview

After this introduction the thesis begins in Chapter 2 with a description of our technique. We present the basics of our heterostructure composition and the fabrication procedures. A special section deals with our capacitance measurement apparatus, which permits quantitative spectroscopy of discrete quantum levels in the structures containing as few as one electron.

Chapter 3 reviews the previous results of our group, which motivated experiments presented further on. We will describe a profound violation of Coulomb blockade in quantum dots: we will show that under certain conditions, electron additions can occur in “pairs” or even “bunches” [29, 30, 32]. By summarizing our experimental findings, we will show that those suggest a relation between electron localization and the pairing phenomena [39]. To test this hypothesis, we have produced two experiments [33, 34] to study the localization-delocalization transition in quantum dots in a controlled fashion, which we describe in Chapter 4 and Chapter 5.

In the first experiment [33] we probe the spatial extent of electronic wavefunctions

by investigating the dependence of the addition spectra on changes in the dot confining potential. We describe the localization-delocalization transition in quantum dots at zero magnetic field. Chapter 4 establishes the existence of electronic states localized at the dot's periphery and arising at densities just below the critical density.

To fully investigate the effect of magnetic fields on electron localization, we created a dot with an artificially introduced disorder potential [34, 40]. Chapter 4 present results of localization in such a “model” disorder. We determine the conditions under which a low-density electron puddle becomes unstable and actually breaks up into smaller fragments.

Finally Chapter 6 concludes with possible directions for future research. Two appendices present a detail description of our fabrication methods. One lists the recipes we used and the other describes a setup procedure for the electron beam microscope.

Chapter 2

Single Electron Capacitance Spectroscopy

This chapter describes “Single Electron Capacitance Spectroscopy” (SECS). SECS was initially invented by Ashoori [29, 30], and has been significantly improved over the years in our lab. These developments have allowed us to take most of the data presented in this thesis.

SECS permits detailed measurement of the ground state energies of quantum dots, containing a variable and known number of electrons. We position a quantum dot between two plates of a tunnel capacitor. Electrons may tunnel between the dot and the bottom plate, while a large barrier forbids tunneling to the top plate. By adjusting the voltage applied across the plates, single electrons are caused to tunnel onto and off the dot. Once an electron tunnels onto the dot, it induces an image charge on the top plate. By integrating an ultra sensitive cryogenic home-built amplifier on the chip containing the sample, we detect and precisely measure this image charge.

To optimize the signal-to-noise-ratio, we employ a conventional lock-in technique. In addition to applying a dc bias across the tunnel capacitor, we force single electron tunnel back and forth between the dot and the bottom plate using an ac voltage. We then synchronously detect signals due to electron tunneling. Peaks appear in the response at those particular positions in dc bias at which the quantum dot energy level is resonant with the chemical potential in the bottom plate. We convert the

dc bias scale into an energy scale for the dot, using a simple scale factor, deduced from the sample geometry. Thus, we measure the ground state energy levels of a dot, containing specifiable number of electrons as a function of an external parameter (magnetic field, shape and strength of the confinement potential) In addition, by measuring the phase of the signal at different frequencies, we deduce the tunneling rate of the single electrons relative to the frequency of the ac excitation.

We begin with our wafer design. Then we describe how we create dots with different confinement potentials. Next we explains the details of capacitance measurements. Finally, we point out the advantages of SECS over the conventional transport techniques.

2.1 MBE Wafer

Figure 2-1A shows the essential structure of our samples. The sample is a GaAs/AlGaAs modulation-doped [20] heterostructure grown by molecular beam epitaxy. Figure 2-1B displays the corresponding conduction band diagram. Our substrate is intrinsic GaAs covered with a cleanup MBE layers, which trap out Si atoms which might otherwise migrate into our structure. First, we grow a heavily doped GaAs contact layer that remains conductive at low temperature. This layer serves as the bottom plate of our tunnel capacitor. On top of the contact layer, we grow a GaAs spacer, a GaAs/AlGaAs tunnel barrier and a GaAs quantum well. The last layer defines a two dimensional (2D) electron system. Our processing procedure, described in section 2.2, further confines electrons to small regions within the GaAs quantum well, thus defining our dots. The quantum well is covered by a blocking GaAs/AlGaAs barrier and a GaAs cap layer. A top plate of the capacitor is formed at the fabrication stage by evaporating Cr/Au gate on top of the structure.

The exact thicknesses of the layers, from bottom to top, are as follows: 6500 Å GaAs undoped clean up buffer; 6500 Å GaAs/AlGaAs undoped clean up superlattice; 2000 Å GaAs n+ doped contact layer; 400 Å GaAs undoped spacer; 80 Å GaAs/AlGaAs superlattice tunnel barrier; 175 Å GaAs undoped quantum well; 500

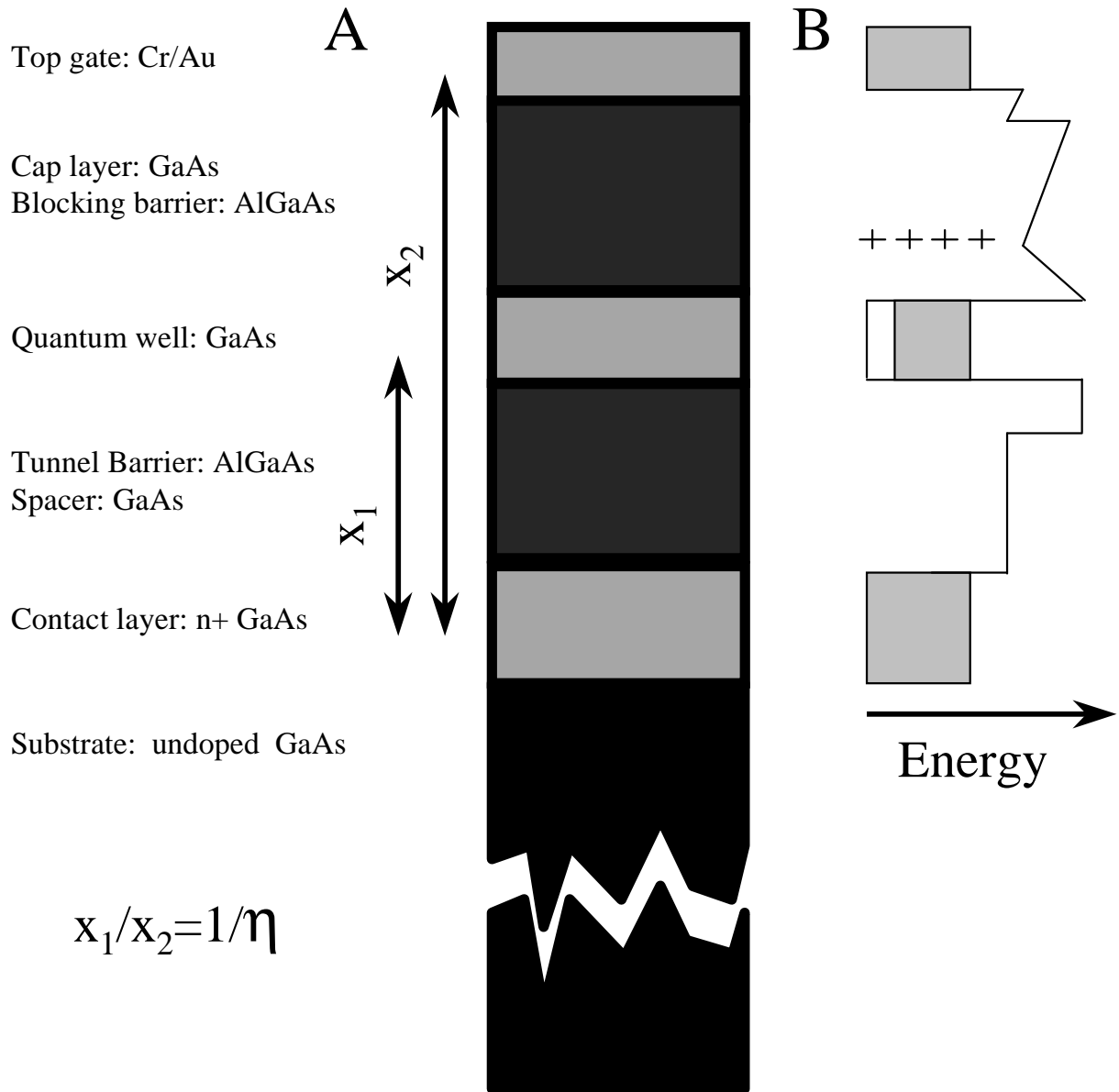


Figure 2-1: (A) Structure of our samples with layer thickness shown. (B) Conduction band energy diagram of our samples.

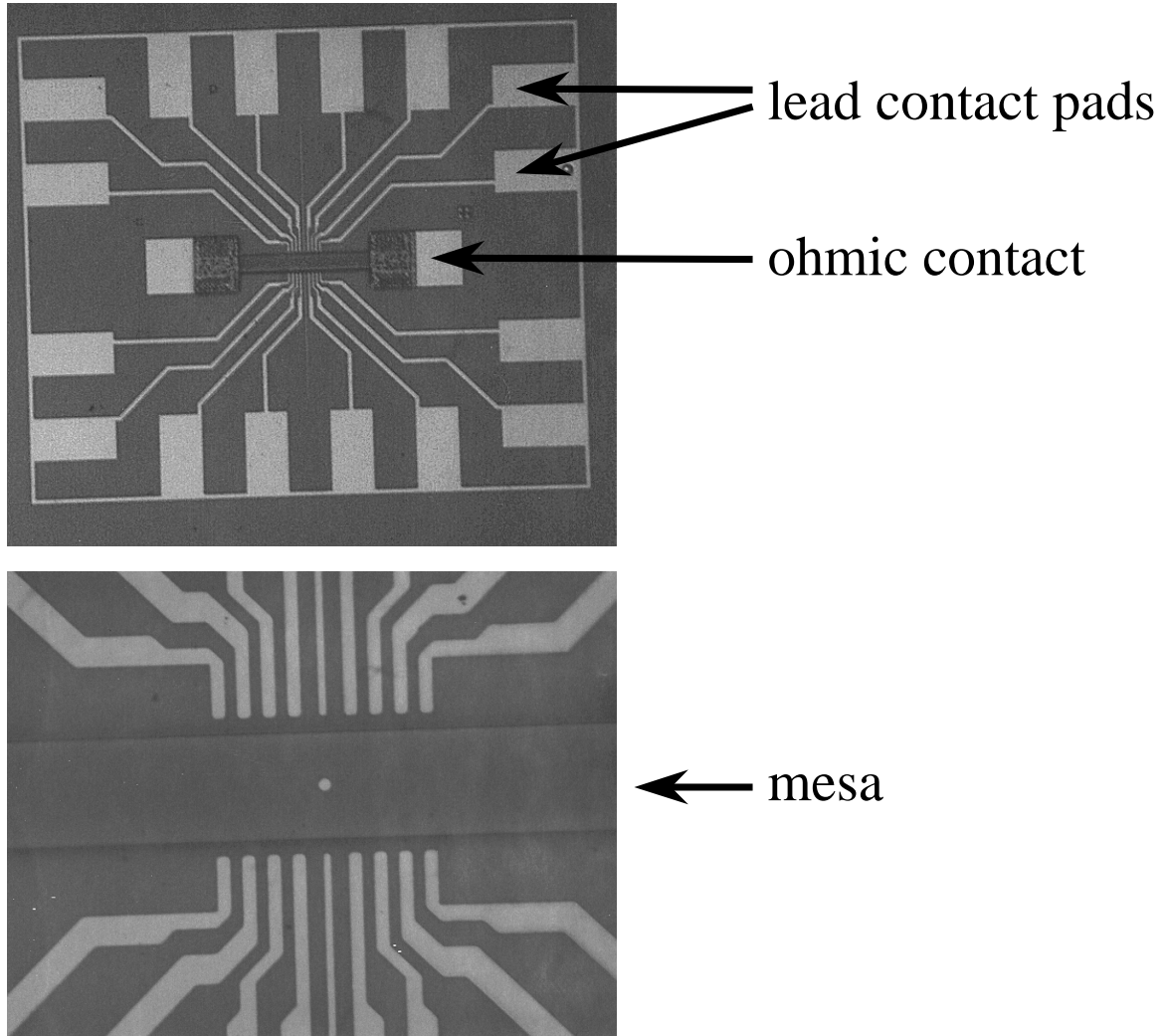


Figure 2-2: Top panel shows a photograph of the entire sample. One can see a mesa with ohmic contacts and a pattern of sixteen leads converging to the center of the mesa. Bottom panel is a zoom-in into the mesa center. Mesa is about $40\mu m$ wide. Lead contact pads are $100 \times 200\mu m$.

Å AlGaAs undoped blocking barrier, 300 Å GaAs undoped cap layer. We introduce Si δ doping in the middle of the blocking barrier 200 Å from the quantum well in order to provide electrons for the quantum well.

The two barriers in our wafer are very different. The lower one (tunnel barrier) allows electrons to tunnel between the bottom plate and the quantum well. The upper one (blocking barrier) is thick enough to prevent electrons from tunneling between the quantum well and the top plate.

In our tunnel capacitor only one electron is induced to tunnel between the contact layer and the discrete state in the well. Since electrons travel only a fraction, $1/\eta$, of the distance between the plates of the tunnel capacitor (see Figure 2-1), the amount of charge induced on the top plate is e/η . Therefore, the closer the quantum well is to the top plate (i.e. the thicker the tunnel barrier is), the more image charge is induced in response to the single electron tunneling event. To make the tunnel barrier thick without sacrificing its transparency, we grow the barrier as a superlattice and add the spacer layer underneath it.

2.2 Fabrication of Vertical Dots

Here we describe the fabrication process that we devised to create our quantum dots. Our wafer contains the quantum well sandwiched between the contact layer and the top surface, as was described in section 2.1. Electrons in the well are already confined in the direction of the growth. The goal of the fabrication process is to further confine these electrons laterally to small pockets within the quantum well plane, and to make contacts to the top and the bottom electrodes of the tunnel capacitor. Our measurement apparatus requires that a great care be taken to minimize shunt capacitance between the leads to the top and the bottom plate (see section 2.3).

We start by performing three preliminary processing steps on a piece of wafer using optical lithography. We define a mesa, make ohmic contacts, and lay out metal leads. Photographs of a prefabricated sample are shown on Figure 2-2.

The mesa is defined in the form of an elongated rectangle by wet etch. The etchant

used ($H_2SO_4 - H_2O_2 - H_2O$) produces anisotropic edge profiles [41]. We intentionally align the longer side of the mesa with the $\langle 1-10 \rangle$ crystallographic direction to yield an outwards edge profile along this side of the mesa. The etch removes 4500 Å of material, cutting deep below the contact layer, thereby limiting the bottom electrode to the region underneath the mesa.

Two Ni/Ge/Au contacts are deposited at both short sides of the mesa. They are annealed all the way through to the bottom electrode, so that they contact both the 2D gas in the well and the bottom electrode. Even though our measurements utilize only one contact, the second is necessary for testing the contacts at low temperature prior to starting experiments.

Outside of the mesa we pattern multiple Cr/Au leads converging to the small region near the center of the mesa. Each lead starts with a bonding pad and stops a short distance from the mesa edge. Once the dots are defined on the mesa, each is used to connect to one dot. Because the previous etching procedure eliminated the contact layer underneath the leads, the capacitance between each lead and the contact layer is small.

Once this preliminary fabrication is complete, we turn to the actual creation of the dots. This process involves two or three electron beam lithography steps. These steps vary from one experiment to another [29, 32, 33, 34] and consequently are outlined below in separate sections.

2.2.1 Electron Beam Lithography

Our choice of electron beam lithography over other lithographical methods is influenced by two major factors. First, it can reproducibly make features of about 60 nm. Second, it allows us to make modification to a pattern easily and quickly without the need to make additional masks.

One of the problems inherent to lithography is that of alignment of several subsequent patterns. In our case this is particularly difficult because the typical features of our patterns are extremely small. We solve this problem by careful designing proper alignment marks.

Another pitfall we encountered is the need to control the resist profile with great precision. In our fabrication process described below we deposit several thin metal films. In order to insure the continuity of the films, some of the depositions are performed at different angles. The success of the following lift-off procedure depends to a large degree on the quality of undercut of the resist profile. However, very large undercut undermines our ability to make sharp features, and the top resist layer often falls without the support of the bottom layer. We adopted a procedure with two development steps on a bilayer resist similar to that outlined in David Berman's thesis [42]. Figure 2-3 shows the effect of this development procedure on pattern profiles.

2.2.2 Individual Circular Dot

Early experiments [29, 31, 32] described in Chapter 3 were conducted on individual single circular dots. The following principle [43, 44, 45] was chosen to confine electrons to small pockets within the quantum well plane. Almost every A_3B_5 material, and GaAs in particular, has an extremely large density of surface states in the middle of the bandgap. In other words the Fermi level at any surface of the material is pinned to the middle of the bandgap, and a depletion layer exists under the surface of the material.

To make a single dot, we form a small Cr/Au disk using electron beam lithography on top of the etched mesa. This disk is used as a mask for the reactive ion etch, which removes 300 Å of material throughout the mesa. Depletion under the etched surface confines electrons to the region of the well underneath the disk. We refer to this region as “the dot” and to the disk as “the top gate”. Usually we make many dots on one mesa, each aligned with one of the previously defined leads.

We note that because of the depletion of the two-dimensional gas in the quantum well, the previously defined Ni/Ge/Au contacts contact only the lower $n+$ layer (see Figure 2-4).

In the next lithographical steps we define narrow metal patches that run up the mesa edge and connect the dots on the mesa to the leads, which are located just off

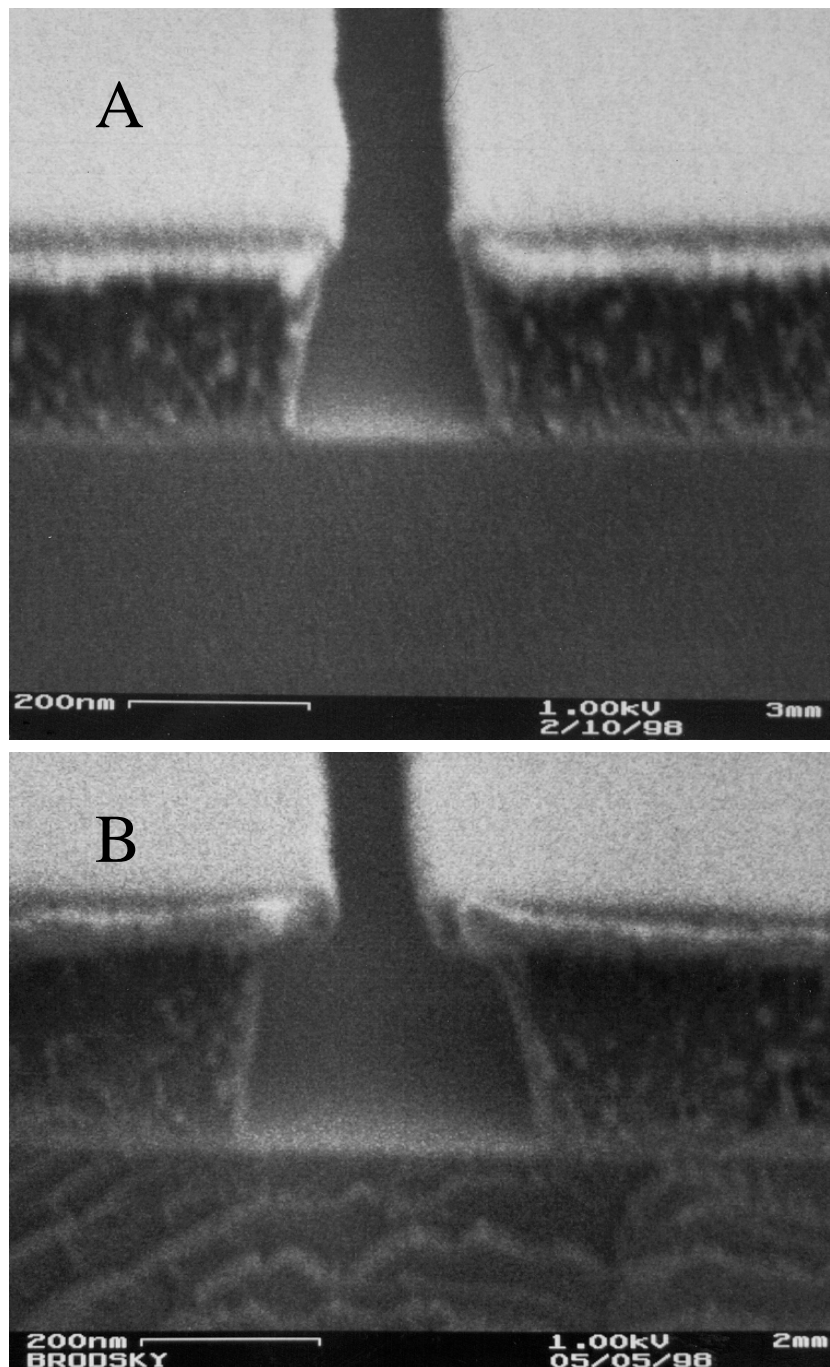


Figure 2-3: Effect of using a two-step development procedure. Profile of a single-pass line written in a bilayer resist. (A) For one step development procedure. (B) For two step development procedure. Second developer attacks only the lower layer. This results in larger undercut and more narrow line. The actual scale is indicated at the bottom each micrograph by 200 nm line.

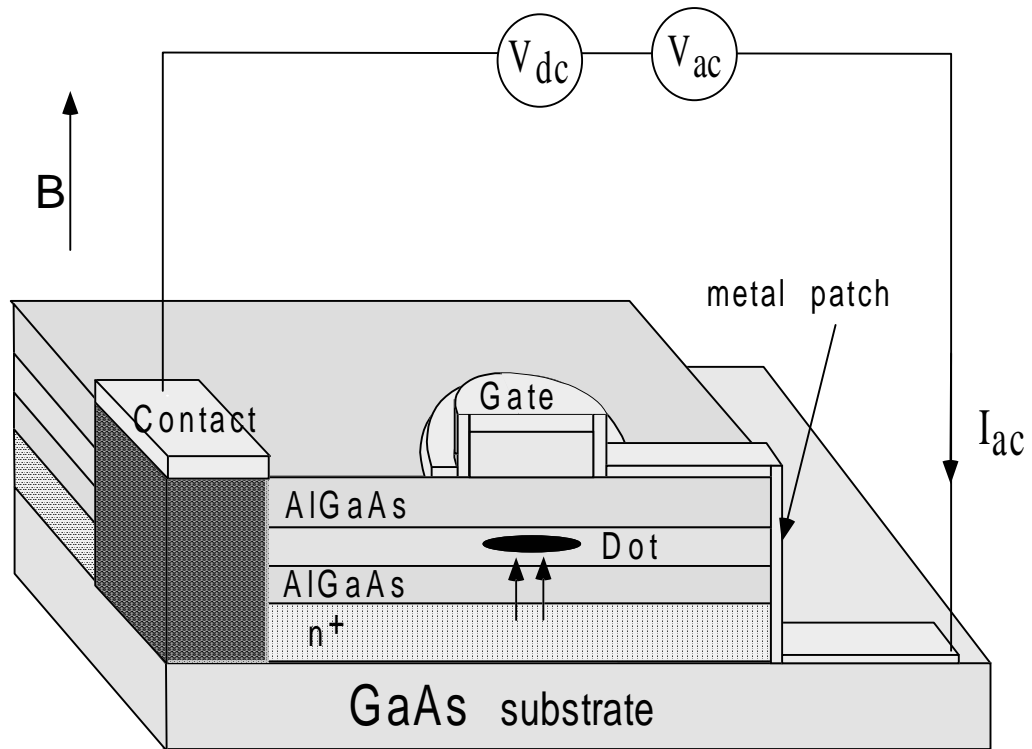


Figure 2-4: A schematic cut through our samples. Electrons are confined to the region under the gate, which we refer to as “the dot” Electron transfers occur between the $n+$ contact layer and the dot as indicated by arrows. A metal patch runs up the mesa edge and connects the dot to nearby electronics.

the mesa. The Cr/Au evaporation at this step is done at two angles. This and the outward edge profile of the mesa ensure that the patches do not break at the edge of the mesa.

A rough schematic cut through our dot is depicted in Figure 2-4.

In the described process the general shape and size of the dot is predominantly determined by the shape and size of the initial metal disk. In the experiments [29, 31, 32] described in Chapter 3, dots were defined by using metal disks with diameters ranging from 300 nm to 2 μm .

2.2.3 Dot with Adjustable Confinement: Putting an Additional Gate Around a Dot

SECS precisely measures the energies required to add individual electrons to a quantum dot. One of our experiments [33] probes the spatial extent of electronic wavefunctions by investigating the dependence of these energies on changes in the dot confining potential. To control the dot confining potential in situ, we fabricate an additional side gate.

Although the first fabrication step remains almost the same as described in section 2.2.2, two modifications have been made. As before, a small Cr/Au top gate on the top surface is formed. This top gate serves as a mask for etching, which completely depletes the quantum well layer outside the covered region, thereby producing the quantum dot below the top gate. However, the shape of the gate is different: it has a rather long tail extending sideways. Figure 2-5 shows two micrographs of the sample. This tail is made narrow enough, that there are no electrons beneath it, and the dot itself is still circular. Finally, we decided on utilizing a wet etching procedure, rather than a dry etching for the reasons listed below.

In the next a thin film of Cr/Au is evaporated over the formed structure. We evaporate without any tilt, and because the film is adequately thin it actually breaks at the edges of the previously fabricated top gate and can be contacted separately (see Figure 2-5). This new gate serves as a side gate allowing repulsion of electrons

from the edges of the dot through the application of a negative potential.

At the last step, we connect the dot and the side gate to the leads by patches. The last evaporation is a double angle evaporation to ensure that the patches do not break at the edges. One such patch contacting the dot through its tail can be seen on the Figure 2-5.

We noticed that the coupling between the side gate and electrons in the dot depends upon the chosen etching procedure; the wet etch provides much better coupling. We think that the wet etch produces a smaller side depletion resulting in a larger electron puddle. The larger the electron puddle is, the closer it is to the side gate. This assumption is not unrealistic. Wet etch procedure has been known to dramatically reduce the surface density of states. This phenomenon is used in fabricating optical devices to reduce nonradiative recombination, which occurs through the surface state [46, 47].

2.2.4 Dot with Artificial Disorder Potential

In a recent experiment described in references [34, 40], we study the effects of disorder on localization in quantum dots. We intentionally create a dot with an artificial “disorder” potential: a potential profile containing two smooth minima separated by a barrier, as in the double dot system described below.

As we mentioned in section 2.2.2, the dot’s geometry is determined mostly by the shape and size of the initial metal disk. Our previous experiments [29, 31, 32] studied individual circular dots.

However, the disorder inevitably present in the system strongly affects the exact shape of dot’s confining potential. In fact, in the low electron density regime, the combined effect of disorder and electron interaction leads to startling observations in the dot addition spectra [29, 30, 32, 39].

Let us first discuss the source of the disorder. We introduced the δ doping Si layer in the middle of the blocking barrier to provide the quantum well with electrons. The positive charge of the donor atoms, which have given up their electron, attracts electrons and binds them to the quantum well. However, this positive charge is not

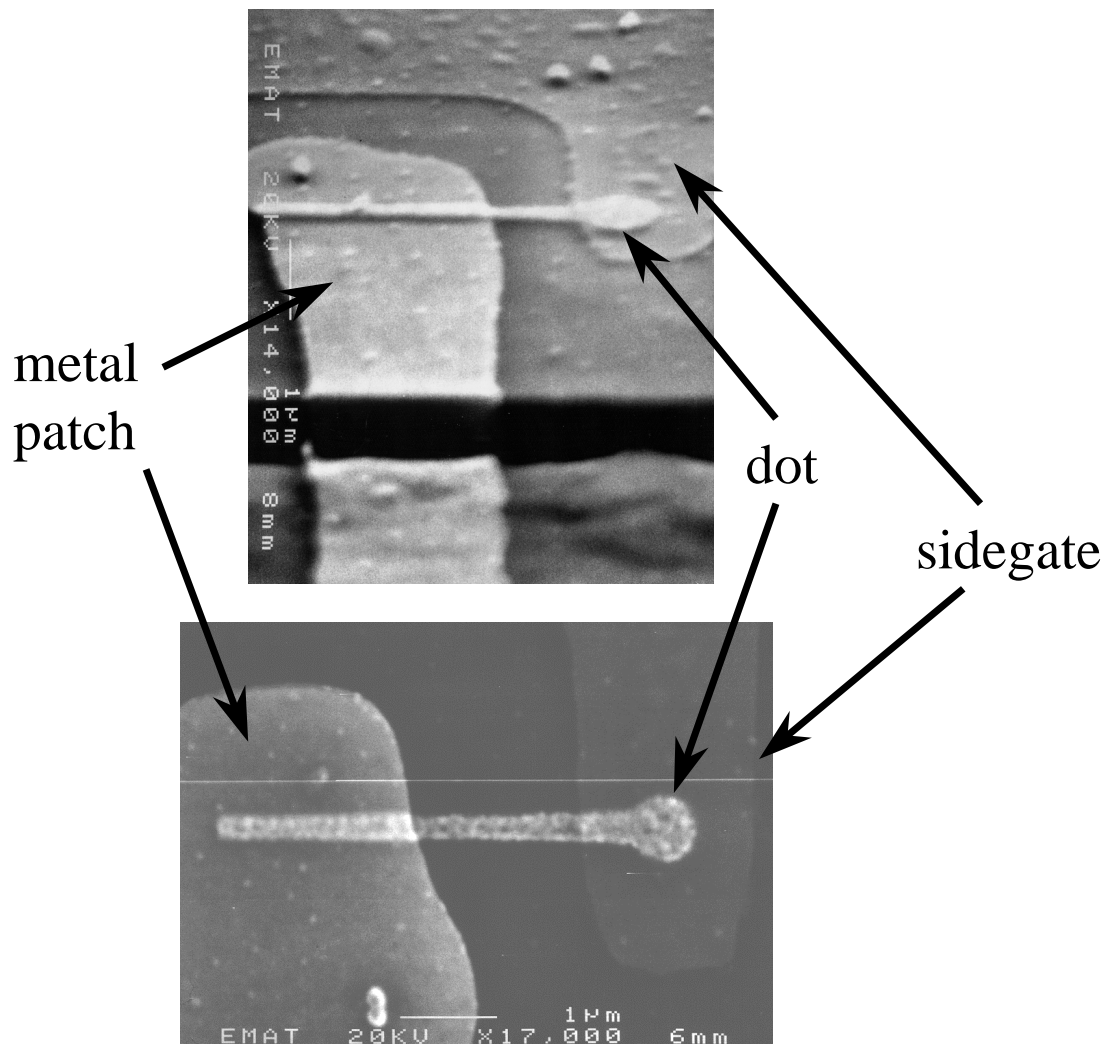


Figure 2-5: Two micrographs of the samples with the sidegate. The top one is a view at an angle, the bottom one is straight from the top. A thin film (thus barely visible on the top view) surrounds the dot without directly contacting it. A metal patch, which connects the dot to our setup is seen on the left. The edge of the mesa can be seen on the top panel. The scale is indicated at each micrograph by $1\mu\text{m}$ bars.

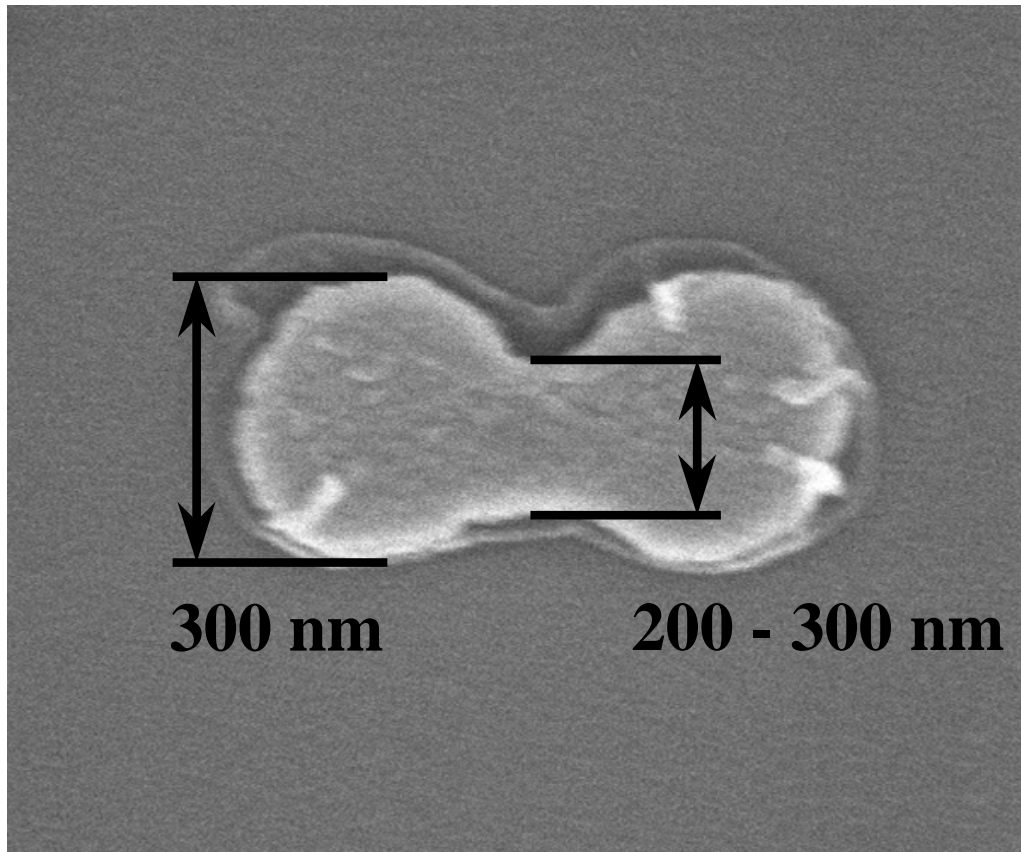


Figure 2-6: Top view micrograph of a dumbbell shaped top gate used to define out double dot system. The dirt around the edges of the structure are left over from the lift-off procedures. We remove it by ozone cleansing.

uniform. The donor atoms within the layer are spaced randomly, and only a fraction (about 30%) of them are ionized. Therefore, there are multiple local minima in the plane of the quantum well underneath positively charged donor atoms.

The scale of lateral variations of the disorder potential within the quantum well plane depends both on the average distance between ionized donors, as well as on the distance between the donor layer and the well. The latter is the largest of for our samples, and the variations of the disorder potential are somewhat diminished. In fact, the distance between the δ doping layer and the quantum well sets the lateral scale of the disorder up to a numerical prefactor [48].

Because of the fixed and finite lateral scale of disorder in our samples, our larger dots are more vulnerable to the presence of disorder. We vary the size of the dot by varying the size of the top gate. We find that our smallest dots with lithographical dimensions 350 nm or less have smooth circular symmetric confinement. See section 5.2 for the data and the discussion. Larger sized dots typically have a confinement potential with more than one minimum.

To create a confinement potential containing two smooth minima separated by a barrier, we define the top gate in the shape of a dumbbell. Figure 2-6 shows an electron micrograph of the top gate before it is connected to the lead. The following dry etching produces the desired double dot system. Each half of the dumbbell gate is 300 nm in diameter, so the resulting potential well under the gate has just two smooth minima.

By varying lithographic dimensions, we control the height of the saddlepoint between two minima, and therefore the strength of “disorder”. We examine a number of samples to investigate the broad range of this disorder strength.

2.3 Capacitive Measurements

The fabrication procedure described in section 2.2 defines the system depicted on Figure 2-7. The dot is arranged between two plates of a parallel plate tunnel capacitor. Electrons may tunnel back and forth between the dot and the bottom plate, while

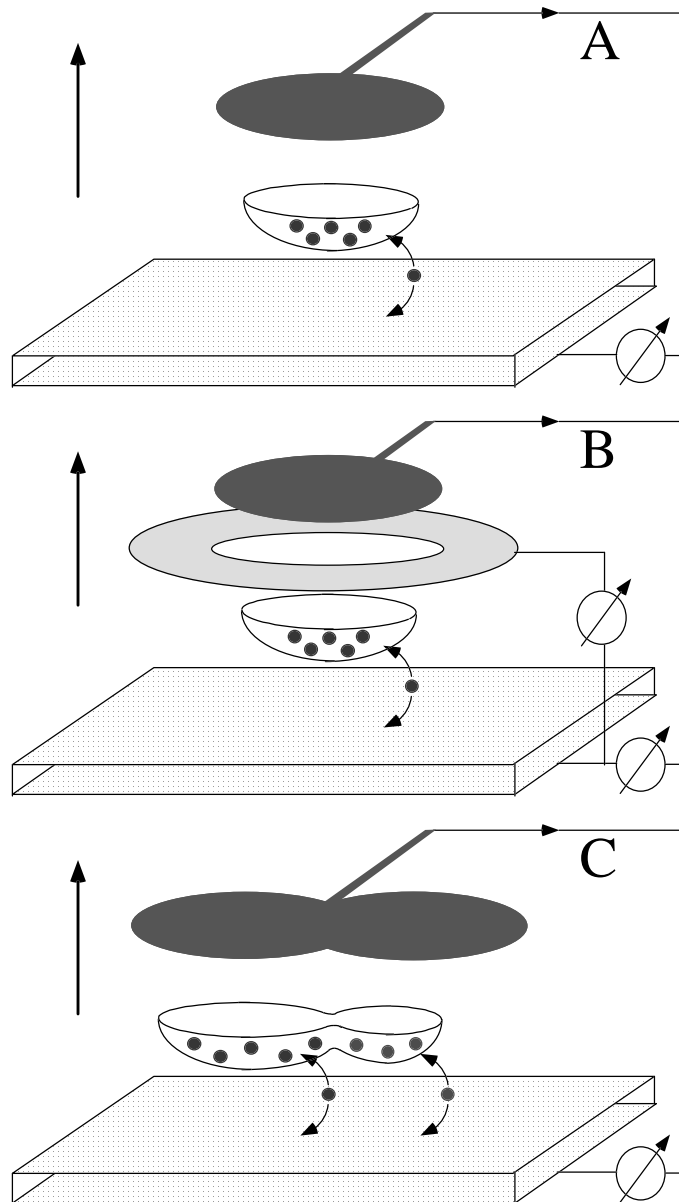


Figure 2-7: Schematic of our setup for three different experiments. The dot is arranged between two plates of a parallel plate capacitor. Electron may tunnel back and forth between the dot and the bottom plate as indicated. Magnetic field is applied along vertical arrows. (A) individual dot. (B) dot with a sidegate used to adjust its confinement in situ. (C) double dot: two smooth minima separated by a barrier. Electron addition to different dot can occur independently

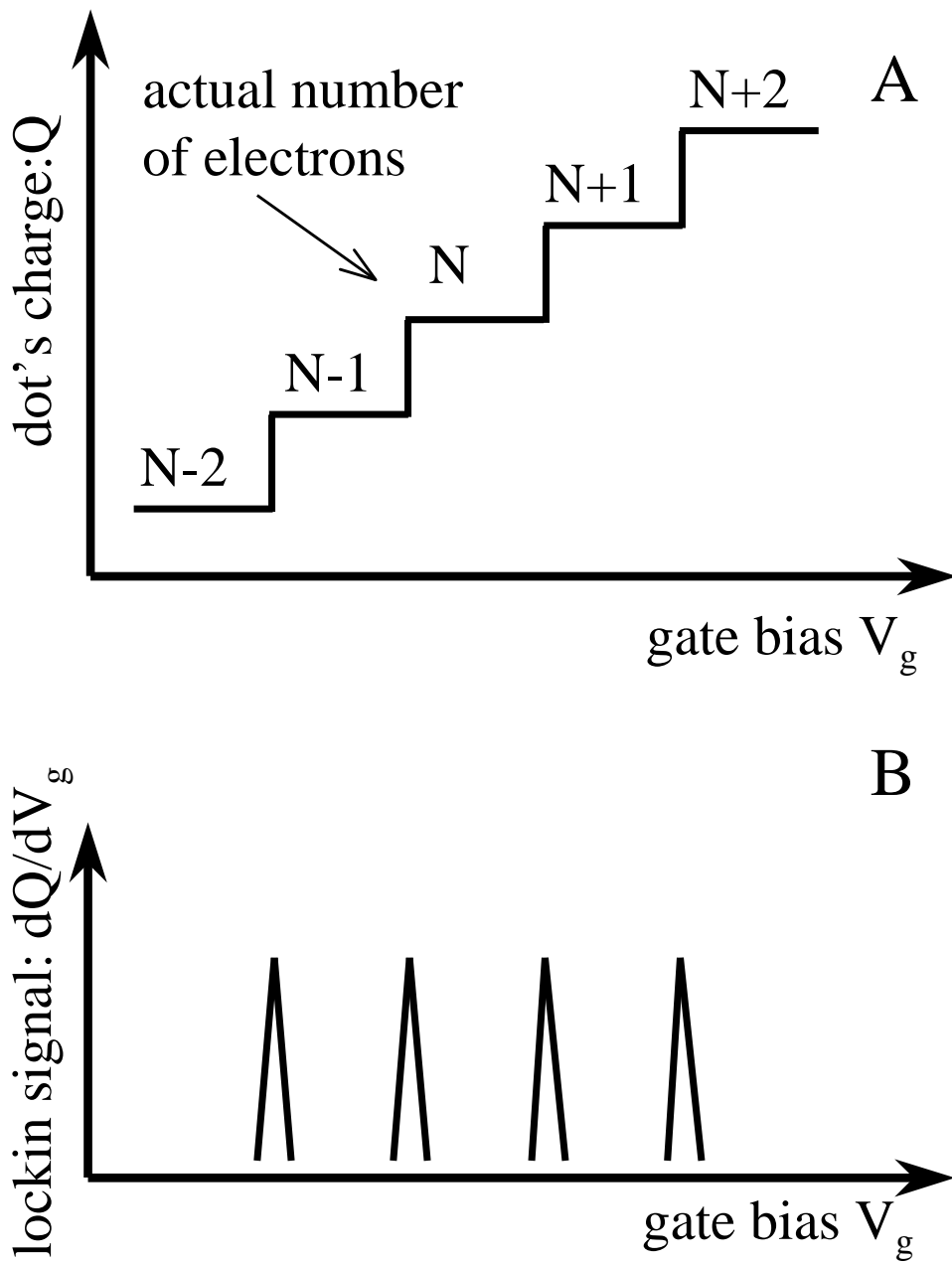


Figure 2-8: A: Schematic representation of the changing charge on the dot. B: Corresponding lockin signal

tunneling to the top plate is forbidden. In our experiment we adjust the top gate bias V_g : the potential applied across the plates of the capacitor. We register the values of the gate bias, at which electrons are added to the dot and convert them into the energy scale for the dot.

Intuitively, our measurement technique can be understood in the following simple terms. Application of a large negative voltage to the top gate depletes the dot completely. By sweeping the gate bias in the positive direction, we add electrons to the dot. Because of Coulomb blockade[11, 13, 14] (see section 1.3), electron additions happen in one by one fashion only at certain values of the gate bias. The schematic dependence of the dot charge on the gate bias is depicted on Figure 2-8A. The increasing charge on the dot induces an image charge on the top plate. This charge is equal to dot's charge up to a numerical factor. To register this image charge, we apply a tiny ac voltage to the bottom plate and feed the signal from the top plate into our lockin. The resulting signal is proportional to the derivative of the dot charge and schematically shown on Figure 2-8B. Let us now turn to a more mathematically elaborated description.

2.3.1 Sample Impedance

Figure 2-9A shows an equivalent circuit diagram representing our samples. The capacitance C_{top} is the capacitance of the top blocking barrier. C_{bottom} is the capacitance of the bottom tunnel barrier shunted by the barrier tunneling resistance R_{bottom} . The values of C_{top} and C_{bottom} depend on the area of the dot and on the heterostructure layer thicknesses. In our experiment, both capacitances have approximately the same value and are about 0.1 fF. As we discussed in section 1.3, the additions of electrons to the dot can be suppressed by the Coulomb blockade. Consequently, R_{bottom} is not a linear circuit element.

However, for our analysis two limiting situations are sufficient. For most values of the gate bias V_g electrons are not allowed to tunnel onto the dot, and R_{bottom} is *infinite*. This is valid provided that the temperature and the excitation voltage is smaller than the Coulomb gap - the charging energy of the dot $E_c = e^2/C_{dot}$. For

the values of V_g , at which an electron can be added to the dot, R_{bottom} has a finite value, that we denote by R_{bottom}^* . R_{bottom}^* depends primarily on the heterostructure parameters. The samples have been designed, so that the tunneling frequency:

$$f_{tunnel} = \frac{1}{2\pi R_{bottom}^* C_{bottom}} \quad (2.1)$$

is greater than the frequency range of our measurements. Thus, once a quantum state in the dot is aligned with the Fermi level in the bottom electrode, there is always enough time during one half cycle of the measuring frequency for charge to move onto the dot from the bottom electrode and bring the two into equilibrium. So in this case R_{bottom} , can be considerate to be *zero*.

In both of the above mentioned circumstances the sample impedance is capacitive (as shown on Figure 2-9B), but the exact values are different. When $R_{bottom} = 0$, the capacitance between the top and the plate is just $C_{sample} = C_{top}$. When $R_{bottom} = \infty$, this capacitance is:

$$C_{sample} = \frac{C_{top}C_{bottom}}{C_{top} + C_{bottom}} \approx \frac{C_{top}}{2} \quad (2.2)$$

Hence, the sample capacitance increases for the values of V_g at which electron additions occur. Although this increase is very tiny (about 0.1 fF), it can be measured precisely by the method delineated below.

2.3.2 Measurement Apparatus Design: Pitfalls and Solutions

Essentially, our sample is a capacitor C_{sample} , whose value changes as we scan the bias V_g between its two plates. We apply an ac excitation V_{exc} to the bottom electrode of our tunnel capacitor and feed the signal from the top gate into a measurement apparatus. This way, the excitation voltage is divided between the sample capacitance and the input capacitance of the apparatus as shown on Figure 2-9C:

$$V_{out} = \frac{C_{sample}}{C_{sample} + C_{input}} \times V_{exc} \quad (2.3)$$

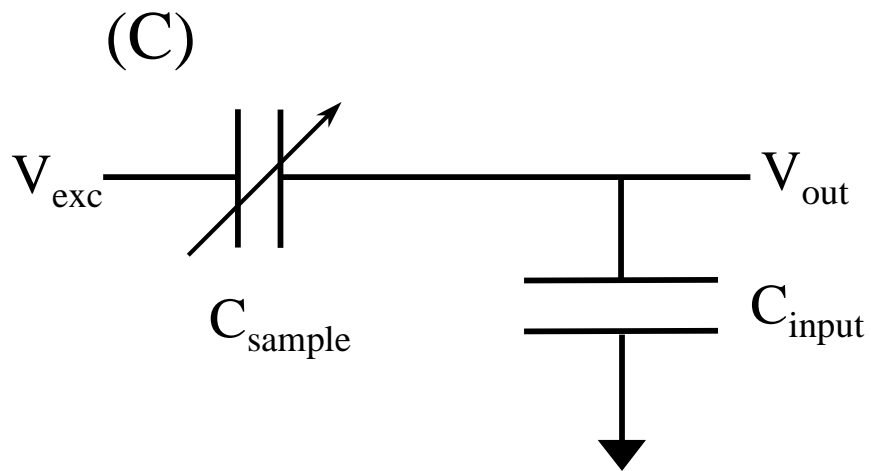
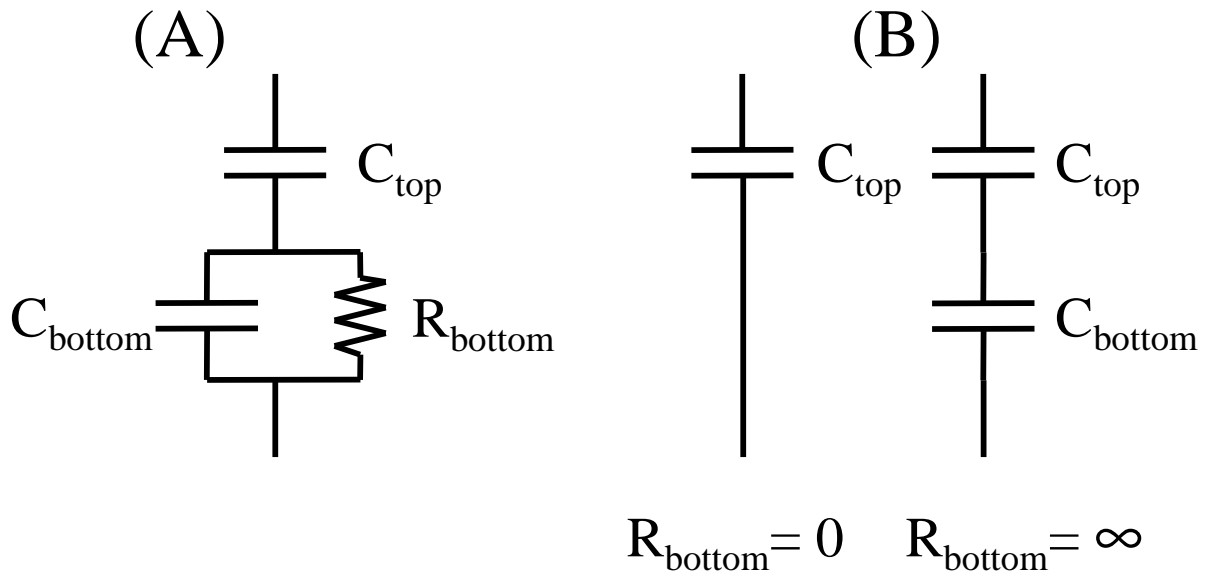


Figure 2-9: A. Equivalent circuit diagram of the sample. B. Corresponding impedance for $R_{bottom} = 0$: C_{top} only and for $R_{bottom} = \infty$: C_{top} and C_{bottom} in series. C. The simplest diagram for capacitance measurements. The sample is represented by a variable capacitance C_{sample} . C_{input} is the input capacitance of the measurement apparatus

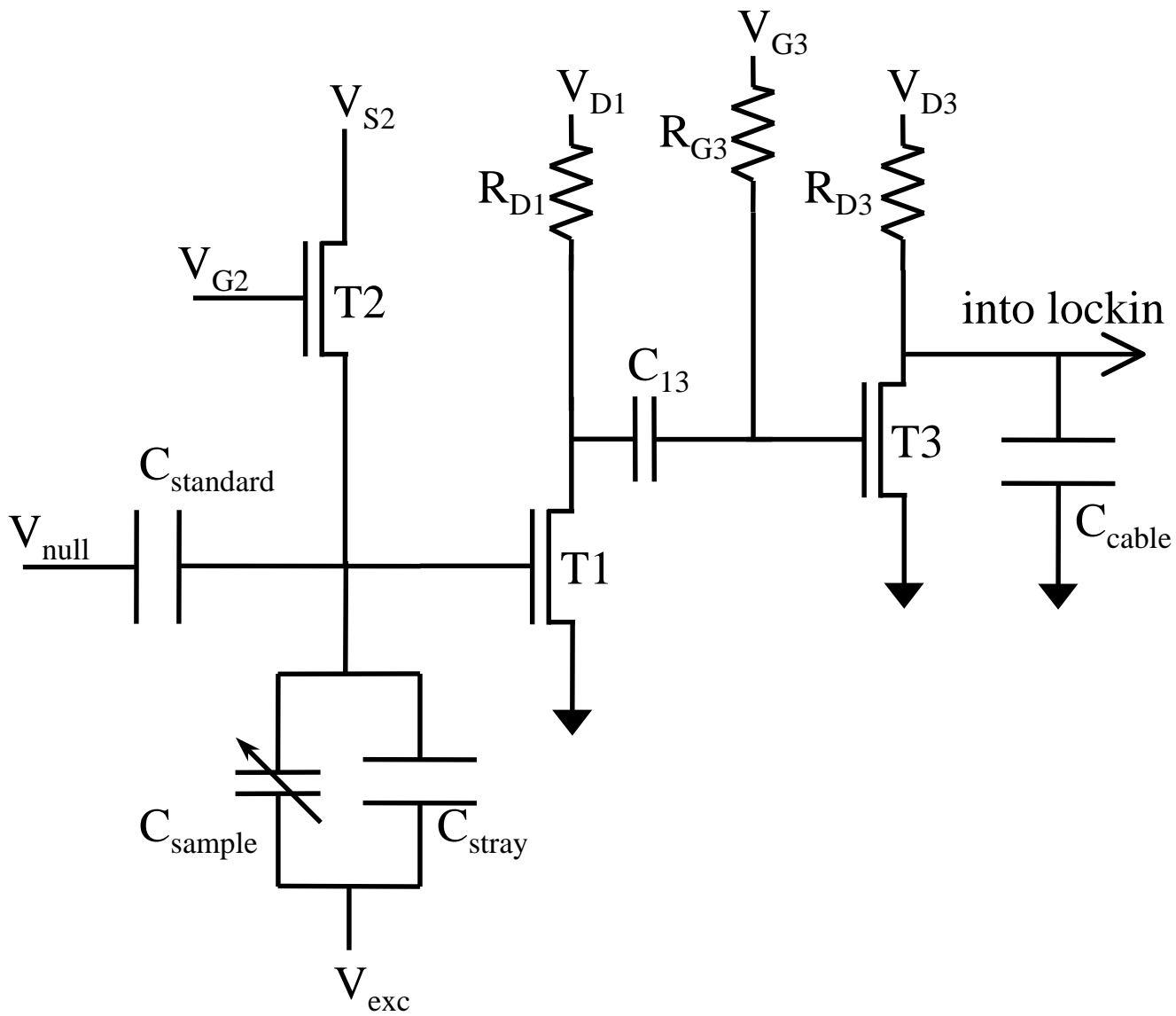


Figure 2-10: Diagram of the two stage cold amplifier

The measurement instrument (our lock-in) registers V_{out} . In effect, this is a two terminal measurement of the sample impedance: the excitation *voltage* is applied across the sample and the resulting *current* is measured by reading the voltage across the input impedance of the measuring instrument. This current is equal to the charge induced on the top plate of our tunnel capacitor during one period of the excitation and in turn is equal to the charge of the dot up to a numerical factor. Thus our circuit can be thought of as an ac electrometer.

There are two obvious ways to maximize the output signal. The first one is to increase the excitation voltage V_{exc} , and the second one is to minimize the input capacitance. However, V_{exc} limits the energetic resolution of our experiments and we are coerced to keep it under $100\mu V$ rms. Also, signal from single electrons does not increase once $V_{exc}/\eta > k_B T$ [29]. Minimization of the input capacitance becomes especially tricky because the experiments are conducted at ultra low temperatures, which requires huge cryogenic systems. As the result, the sample is situated at least 10 feet away from the lock-in, and the enormous capacitance of the cable connecting the two shunts the input impedance of the lockin. This capacitance is at least 300 pF, making $V_{out} \approx 0.3pV$. This is practically not a measurable quantity.

To circumvent this problem, we developed a two-stage cryogenic amplifier, which is positioned inside the refrigerator within 1 mm of our samples. The basic idea behind this amplifier is that it operates as an impedance matcher with a small gain [29]. With a low capacitance input, it drives high capacitance cables. We build the amplifier from commercially available high electron mobility transistors (HEMT) as shown on Figure 2-10. The signal from the sample C_{sample} is fed into transistor T1 and then further amplified by T3. The output of T3 is connected via a long cable to the input of the lock-in amplifier, which we position right on the top of the fridge. Since most of our experiment is conducted at high magnetic fields, the amplifier is mounted in a fashion which leaves its characteristics practically unaffected by an applied magnetic field.

To obtain high sensitivity, care is taken to further minimize the input capacitance C_{in} of the amplifier. First, the HEMTs chosen for the amplifier have the smallest

input capacitance. For an unpackaged transistor $C_{in} \approx 1pF$. We further reduce it by cleaving the transistors. The measurement transistor (T1 in the diagram) is actually only one third of a chip we buy. Second, we use another cleaved transistor (T2) and not a resistor chip to set the gate bias V_{S2} on the T1. This is because the thin film chip resistors available have appreciable capacitance between their terminals. The resulting input capacitance of our setup $C_{in} \approx 0.3pF$.

Another problem that obstructs our measurements is the existence of a large stray capacitance C_{stray} in parallel with C_{sample} . During the fabrication process, we try to minimize C_{stray} by minimizing the direct capacitance between the contact layer and the top gate. Nevertheless, because of the minuscule dimensions of our chip layout there exists a $C_{stray} \approx 150fF$, which is three orders of magnitude larger than the capacitance changes we measure. This extra capacitance adds a large, though constant, component to our signal at the input of the amplifier, thus significantly degrading the signal to noise ratio. However, exactly because this component is constant, we can eliminate it by using a bridge technique [29, 30]. We introduce another fixed capacitance into the circuit $C_{standard}$ and apply an ac voltage to it. This voltage V_{null} is at the excitation frequency and exactly 180° degrees out of phase with the excitation V_{exc} . The large signal due to C_{stray} is nulled by adjusting the nulling voltage V_{null} on $C_{standard}$.

The use of a two-stage circuit is advantageous in attaining larger gain from the amplifier. On one hand, the gain of the amplifier increases as we pinch off the transistors. On other hand, the output resistance also increases with a pinch off. A huge capacitive load on our amplifier $C_{cable} = 300pF$ imposes an upper boundary on the output resistance:

$$R_{out} \leq Z_{load} = \frac{1}{j\omega C_{cable}} \approx 1K\Omega \quad (2.4)$$

The two-stage arrangement allows us to close the first transistor T1 significantly, because it does not drive a large load; and to pass more drain current through T3 while leaving in more open state. This way gain is achieved on the first stage of amplification and the second stage actually drives the load operating around unity

gain. The 100pF capacitor C_{13} between the two transistors has negligible impedance for our operation frequency. It just separates dc voltages between T1 and T3 circuits.

Finally, let us mention two empirical rules that we follow to improve the signal to noise ratio. For the transistors that we use, there exists yet another observed limitation: the input noise of our transistor increases drastically when it dissipates more than $5\mu W$ of power. So we keep the power dissipated by each T1 and T3 under $5\mu W$. Also to reduce $1/f$ noise we operate at the frequency of $f = 600kHz$. Given our load of $C_{cable} = 300pF$, the maximal gain of 10 is achieved for $f < 50kHz$ and at $f = 600kHz$ the gain is only about 4. However, the noise decreases with frequency as well and we find that $f = 600kHz$ to be optimal for the best signal to noise ratio for our amplifier.

To summarize, we succeeded in implementing an amplifier with a low input capacitance of $C_{in} \approx 0.3pF$, an input noise of $\approx 10nV/\sqrt{Hz}$, and an amplification of around 10 and an output impedance of $R_{out} = 1k\Omega$. This translates into charge sensitivity of $0.01e/\sqrt{Hz}$.

2.3.3 Data Acquisition

The resistors R_{D1} and R_{D3} are used to set up source- drain current through the transistors T1 and T3. Both of the resistors cooled to helium temperatures to diminish Johnson noise. The gates of both transistors T1 and T3 are biased by V_{S2} and V_{G3} correspondingly (see Figure 2-10). While a thin film resistor R_{G3} is used to bias the transistor T3, the transistor T1 is biased through another transistor T2. To ensure that our setup is sensitive to electron tunneling between the contact layer and the dot in *synchrony* with the ac excitation we deliberately choose the biasing resistors to be much greater than the transistor's input impedances:

$$R_{bias} \gg \frac{1}{\omega_{exc} C_{in}} \quad (2.5)$$

For our excitation frequency of $f_{exc} = 600kHz$, a value of $R_{G3} = 10M\Omega$ satisfies this requirement. Since the gate bias for the transistor T1 is established through the

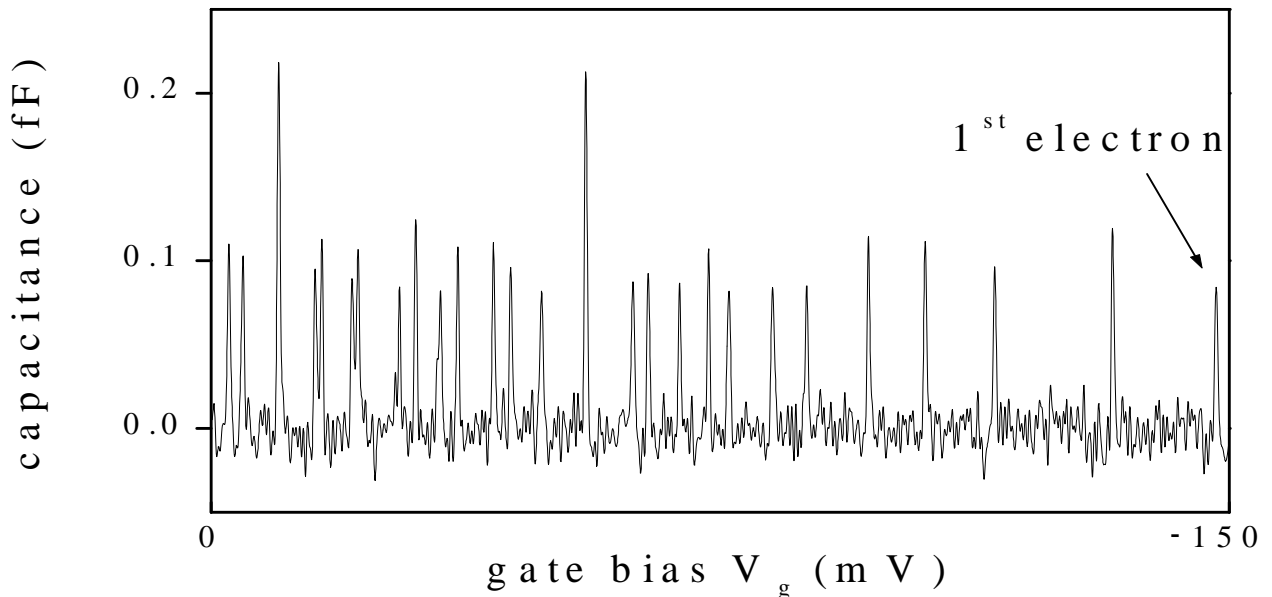


Figure 2-11: Experimentally measure capacitance trace as a function of the gate bias V_g . Each peak corresponds to an electron addition to the double dot described in section 2.2.4. Two peaks of double height actually occur because of simultaneous but independent additions to each dot [34].

transistor T2, we pinch T2 off by V_{G2} , so that its source-drain resistance is much larger than 10 M Ω .

Once the transistors are biased and the stray capacitance is nulled off, we monitor the off-balance capacitance signal while slowly sweeping the top gate bias across our samples. The resulting capacitance trace is shown on Figure 2-11. Each peak corresponds to the addition of one electron to the quantum dot. The validity of this picture has been verified as explained in references [29, 30, 49].

2.4 Advantages of Vertical Structures

Sections 2.3 and 2.2 establishes our ability to study electron additions to vertical quantum dots of various sizes and geometries. These dots are called vertical dots because

electron transfer occurs vertically and not in the plane of the two-dimensional system. In two aspects our dot are beneficial over the more traditional lateral structures [11].

In general, quantum dots provide convenient test devices for studying the quantum mechanics of coherent, interacting charged systems. But only our system permits variation of electron density, a critically important parameter that changes the effective strength of electron interactions. We note that since the Fermi energy $E_F \propto n$ in two dimensions and the electron interaction energy $E_{ee} \propto n^{1/2}$, the ratio $E_F/E_{ee} \propto n^{-1/2}$. Therefore, the lower the electron density, the greater the role of electron-electron interaction.

Also the traditional transport techniques for studying lateral quantum dots [11] sense primarily delocalized electronic states. A possible exception is transport studies in vertical structures [28, 50, 51], but again these do not permit variation of electron density. Our method of Single Electron Capacitance Spectroscopy (SECS) has demonstrated the capability of probing both *localized* and delocalized states of electrons. Furthermore, this method allows us to study 2D dots of various sizes and geometries.

These two principal advantages of our samples and technique result in a wealth of exciting experimental finding [29, 31, 32, 33, 34], which we will describe in the following chapters.

Chapter 3

Detailed Study of Single Vertical Quantum Dots.

This chapter is devoted to a historical overview of previous experiments conducted in our group on vertical quantum dots. The results of these early studies are what motivated us to produce the two experiments [33, 34] presented in the next chapters.

3.1 Early Observations

The first observation of a capacitance signal resulting from single electron tunneling into discrete quantum levels of a quantum dot was reported in the pioneering work by Ashoori [29]. The wafer structure and the fabrication procedure were similar to that described in section 2.2.2. An earlier version of our cryogenic amplifier (see section 2.3) was used in these measurements. A schematic of the experimental setup is shown in Figure 3-1. The dot is arranged between two plates of a parallel plate capacitor. Electron may tunnel back and forth between the dot and the bottom plate as indicated. A magnetic field is applied along vertical arrows. The experiments consist of monitoring the capacitance signal resulting from tunneling of signal electrons from the metallic contact layer to the levels in the dot as we scan the gate bias V_g : a potential applied across the plates of the capacitor. (see section 2.3). Charge transfer only occurs for bias voltages V_g at which a quantum level resonates with the Fermi energy

of the contact layer. This creates a sequence of distinct capacitance peaks whose bias position can be directly converted to an energy scale for the dot [29, 30]. For the first time the ground state energy in a quantum dot has been measured and followed as a function of magnetic field for an *arbitrary* number of electrons. Particularly striking is the spectra of dots with low electron occupancy, i.e. dots that contain low electron density.

Dots of two sizes were studied. The top circular gate used to define the smaller dot was 350nm in diameter, while the larger dot was defined by a $1\mu\text{m}$ disk. Two important and somewhat dissimilar results have been obtained.

The experimental spectra of small dots [31, 52] shows electronic states well separated by Coulomb blockade. The spectra reproduce many features of a simple non-interacting electron model with an added fixed charging energy [53, 54]. In other words, the first few electrons are shown simply to fill single particle states of a roughly parabolic confinement potential. In detailed observations deviations due to electron-electron interactions are apparent. First, the exchange interaction induces a two-electron singlet-triplet transition. Second, self-consistency of the confinement potential causes the dot to assume a two-dimensional character, and features develop in high magnetic field which are attributed to quantum Hall regime.

On the contrary, the spectra of large dots [29, 30] appears entirely different. Low energy spectra consist of *randomly* spaced discrete electronic states. The analysis performed in the paper [29] shows that such energy spacing cannot be caused by lateral confinement. Instead, potential fluctuation in the quantum well must create local minima, which localize electron puddles. The most intriguing feature in the spectra is a presence of “paired” electron additions. In several cases at zero magnetic field, two electrons enter the well at the same gate bias. Usually, electrons avoid entering the same potential minimum due to electron repulsion (Coulomb blockade). The experiments observe the reverse. The fact that this phenomenon is observed in many low lying levels suggests a possible physical mechanism.

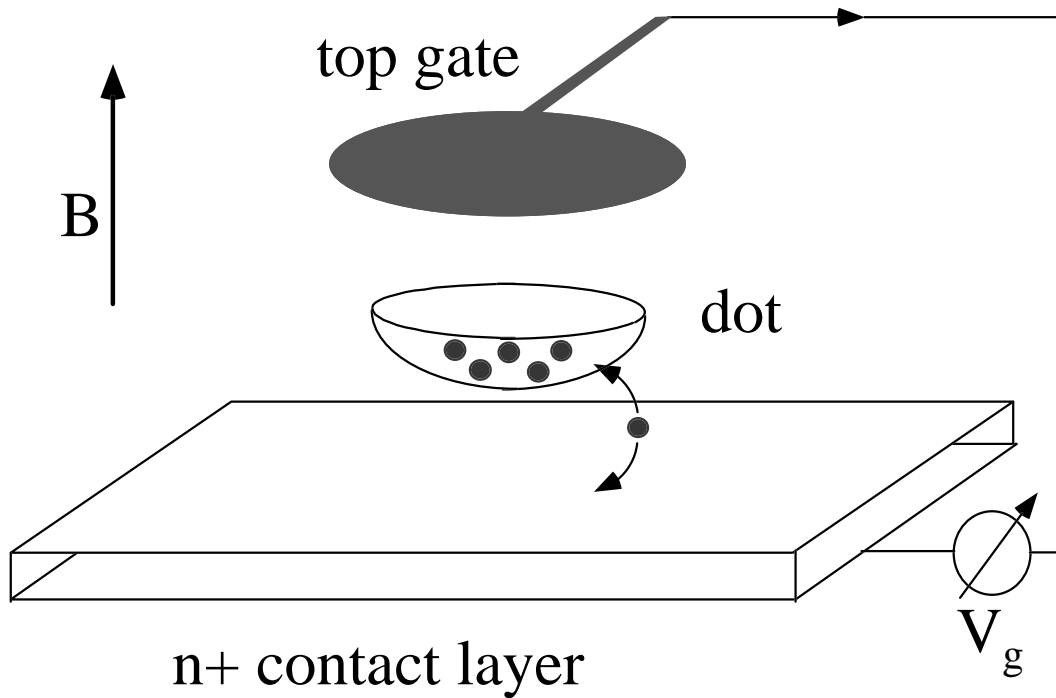


Figure 3-1: Schematic of vertical dot samples. The dot is arranged between two plates of a parallel plate capacitor. Electron may tunnel back and forth between the dot and the bottom plate as indicated. A magnetic field is applied along vertical arrows.

3.2 Periodic and Aperiodic Bunching in the Addition Spectra of Quantum Dots

The early observation of the profound violation of Coulomb blockade led to a systematic study of vertical dots of different sizes and densities [32], which is presented in the rest of this chapter. Eight individual circular vertical dots defined as described in section 2.2.2 were studied. The lithographical diameters of the top gate ranged from $0.2 \mu\text{m}$ to $1.6 \mu\text{m}$.

It was found that in dots with lithographic diameters larger than $0.4 \mu\text{m}$ containing small numbers of electrons, electron additions are sometimes grouped in bunches comprising from 2 to 6 electrons. The exact pairing seen previously [29, 30] is apparently a limiting case of this more general tendency. Surprisingly, in dots with diameters of $0.4\text{-}0.5 \mu\text{m}$, the bunching occurs *periodically* with electron number. Approximately every fifth electron addition peak pairs with a neighboring peak. The details of the addition spectra yield critical clues about the nature of the bunching.

As the electron density is increased in dots of all sizes, the pairing eventually ceases, and a periodic Coulomb blockade spectrum develops. However, application of magnetic field causes the pairing effect to reappear thus creating a boundary between periodic and “paired” part of the spectra. The boundary for the onset of the bunching is remarkably similar for all dots in which bunches are observed, regardless of their size.

We begin with very thorough consideration of an addition spectrum of one particular dot that shows periodic “paired” electron additions. Then, we generalize our finding by discussing the condition under which these phenomena occur. We will show that these suggest a relation between electron localization and the pairing phenomena [39]. Finally, we will consider how this suggestion can be tested.

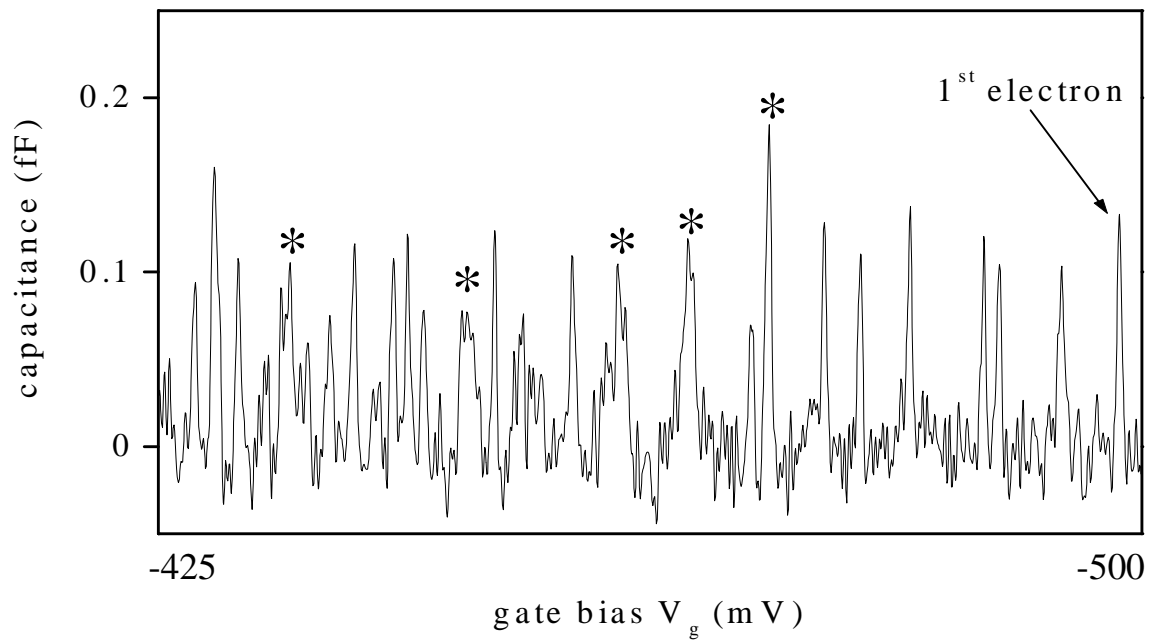


Figure 3-2: Experimental capacitance trace. Peaks in the capacitance occur at gate voltages for single electron additions to the quantum dot. The peaks are spaced rather randomly and many closely spaced electron addition are seen. Some are marked by stars.

3.2.1 Large Dot Spectra in Zero Magnetic Field

Figure 3-2 displays the electron addition spectrum at zero magnetic field for a dot of 500 nm lithographic diameter. For gate biases below -500 mV, the quantum dot is empty. Peaks in the capacitance occur at gate voltages for single electron additions to the quantum dot[29]. The peaks are spaced rather randomly and many closely spaced electron addition are seen. They are marked on the figure. Figure 3-3 shows another part of the same spectrum for higher gate biases V_g . Some of the peaks shown are of double height indicating the tunneling of two electrons in the dot at the same gate voltage. Remarkably, pairing of electron additions occurs nearly periodically. For even higher values of the gate bias, the spectrum evolves into a nearly periodic set of peaks, as is typical for Coulomb blockade.

Altogether, we can distinctly resolve about 600 electron additions in this dot. The gate voltage scale can be directly converted to an energy scale $\Delta E = 1/\eta\Delta V_g$ with the lever-arm $1/\eta \sim 0.5$ for these structures determined from the geometry of the dot as described in[29] (see also definition of η on Figure 2-1). The gate voltage position of the Nth capacitance peak, when multiplied by the lever arm, directly measures the chemical potential μ_N of the dot containing N electrons [14].

Fourier analysis of the spectrum clearly illustrates its evolution with the gate bias V_g . Figure 3-4 shows the Fourier transform of the measured capacitance for successive gate voltage intervals of equal length. The position of the Fourier transform peak reflects the number of electron additions per gate voltage interval. For more positive values of V_g (bottom traces), only a single dominant frequency component is present in the spectrum. As the gate bias is made more negative, the position of the Fourier transform peak shifts towards lower electron counts. In other words, for more negative gate bias fewer electrons are added in a gate voltage interval. This reflects a decrease in the gate capacitance C_g due to lateral contraction of the electron droplet. At voltages more negative than -400 mV, the single peak evolves into a broad low frequency spectrum. The broadening indicates that the gate voltage spacings between electron additions become uneven.

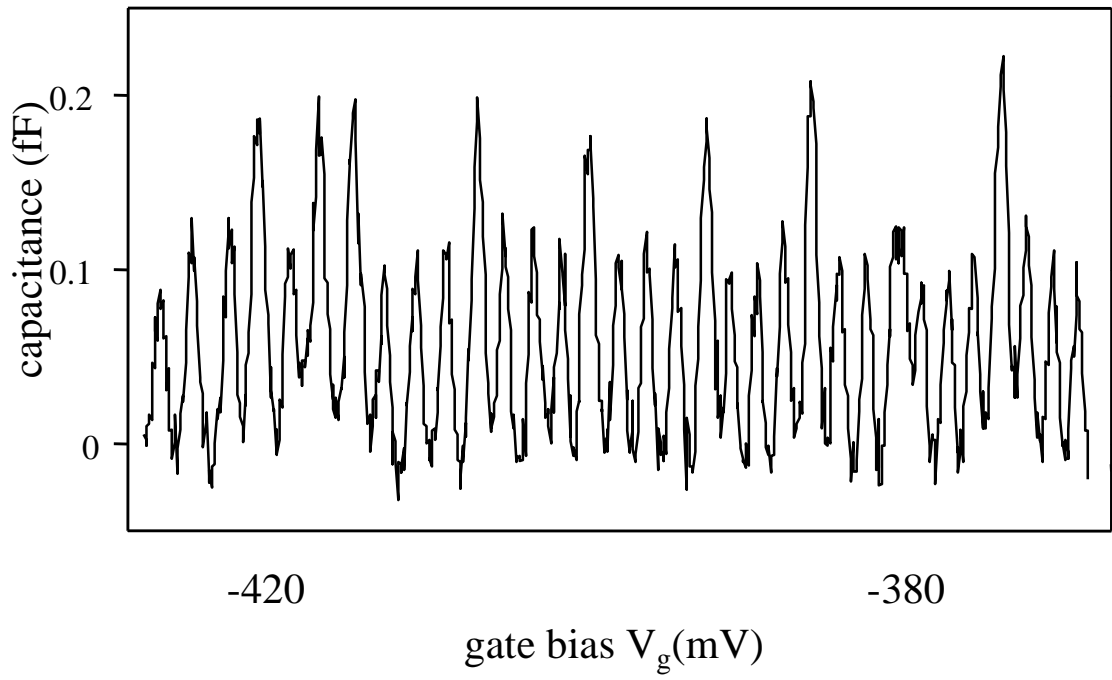


Figure 3-3: Another capacitance trace for higher gate biases V_g . Some of the peaks shown are of double height indicating the tunneling of two electrons in the dot at the same gate voltage. Remarkably, pairing of electron additions occurs nearly periodically.

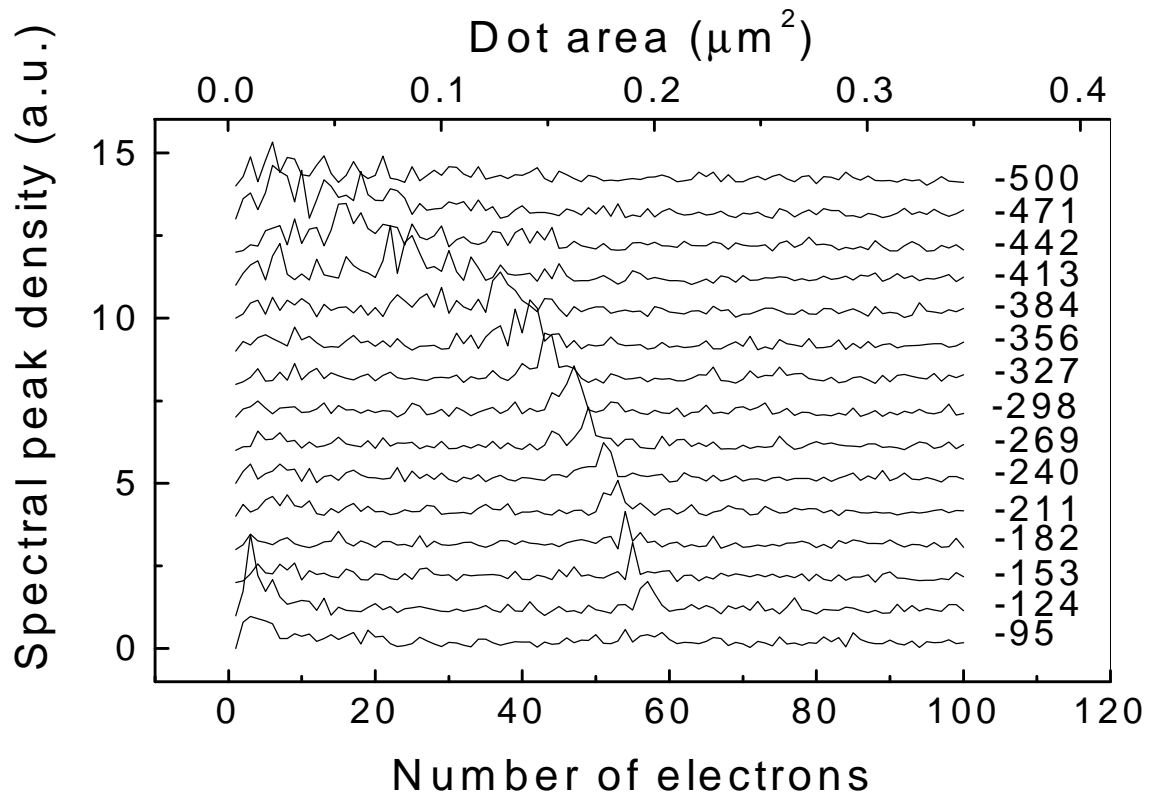


Figure 3-4: Fourier transform of the measured capacitance for successive gate voltage intervals of equal length. The position of the Fourier transform peak reflects the number of electron additions per gate voltage interval. The peak positions can be recalculated into the area of the dot (see text). The resulting area scale is shown on the top axis.

The peak positions in Figure 3-4 can be recalculated into the area of the dot by the following method. The position of the Fourier peak give us the mean spacing between the capacitance peaks in the gate voltage ΔV_g . This spacing, in turn, is inversely proportional to the gate capacitance: $\Delta V_g = e/C_g$. Assuming a simple parallel plate capacitor model for the gate-dot capacitance, we assess the dot area. The resulting area scale is shown on the top axis. Another independent way to determine the size of the dot from magnetic field position of quantum Hall features in the spectrum will be presented in the next section.

3.2.2 Evolution of the Spectra in Magnetic Field

The evolution with magnetic field of a portion of the electron addition spectrum is shown in Figure 3-5. The grayscale map displays the first 150 additions, with capacitance peaks visible as black traces. Examination of the bottom of Fig 3-5 shows that the first 7 electrons enter the dot at widely spaced voltages. They may enter into a single potential minimum or minima spaced closely enough that the Coulomb repulsion between the sites is sufficient to keep the peaks widely spaced. Beyond the 7th electron trace, something extraordinary occurs. Three electrons enter the dot in very rapid succession in gate voltage over the full range of magnetic fields. The next two electrons also join in a bunch (pair). For higher electron occupancy (N), other bunches can be seen. We note that the experiment shows no hysteretic effects. The bunching is a phenomenon which occurs in a dot in *equilibrium* with its surroundings.

After about 40 electrons are added to the dot, the bunching develops into a periodic pattern, with one bunch appearing for each 4-6 electrons added to the dot. As N is increased beyond about 80, the bunching ceases for zero magnetic field. Instead, the electron additions occur with nearly perfect periodicity, as is typical of Coulomb blockade. However, for nonzero magnetic field strengths, the bunching phenomenon returns. Bunches again occur periodically in gate voltage, and the period is about the same as that for the zero field bunches. A zoom-in of this behavior is shown in Fig 3-6. The onset of bunching shifts to larger magnetic fields with increasing concentration, and the bunches are no longer observable at fields of up to 13 Tesla

for more than about 200 electrons in the dot.

There is a region devoid of electron additions in the spectrum on both sides of any bunch. The mean interval between electron additions hence remains the same on a larger scale, even though individual traces have bunched. This is clearly noticeable for small N . At large N , Figure 3-6 reveals that the spacing between the non-bunched additions at nonzero magnetic field is larger than the spacing at zero field where the bunching phenomenon is not present.

Certain features, which develop in the spectrum at large electron number N and at high magnetic fields, can be attributed to Landau quantization in two dimensional electron system [31, 52]. Hartree calculations [55] shows that the bottom of the dot's confinement potential is "flattened" considerably by the presence of electrons, and in the interior can be considered as a small two-dimensional (2D) system. The chemical potential of a 2D system exhibits well-known drops as Landau level depopulate in the magnetic field.

Since the gate voltage position of the capacitance peak reflects the chemical potential of the dot, the behavior of each electron trace can be described roughly as follows. The magnetic field at which all electrons fall into the lowest Landau level, $\nu=2$, can be readily identified as a maximum in the traces at around $B \approx 2T$ [31, 52]. As in two-dimensional systems, the chemical potential peaks just as higher Landau levels depopulate completely. A line marked as $\nu = 2$ on Figure 3-5 is drawn through these maxima on each trace. Jumps in the traces at higher magnetic fields, where both spin levels of the lowest Landau level are filled, are usually interpreted as single electron spin-flips [54, 12]. The flatness of the traces around $B=6$ T demarcates total spin polarization of the dot. We refer to this range as the vicinity of $\nu=1$. For higher fields, the traces rise nearly linearly with magnetic field.

The position of $\nu = 2$ in the magnetic field provides another estimate of the dot area. In a dot with flat-bottom potential, the area of the dot is related to the Landau level filling fraction ν by $A = N(hc/eB\nu)$. This estimate agrees very well with the one obtained from the Fourier transform method.

The bunching phenomenon appears to be responsive to Landau quantization. Con-

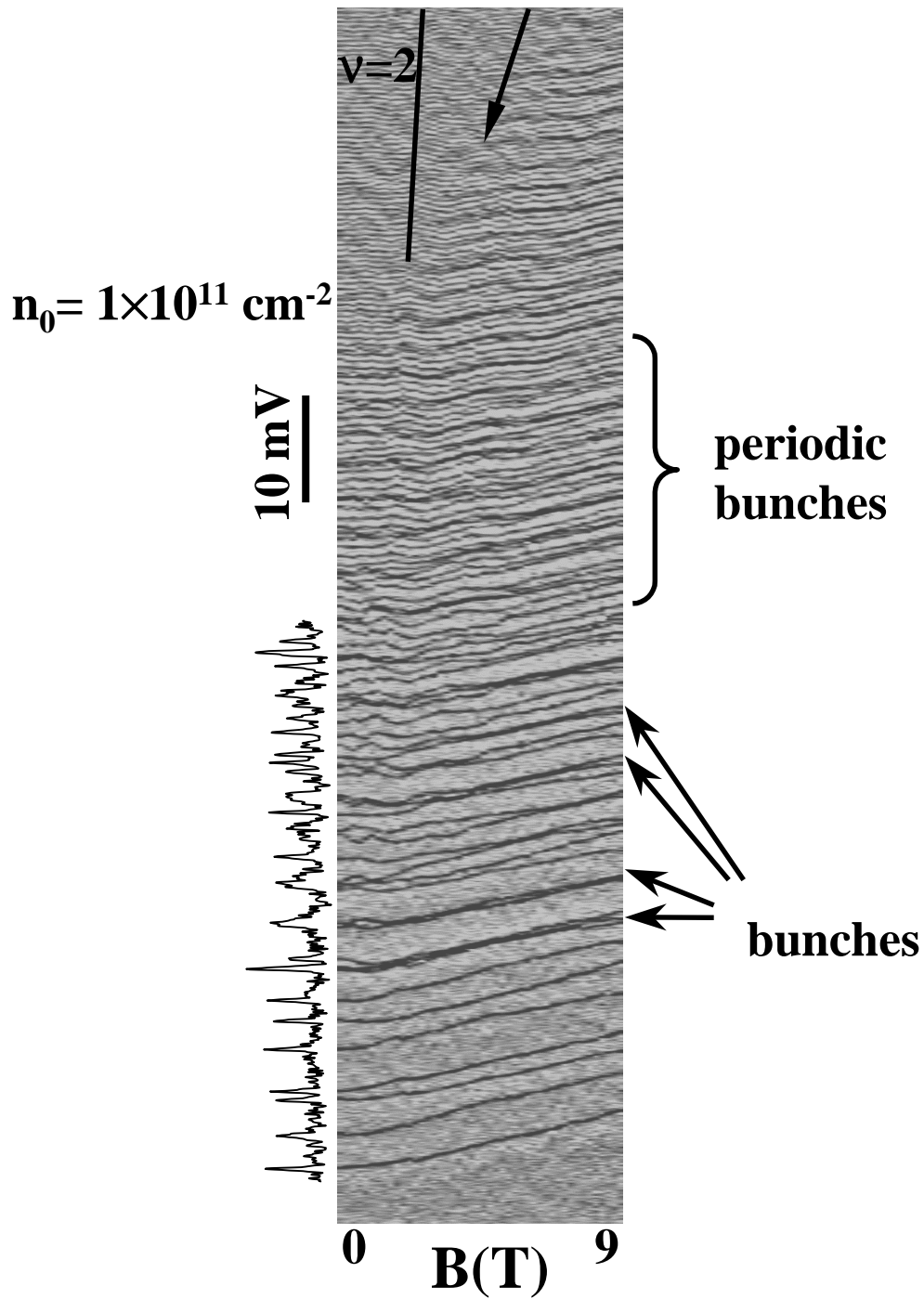


Figure 3-5: Grayscale image of the measured capacitance. Vertical scale - gate voltage (electron density). Horizontal - magnetic field. One capacitance trace taken at $B = 0$ is shown. A line marked $\nu = 2$ is drawn through the maxima at each trace (see text). At low electron density many bunched electron addition can be seen. Above the critical density $n_0 = 1 \times 10^{11} \text{ cm}^{-2}$ the spectrum is periodic at low fields. Note sharp boundary marked by an arrow. To the right of the boundary the bunched additions develop a periodic pattern.

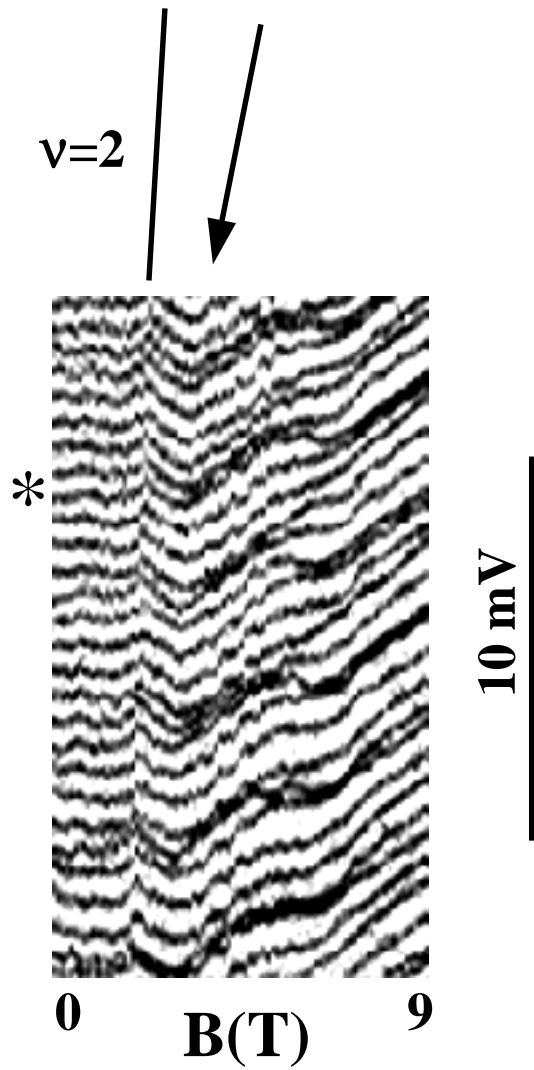


Figure 3-6: Grayscale image of the measured capacitance. Zoom in into a part of spectra shown on Figure 3-5. A line marked $\nu = 2$ is drawn through the maxima at each trace. The boundary is marked by an arrow. An asterisk denote a pair of bunched traces.

sider the bunched pair of traces in Figure 3-6 denoted by an asterisk. These traces are fairly representative of all of the other traces which appear as electron pairs. Starting at some nonzero magnetic field the two traces are seen to stick together but then they split as the field approaches that which yields $\nu=1$. Passing through $\nu=1$, the lower trace of the bunched pair splits from the trace above it only to join with the trace below it.

3.2.3 Tunneling Rates

The bunching phenomenon is reflected in the rate at which electrons tunnel into the dot. At zero magnetic field, the rate of electron tunneling between the $n+$ substrate and the quantum well is about 5 MHz . Measurements at a much lower frequency of $f = 200\text{ KHz}$ are sensitive only to the tunneling resistance if the tunneling is strongly suppressed by electrons correlations within the dot[31, 12]. At very low temperatures ($T < 0.1\text{K}$) the tunneling rate drops substantially in particular regions of magnetic field and electron occupancy.

Figure 3-7 shows a measurement of the addition spectrum of the same dot at base temperature $T = 50\text{ mK}$ after thermal cycling up to room temperature. The details of the addition spectrum of the dot are modified, but the overall bunching behavior remains qualitatively unchanged. For low N , shown on the bottom part of Figure 3-7, the contrast in all electron traces is the same over the entire range of magnetic field, indicating that the electron tunneling rate is much larger than the measurement frequency. The middle segment of Figure 3-7 displays the capacitance spectrum in a range of larger N (75-95 electrons in the dot). Notice here that some of the traces extinguish as the magnetic field increases. As the peaks diminish in strength, the phase of the electron tunneling signal lags relative to the ac excitation [31]. This detectable decay of the tunneling rates begins in the vicinity of $\nu=1$, for sufficiently large number of electrons in the dot.

The only traces observable at the highest magnetic field of $B=13\text{ T}$ in Figure 3-7 extend from paired traces. Examination of the intensity and phase of these unextinguished traces shows that they typically result from only a single electron

rather than two electrons tunneling. We note that the dc bias in the experiment is adjusted very slowly so that the electron occupancy in the dot changes even though peaks are not seen in the capacitance experiment. Finally, at higher N (Figure 3-7, upper part), the bunching disappears, and all traces extinguish equally.

3.2.4 Universality of the Bunching Phenomena

The bunching emerges as a universal behavior. We have seen the bunches in all the investigated quantum dots with lithographic diameters greater than $0.4 \mu\text{m}$. The bunching is absent in the spectra of smaller dots [31, 28]. The appearance of the bunching in larger dot is governed *not* by number of electrons but the electron density in the dots.

At zero field, the bunching is observed below a critical electron density ($n_0 = 1 \times 10^{11} \text{cm}^{-2}$ in all of our samples). With increasing density n , the spacing between peaks becomes regular at zero magnetic field. We observe that application of a high perpendicular magnetic field increases n_0 linearly, creating a sharp *boundary* between periodic and “paired” (or “bunched”) parts of the addition spectrum. The boundary for the onset of the bunching is remarkably similar for all dots in which bunches are observed, regardless of their size. This boundary moves to higher magnetic fields as the average electron density (note, *not* N) in the dot is increased roughly according to the linear relation:

$$n_0 = (1 + 0.1 \times B[\text{Tesla}]) \times 10^{11} \text{cm}^{-2}. \quad (3.1)$$

The nearly periodic bunching (pairing) pattern is observed for dots created with lithographic diameters of about $0.5 \mu\text{m}$. For larger dots, the bunches appear to occur randomly with gate voltage rather than periodically. The details of the random bunching pattern vary with thermal cycling of the sample to room temperature. In sharp contrast, the *periodic* bunching behavior remains qualitatively unchanged. The same 5-electron period is consistently detected for different thermal cycling and different samples of the same size.

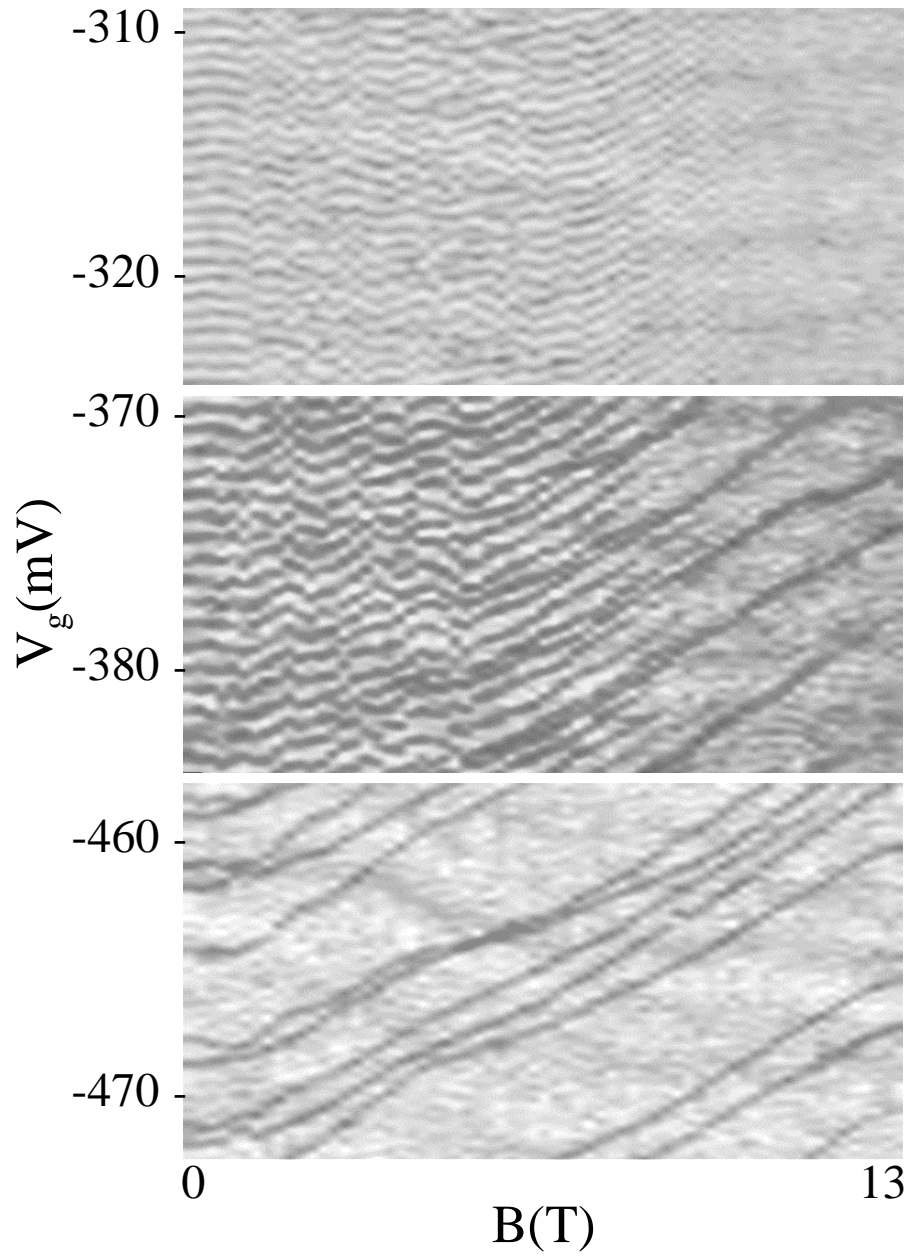


Figure 3-7: Segments of the addition spectra showing difference in the tunneling rates.

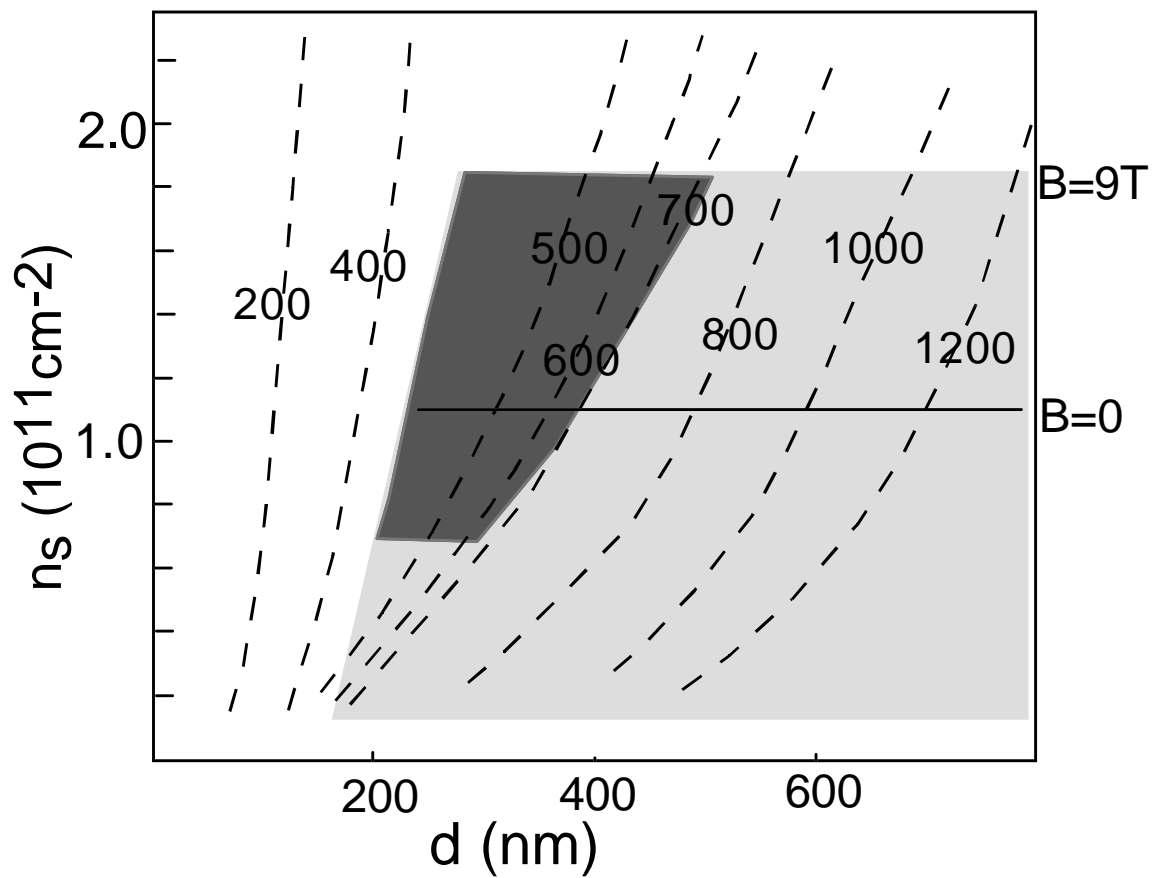


Figure 3-8: Experimental phase diagram for $B = 9T$. Dashed curves show variation of lateral diameter d of electron puddles with the electron density for different dots. Shaded area denotes the range of bunching; dark shading indicates the range of periodic bunches. The density limit at $B = 0$ is demarkated by a horizontal line

Our findings are summarized in an approximate phase diagram shown on Figure 3-8. Each dashed curve represents the evolution of one measured quantum dot sample. As we increase the electron density n_s within the dot, the lateral diameter of the electron pool d also grows. The diameter d is determined from the average spacing between addition peaks as shown in section 3.2.1. The bunching is absent either for very small dots at arbitrary electron density or at sufficiently large electron density in arbitrary large dots (nonshaded area). The shaded area demarcates conditions under which the bunching occurs. The dark shaded area corresponds to the periodic bunching. The density limit at zero magnetic field is shown by a horizontal line.

We believe that pairs of electrons in the quantum dot, previously observed by Ashoori [29] and reviewed in section 3.1, are a special case of the bunches in the regime of electrons strongly localized within a large ($1\mu m$ lithographic diameter) dot. In dots of similar size, we have seen more examples of bunches with traces of two and sometimes three electrons that exactly or nearly overlap over a range of magnetic fields. In general, paired traces from dots with smaller lithographic diameters do not coincide exactly.

3.3 Why is it that the Pairing is Related to Localization?

Taken together, our experimental findings suggest a relation between electron localization and the pairing phenomena [39]: the pairing occurs once the electron droplet within the dot splits into several fragments.

First, small dots do not display the bunching effect. We have determined (see Chapter 5) that dots with lithographical dimensions less than 350 nm have smooth circular symmetric confinement, and consist of a one electron puddle. Second, in larger dots, the bunching appears only at low densities when distinct electron puddles may exist. The size of large dots significantly exceeds the effective screening length (the distance to the top gate), and the direct Coulomb repulsion between different

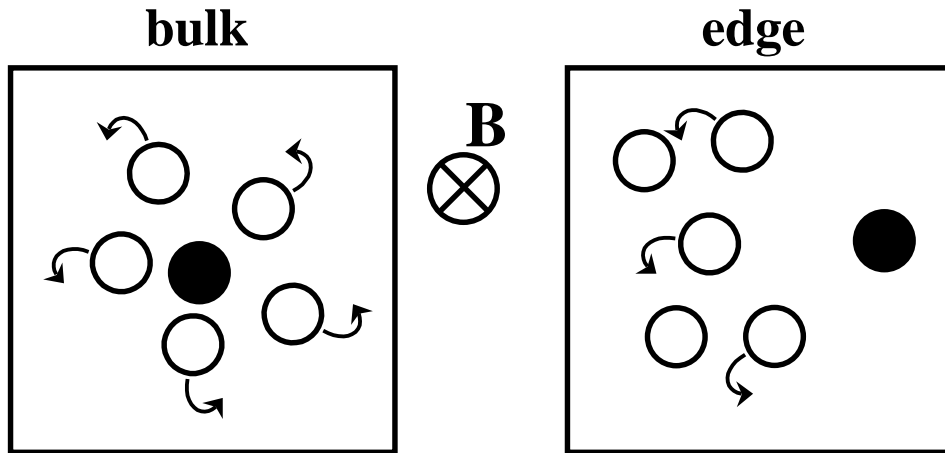


Figure 3-9: Diagram for electron tunneling in the 2D system.

electron droplets may be strongly suppressed. The addition of an electron in one region may not inhibit the addition of a second electron in a remote location. Third, the application of high magnetic fields restores the bunching phenomena at higher densities. The strong magnetic field squeezes the electron wavefunction and may facilitate trapping of electrons in local minima of a disorder potential.

Finally, the contrast observed in the tunneling rate is consistent with the idea that the two bunched electrons enter into spatially different regions within the dot. The drop of the tunneling rate at high fields illustrated on Figure 3-7 can be considered as a special case of the Coulomb gap observed for larger systems [56, 57, 58, 59, 60]. The origin of tunneling suppression can be understood semiclassically (Figure 3-9). The tunneling process suddenly introduces one more electron into a dot thereby creating a local density disturbance. The effective tunneling rate depends on the relaxation rate of this disturbance. In simple words, a “newcomer” needs to push its neighbors around to minimize the Coulomb energy. The high magnetic field causes electrons to

move in circles and slows the relaxation rate. The higher tunneling rate observed for one trace in each bunch can be explained if the electron is added into the edge of the dot. This electron has fewer and more distant neighbors compared with an electron introduced into the bulk of the dot.

Localization in a dot is caused either by a fluctuating potential or may arise intrinsically within a single dot due to interactions. The reproducibility of the periodic bunching pattern in several different dots and upon different thermal cycling of the same dot cannot be ascribed to a peculiarity of the disorder potential.

We hypothesized that disorder and electron-electron interactions within the low-density droplet split it into two or more spatially separate droplets, and the pairing arises once this localization occurs. We have produced two experiments to study this localization-delocalization transition in a controlled fashion. One recently established the existence of electronic states localized at the dot's periphery and arising at densities just below the critical density n_0 [33]. The other convincingly demonstrated that a high magnetic field abruptly splits a low-density electron droplet placed in a disorder potential into smaller fragments, and the paired electron additions to the dot result from an unexplained cancellation of electron repulsion between electrons in these fragments [34]. We will describe these two experiments in Chapters 4 and 5.

3.4 Theories Proposed

Our experiments have triggered intensive theoretical efforts. Despite of several theories that were put forward in recent years [61, 62, 63, 64, 65, 66] to explain the origin of the pairing phenomena, it is not yet understood. As a final point in this chapter we will briefly mention several of the proposed models.

Wan, Ortiz and Phillips [61] suggested an explanation based on the lattice polaronic mechanism. The authors showed that since GaAs is a weakly polar semiconductor, coupling to optical phonons is sufficiently strong to mediate a negative- U pairing state. Raikh and Glazman [62] demonstrated that electron-electron repulsion, screened by a close metallic gate, can lead to electron pairing for specially arranged

compact clusters of localized states in a disordered dot. Both models predict a dramatic suppression of the tunneling rate as soon as two electrons are joined into a pair, since both electrons must be added into the dot in a coherent fashion. Having studied large number of pairs in the frequency range $50 \text{ KHz} - 1 \text{ MHz}$, we have never observed a significant drop of the tunneling rate when the traces merge. This suggests that the paired electrons tunnel into the dot *independently*. The data indicate that filling one state of a pair has no effect on the energy of the other state in the pair.

Avishai, Berend and Berkovits [65] proposed a classical model in which a large semiconductor quantum dot is viewed as a collection of metallic electron islands with capacitive and inductive coupling among them. The model results in a peak spacing distribution, which has a maximum at small spacing values. It can explain the occasional occurrence of couples or even triples of closely spaced Coulomb-blockade peaks, as well as the qualitative behavior of peak positions with the magnetic field. While this model explains some of our data, it does not address the principal issue: what is the mechanism that splits a large dot into fragments? Furthermore, being a classical model, it does not take into account electron interaction and, as a consequence, does not give reasons for the appearance of the bunching only at low electron densities.

Another two classical models were presented by Koutrakov and Shklovskii [63] and Levitov [67]. Both models treat electrons as classical charges. The first theory describes the addition spectra of a dot in which the density of electrons is small and the external disorder is very weak, so that electrons in the dot form the Wigner crystal. This type of dot is referred to as “the Wigner crystal island”. The electrons are assumed to reside in a parabolic external confinement. Due to the crystalline symmetry, the center of confinement can be situated at distinct positions with respect to the crystal. With increasing electron number the center of the crystal periodically hops from one such location to another. Calculations show that at the moment when these rearrangements occur, several electrons can enter the dot simultaneously. In our experimental conditions a dot can be thought of as a Wigner crystal island only in the highest magnetic fields. Classical point charges cannot describe the electron density at zero field.

The calculations by Levitov [67] based on earlier work by Bedanov *et al.* [68] showed that classical point charges in a confinement potential form a nearly triangular lattice with significant lattice deformation only the dot edges. The edge electrons are practically frozen and can move only along the perimeter. The radial displacements for outer-shell electrons and for the inner ones differ by several orders of magnitude. Levitov demonstrated that, for a classical dot containing 50-150 electrons, 4 electrons enter the delocalized center of the dot in succession, and the 5th enters the localized circumference. While this model may explain the periodicity seen in our data and its increasing prominence at large magnetic field, it still does not explain the pairing.

Only recently, and in fact just after our new localization experiments [33, 34] were produced another theoretical work was published by Canali [66]. This work carries out a full quantum mechanical calculation of the addition spectra of dots containing a small number of particles in the limit of strong disorder and with a short range Coulomb repulsion. Both these assumptions are justified for our experiments. The background potential fluctuation are large: of the order of $5mV$ [29, 30]. The presence of the top gate cuts off the Coulomb repulsion.

Canali's simulations identify two different regimes where two successive electron additions almost coincide. The first case takes place for small values of the direct Coulomb repulsion but strong on-site repulsion, which favors the appearance of a dense droplet with neither holes nor doubly occupied states. Both electrons in the pair tunnel into the edges of the dot but in spatially distinct regions. The second situation is much more interesting. It occurs in the strongly correlated regime, with strong values of direct Coulomb interaction competing with the on-site repulsion and the disorder. In this case, pairing is characterized by the formation of two puddles of electrons. Doubly occupied states appear in between the two puddles, and one of the two electrons tunnels into this state.

So far, this last calculation is the most realistic modelling of our dots. The closely spaced electron additions in this regime bear strong similarities to the pairing seen in our experiments. The published model does not include the effect of the magnetic field, but a new series of calculations is under way.

3.5 Summary

This chapter provides a historical overview of previous experiments conducted in our group on vertical quantum dots. Our capacitive technique: Single Electron Capacitance Spectroscopy (SECS) precisely measures the energies required to add individual electrons to a quantum dots. We described the early SECS experiments and presented a detailed study of individual circular quantum dots of various sizes and electron densities.

We found that in dots with lithographic diameters larger than $0.4 \mu\text{m}$ containing small numbers of electrons, electron additions are sometimes grouped in bunches comprising several electrons. Surprisingly, in dots with diameters of $0.4\text{-}0.5 \mu\text{m}$, the bunching occurs *periodically* with electron number. Approximately every fifth electron addition peak pairs with a neighboring peak.

As the electron density is increased in dots of all sizes, the pairing eventually ceases, and a periodic Coulomb blockade spectrum develops. However, application of magnetic field causes the pairing effect to reappear, thus, creating a boundary between periodic and “paired” part of the spectra. The boundary for the onset of the bunching is remarkably similar for all dots in which bunches are observed, regardless of their size.

The details of the addition spectra yield critical clues about the nature of the bunching. We hypothesized disorder and electron interactions within the low-density droplet split it into two or more spatially separate droplets, and pairing arises once this localization occurs. In next two chapters we will present two experiments [33, 34] we produced to study this localization-delocalization transition in a controlled fashion.

Chapter 4

Localization-Delocalization

Transition in Quantum Dots

Detailed study of the pairing phenomena in quantum dots presented in Chapter 3 led us to conjecture a relationship between the pairing and localization in our dots. We hypothesized that disorder and electron-electron interactions within the low-density droplet split it into two or more spatially separate droplets, and pairing arises once this localization occurs. This chapter describes the results of the first [33] of the two experiments [33, 34] that we produced to study the localization-delocalization transition in a controlled fashion.

Our technique precisely measures the energies required to add individual electrons to a quantum dot. The spatial extent of electronic wavefunctions is probed by investigating the dependence of these energies on changes in the dot confining potential. We find that for low electron densities, electrons occupy distinct spatial sites localized within the dot. At higher densities, the electrons become delocalized, and all wavefunctions are spread over the full dot area. The transition occurs around the critical electron density $n_0 = 1 \times 10^{11} \text{cm}^{-2}$, below which paired electron additions appear (see section 3.2.4). For densities just below the critical density, our data establish the existence of electronic states localized at the dot's periphery. In the latter regime the paired electron additions develop a periodic pattern. We convincingly demonstrate that electrons in each pair are added to spatially separated regions within the dot: a

localized periphery and delocalized inner core. Unexpectedly, some of the localized electrons appear to bind with electrons in the dot center.

4.1 Added Electron: Where Does It Go?

The fabrication procedure for the samples used in this experiment is outline in section 2.2.3. Figure 4-1 depicts a schematic of the experimental setup. As before, we position the dot inside a tunnel capacitor, which is formed by the $n+$ contact layer and the top gate. Electrons may tunnel back and forth between the dot and the capacitor bottom plate ($n+$ layer) as indicated in the figure. In this experiment, we added an additional side gate that encircles the dot. Application of a negative voltage to this side gate squeezes the dot and repels electrons from the edges.

In measuring the electron addition spectra of these dots, we first apply a large negative potential to the top gate, V_t , repelling all the electrons from the quantum dot. Then, we scan V_t towards more positive voltages, drawing the electrons back into the dot one by one. To detect the electron additions we measure the ac capacitance between the top gate and the contact layer at a frequency of 600 kHz. At V_t values corresponding to the electron additions, an electron oscillates between the dot and the contact responding to the small (about $80 \mu V$) ac voltage and increasing the measured ac capacitance [29].

The electron addition energies are far less sensitive to the side gate potential than to the top gate potential reflecting the difference in the geometrical capacitance. First, only the fringing fields emerging from the side gate affect the dot. Second, this field decays strongly, moving toward the interior of the dot because of the screening by the bottom and top metal electrodes [69]. Moreover, because of this decay, the sensitivity of a particular electronic state in the dot to changes in the side gate potential V_s depends on the position of this state within the dot. The peripheral states are more susceptible to changes in the voltage V_s than the states in the dot's center.

Thus, the side gated samples allow us to determine where in the dot we actually add an electron. It would be particularly interesting to use this new tool on dots that

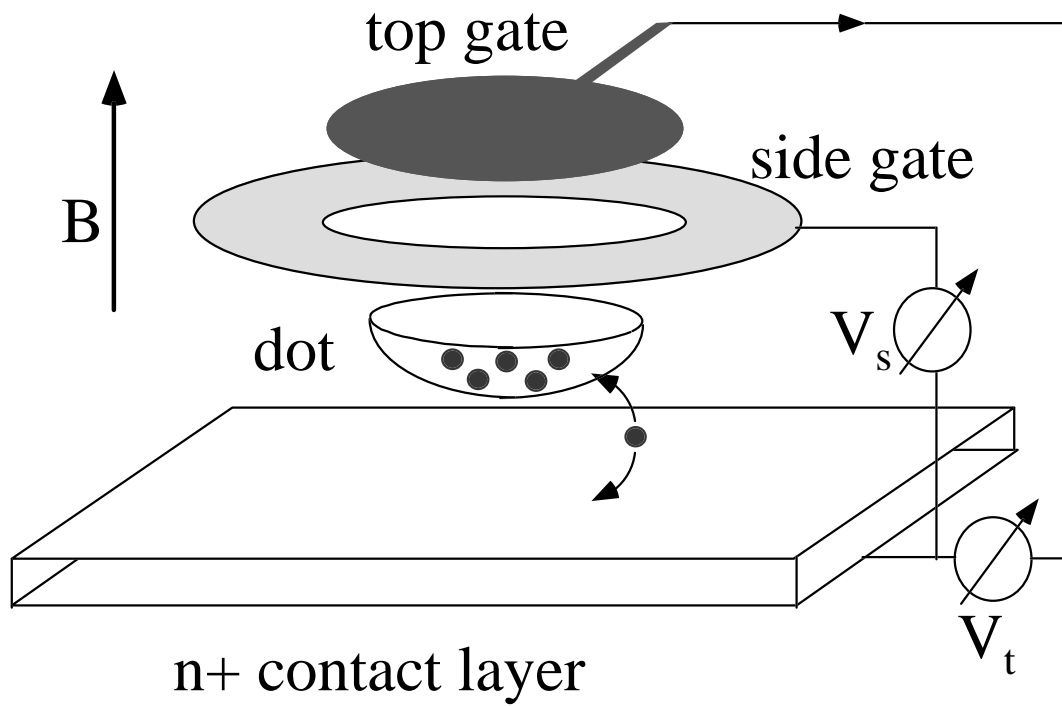


Figure 4-1: Schematic of quantum dot structure with side gate and scheme for application of bias voltages.

exhibit the paired electron addition.

4.2 Probing Localization: Experimental Results

4.2.1 Localization in Zero Field

We study the electron addition spectrum at zero magnetic field for a dot of 500 nm lithographic diameter. We choose to study a dot of this size because it shows the periodic bunching for densities below $n_0 = 1 \times 10^{11} \text{cm}^{-2}$ (see Chapter 3).

Capacitance traces (measured versus scanned V_t) taken for different values of the side gate bias V_s are plotted together on the grayscale panel in Figure 4-2A. Each dark trace represents a capacitance peak resulting from a single electron addition. The evolution of the addition energies with V_s can be easily perceived this way. The slope of a peak as a function of V_s effectively measures the probability for an electron in the respective electronic state to reside at the periphery of the dot.

At small electron numbers (bottom of Figure 4-2A, the slope is small and varies strongly from peak to peak. Note that the spacing in V_t also fluctuates strongly. In our dots, the single-particle quantum level spacing is about 1/10th the charging energy. Hence, the energy of spatial quantization cannot be the origin of the strong fluctuations in the addition spectrum. The large fluctuations in peak spacing and slope indicate that electrons are localized and interact weakly with each other. On average, the slopes of traces increase with electron number and the spacing between traces decreases.

As more electrons are added to the dot, the electron droplet expands laterally. This increases the capacitance of the puddle to the top gate and results in a decrease in the spacing as a function of V_t . The average lateral expansion also explains the increase in the coupling to the side gate and, respectively, the increase of the slope. Above a critical density $n_0 = 1 \times 10^{11} \text{cm}^{-2}$ (about 100 electrons in this dot) corresponding to the very top of the panel in Figure 4-2A, the slopes of all the electronic states become equal within the experimental resolution. Note that for a perfectly metallic

droplet where all electronic states are similarly spread over the area of the dot, one expects equal slopes for all traces with V_s and precisely periodic electron additions as a function of V_t (Coulomb Blockade). We conclude that above the critical density, electrons in our dot are completely delocalized.

We now center our discussion on the intermediate range of electron density just before the delocalization transition. For the gate biases V_t in the middle of Figure 4-2A, the traces can be separated into two distinct groups with respect to their dependence on V_s . The presence of traces with very large slopes is the most noticeable feature. The large capacitance to the side gate means that these states are mainly localized at the edge of the electron puddle. Traces with small slopes originate from electron additions to states with high probability density located near the dot center. We label them as interior states. The distinctness of these two groups establishes that the dot does indeed break-up into an isolated core and periphery regions: near the delocalization transition, the last remaining localized states exist at the perimeter of the dot.

While addition traces associated with the interior states are well separated in the top gate bias V_t by Coulomb blockade, a localized “peripheral” trace can appear very close to an “internal” trace. Closer examination of Figure 4-2C reveals direct crossing between two families of traces. As one still expects Coulomb repulsion between electrons in the two regions, the existence of levels that cross directly (rather than anticross) is a surprise. This behavior corresponds to the pairing behavior described in Chapter 3. At the direct crossings, two electrons enter the dot at the same top gate voltage. The absence of Coulomb repulsion leading to the pairing effect is still a mystery, but we now understand that the paired electrons enter isolated positions within the dot.

Consider the last five localized states seen before the complete delocalization on Figure 4-2B. They, themselves, appear with nearly perfect *periodicity* in the top bias V_t . This means that for densities near the delocalization transition, four electrons enter the delocalized center of the dot in succession and the fifth enters the localized circumference. This observation is reproducible upon different thermal cycling and is

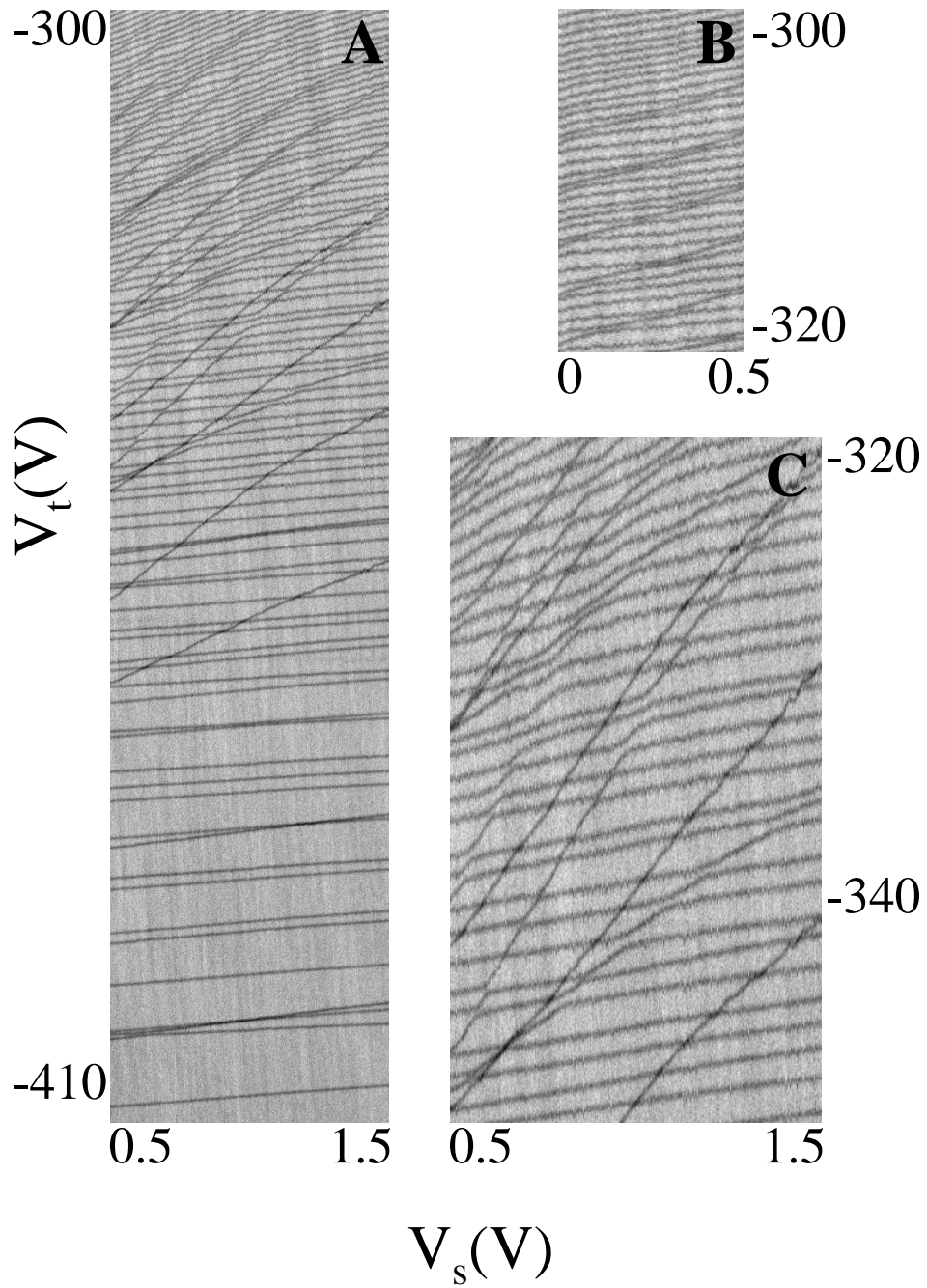


Figure 4-2: (A) Greyscale panel of measured capacitance with dark lines denoting capacitance peaks. Each peak corresponds to an electron addition to the dot. Top-gate voltage scale can be converted to the addition energy scale by multiplying by 0.5 (lever-arm). Temperature, 50 mK. (B)(C) Two zoom in to spectrum (A) (see text)

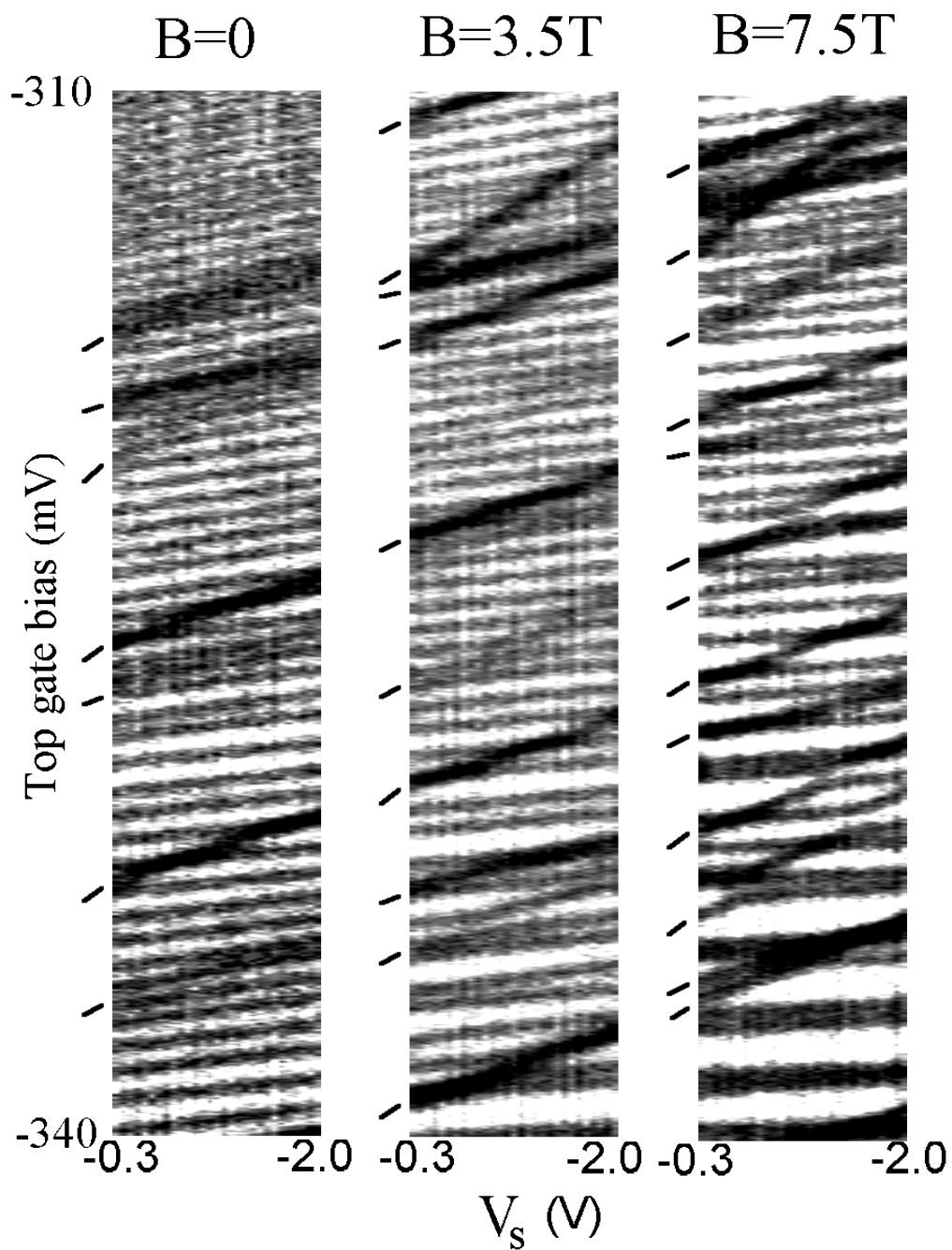


Figure 4-3: Grayscale panels demonstrating the effect of magnetic field on the addition spectra. The temperature, 300 mK. At zero field most traces have only small slopes, indicating that most electrons are either delocalized throughout the dot or localized in the interior of the dot. As magnetic field increases more states (dashes) appear with a steeper slope and are therefore confined to the dot periphery. Magnetic field thus appears to enhance localization of electrons into interior or periphery regions.

consistent with the observation of the periodic bunching pattern under precisely the same conditions in dots of similar sizes. In summary, Figure 4-2 allows us to conclude that one of the electrons in the previously observed bunches is localized at the edge.

4.2.2 Effects of High Magnetic Fields

Application of a magnetic field perpendicular to the plane of the quantum dot strongly affects the addition spectrum. Addition spectra at 300 mK from this region in another quantum dot were taken at several values of applied magnetic field (Figure 4-3). The general behavior of the addition spectrum as the dot evolves from localized to metallic-like with increasing density appears qualitatively unchanged from the dot of Figure 4-2. The traces arising from the remaining states localized at the dot edge are indicated by tic marks in Figure 4-3.

The magnetic field breaks the regular metallic-like pattern of the addition spectrum and tends to localize electronic states at either the center or the periphery of the dot. This is clearly evidenced by the emergence of additional traces with large slope as the field strength is increased. Other traces display a diminished slope at increased fields, indicating that they arise from electronic states that have become localized near the center of the dot. The magnetic field effectively shifts the localization-delocalization transition towards higher electron densities within the dot.

Again we would like to point out the similarity between localization and the bunching phenomena. Chapter 3 demonstrated that application of a high perpendicular magnetic field increases the critical density below which the periodic bunching is observed. Even though for high electron densities the pairing eventually ceases, high magnetic fields restore the pairing effect thus creating a sharp boundary between periodic and “paired” part of the spectra. While it is difficult to quantitatively investigate the effect of the magnetic field using our side gated samples (we have three parameters to vary: V_t , V_s and B), we have designed another experiment that permits thorough studies of the boundary [34, 40]. We will describe this experiment in Chapter 5.

Finally, note that the traces at high fields are not always well separated as a

function of V_t , as the Coulomb repulsion between electrons would ordinarily suggest. In fact, many traces appear “clumped”, similarly to the bunching of levels observed in our previous experiments [32] (see Chapter 3).

4.2.3 Interaction Between Localized and Delocalized States

Figures 4-2 and 4-3 establish our ability to detect localization within the dot. We now focus on the interaction between electronic states localized at the edge and the center of the dot. Closer examination of Figure 4-2C reveals that upon increasing V_t , traces from states localized at the periphery traverse traces from states localized at the dot center. The splitting observed at these avoided crossings (anticrossings) is a measure of the interaction between respective states. The anticrossing opens because the presence of an electron in the lower state causes the addition energy of the crossing state to move up due to hybridization and the Coulomb repulsion between hybridized states. Very detailed calculations of the magnitude of the splitting, albeit for a slightly different geometry can be found in references [70, 71, 72, 73].

The lowest of the edge localized (steep slope) states shown in Figure 4-2C hardly appear to interact with interior electron states at all. More interesting are the edge states that display noticeable interaction with other crossing states.

A typical trace from a periphery state displays anticrossings with all of the traces that it traverses. The strength of the interactions fluctuates strongly over the range, with the splitting values varying by a factor of five. Other localized states display similar strong fluctuations of the splitting values. On average, the splittings are smaller than the peak spacing in the range shown. At higher electron number, the splittings grow to become comparable with the Coulomb blockade peak spacing, indicating an increased interaction between crossing states. Surprisingly, some very unusual anticrossing patterns can be seen here.

We zoom into the part of the addition spectrum immediately preceding the complete disappearance of patterns of anticrossings associated with localized states (Figure 4-4C). To facilitate visualization, the image is skewed to compensate for the slope of the internal states. Close examination of Figure 4-4C reveal a surprising feature:

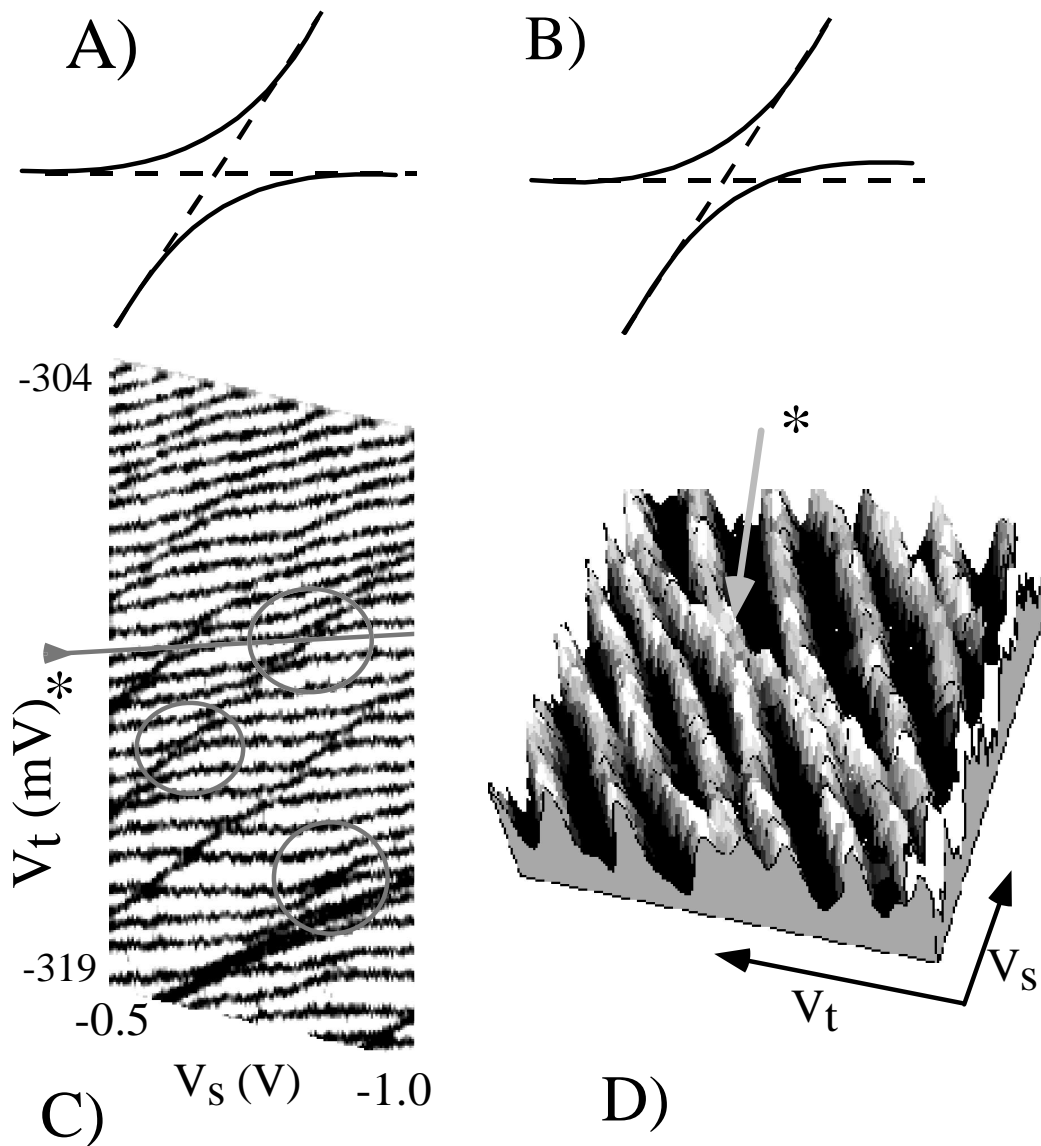


Figure 4-4: (A) Sketch of the expected form for an anticrossing considering quantum mechanical and Coulomb interactions between electrons in different states. The chemical potential of (N+1) electron state (left) is higher than or equal to the chemical potential of N electron state (right). (B) Sketch of an experimentally observed anomalous anticrossing; the chemical potential of (N+1) electron state is lower than the chemical potential of N electron state. In this case, the removal of a periphery electron on the right hand side of the diagram raises the chemical potential of remaining N electrons facilitating the removal of another electron in the interior. (C) Top part of the addition spectrum from figure 4-2A skewed to level the traces of internal electrons. Some of the anomalous anticrossings are denoted by circles. (D) Surface map zooming-in to the anomalous anticrossing marked by an asterisk. The energy levels clearly demonstrate the tendency of states to "stick" together at the anticrossing.

anticrossings fall in two categories schematically depicted in diagrams A and B. While diagram A represents the expected behavior of two crossing quantum states, diagram B is highly unusual.

Intriguingly, at some of the anticrossings, the addition energy for the N -electron state after the anticrossing is higher than the addition energy for the $(N+1)$ -electron state before the anticrossing (diagram in Figure 4-4B). This looks as though the removal of the edge electron (sloped line) from the system actually raises the chemical potential, and correspondingly increases the addition energy for an internal electron (horizontal line). We note that all the anticrossings at lower density seen on Figure 4-2 follow a more typical pattern of Figure 4-4A.

4.3 Localization Results from Electron Correlations

The pattern of the interaction at lower density is generally consistent with the assumption that the localization of the periphery states is caused by strong fluctuations of the background potential. As more electrons are added to the dot, the interior puddle expands laterally and approaches a localized state at the periphery. This expansion appears to increase the interaction between the crossing states. Further, one might expect that the interaction strength should be sensitive to the particular electron wavefunctions of the localized and delocalized states. These may vary strongly, possibly accounting for the large fluctuation in the observed interactions. Examining a typical edge state (Figure 4-2C), we see that the values of the anticrossing fluctuate strongly.

At higher electron density there are, however, a few features in the addition spectrum that appear inconsistent with the irregular single-particle localization by fluctuating potential. First, the last six localized states seen before complete delocalization (Figure 4-2B) appear with nearly perfect periodicity in electron number. This observation is reproducible upon different thermal cyclings and was observed on many different quantum dots [32]. Second, the localized edge states disappear above a critical density that is *identical* for all of our quantum dots. Both observations indi-

cate that the segregation results from electron correlations in a low-density electron droplet. In Chapter 3 we conjectured this hypothesis after having observed the periodic bunching in the addition spectra of quantum dots [32]. The present experiment visualizes directly the localized states confined to the perimeter of the dot.

A surprising observation is the unusual interaction between the edge localized and the bulk states. For electron densities just below complete delocalization the values of the splitting at the anticrossings between the states at the dot's perimeter and the core states become comparable with the spacings in V_t for electrons entering the core. Therefore, the interaction cannot be considered as a weak perturbation for the initial crossing states. Existence of the anticrossing pattern presented on Figure 4-4D makes it evident that the removal of the edge electron from the system actually raises the chemical potential and increases the energy to add an electron to the system. This behavior suggests that there exists a mechanism for attraction between electrons in the crossing states overcoming the usual Coulomb repulsion. Indeed, the clear tendency for electron peaks to move closer to each other over an extended interval of V_s is seen, implying a possible energetic benefit of the paired configuration.

4.4 Possible Physical Mechanisms for Localization

The exact physical mechanism for segregation into an interior puddle and periphery localized states has yet to be determined. We observe segregation only at densities below a critical density of $n_0 = 1 \times 10^{11} \text{cm}^{-2}$. The conventional density dependent parameter that describes the interaction strength is

$$r_s = \frac{1}{a_B \sqrt{\pi n_s}}, \quad (4.1)$$

where a_B is the Bohr radius (about 100 \AA in GaAs) and n_s is the sheet electron density. The critical density n_0 corresponds to $r_s \approx 1.8$.

Strong electron correlation has been shown to induce liquid-to-solid transition in diluted electron systems. According to Wigner [74], the potential energy gained due

to the formation of solid, of the order of $1/r_s$, outweighs the kinetic energy lost, of the order of $1/r_s^2$, for sufficiently low density (larger r_s). Monte Carlo [75] and analytic calculation [76] of the pure system suggest that the solid-fluid transition occurs near $r_s \approx 37$. However, impurities that are present in the system can facilitate formation of a Wigner crystal, therefore shifting the transition to lower r_s . While there is no consensus on the exact value of critical r_s for disordered systems, the published figures of $r_s \approx 7.5$ [77, 78] and $r_s \approx 4$ [79, 80] are greater than $r_s \approx 1.8$ in our system. Also the values of $r_s \approx 6 - 8$ and $r_s \approx 10$ for the recently observed metal-insulator transition for two-dimensional electrons in Si [3, 4] and holes in GaAs [5, 6] are well above the critical r_s in our samples.

However, our critical r_s corresponds to the density range where Eisenstein experimentally observed negative compressibility in a two-dimensional electronic system [81]. The physical essence of negative compressibility is an over-screening of a probe electron by the correlated electron liquid. As a result, the chemical potential of the entire system decreases with the addition of an extra electron. Recently, Levitov [67] demonstrated that negative compressibility give rise to a significant spatial oscillation of the density at the edge of an electron droplet. Whether such oscillations can result in edge states localization remains unclear.

We have already mentioned in section 3.4 a recent theoretical work by Canali [66] that supports our experimental finding. This work carries out a full quantum mechanical calculation of the addition spectra of dots containing a small number of particles in the limit of strong disorder and for a short range Coulomb repulsion. The theory shows that strongly the correlated regime in a dot is characterized by formation of two puddles of electrons. In this regime, two successive electron additions almost coincide. Although these calculations are the most realistic of the proposed models for our dots, it deals only with a very small number of electrons in a rectangular dot (3×4 sites). It is not yet clear how to generalize these results to more realistic geometries.

4.5 Summary

In this Chapter, we described a new method to study localization in small low-density electron puddles placed in a disorder potential. With our capacitive technique, we precisely measured the addition spectra of quantum dots. To probe the spatial extent of electron wavefunctions within our dots, we studied dependence on the addition energies on changes in confinement potential. While electronic states localized near the edge are the most sensitive to changes in the dot's confinement, states residing near the center of the dots are almost not perturbed at all. Thus, we were able to differentiate between electronic states occupying spatially distinct regions within the dots.

We found that for low electron densities, electrons occupy distinct spatial sites localized within the dot. At higher densities, the electrons become delocalized, and all wavefunctions are spread over the full dot area. The transition between two regimes occurs around the critical density $n_0 = 1 \times 10^{11} \text{cm}^{-2}$, which is *identical* for all of our quantum dots. For densities just below complete delocalization, the last remaining localized states exist at the perimeter of the dot. Unexpectedly, these electrons appear to bind with electrons in the dot center. We realized that some features in the addition spectrum appear inconsistent with the irregular single-particle localization by fluctuating potential. This led us to conclude that the spatial separation observed in our dots results from electron correlations in a low-density electron droplet.

While we did not investigate the effect of the magnetic field on the electron localization in great detail, another experiment we produced addresses this issue. Chapter 5 presents the results of this new study.

Chapter 5

Localization in Artificial Disorder: Two Coupled Quantum Dots

Chapter 4 demonstrated that our quantum dots provide a convenient system for studying electron localization on a microscopic scale. Unlike the traditional transport spectroscopic tools for studying lateral quantum dots [11] that sense primarily delocalized electronic states, our method of Single Electron Capacitance Spectroscopy (SECS) [29] has demonstrated the capability of probing both *localized* and delocalized states of electrons. Furthermore, this method allows us to study two-dimensional dots of various sizes and over a broad range of electron densities, a critically important parameter that changes the effective strength of electron interactions.

In quantum dot experiments in high-density dots, the Coulomb repulsion between electrons largely sets the amount of energy required to add an additional electron to the dot. This energy increases by a fixed amount with each electron added. An external gate, capacitively coupled to the dot, can then be used to change the electron number, and electron additions occur periodically in the gate voltage with a period e/C_g , where C_g is the capacitance between the gate and the dot [14, 13].

In contrast, our prior SECS measurements presented, in Chapter 3, have shown that the *low-density* regime appears entirely different. The addition spectrum of a dot larger than $0.4\mu\text{m}$ in diameter and below a critical electron density ($n_0 = 1 \times 10^{11} \text{cm}^{-2}$ in all of our samples) is highly nonperiodic. It contains pairs and bunches: two or

more successive electrons can enter the dot with nearly the same energy [29, 32]. The paired electrons thus show almost no sign of repelling each other. Application of a high perpendicular magnetic field increases n_0 linearly, creating a sharp *boundary* between periodic and “paired” parts of the addition spectrum [32]. We hypothesized that, for densities below this boundary, disorder and electron-electron interactions within the low-density droplet split it into two or more spatially separate droplets, and pairing arises once this localization occurs.

We have produced two experiments [33, 34] to study this localization-delocalization transition in a controlled fashion. One, described in Chapter 4, recently established the existence of electronic states localized at the dot’s periphery and arising at densities just below the critical density n_0 [33]. In this Chapter we report the results of a new approach [34] for studying localization in quantum dots.

We intentionally create a dot with an artificial “disorder” potential: a potential profile containing two smooth minima separated by a barrier, as in the double dot system described in section 2.2.4. Through analysis of addition spectra in magnetic field, we distinguish between electrons localized in either of the two potential wells or delocalized over the entire dot. Our studies conclusively demonstrate that under precisely the same conditions for observation of the paired electron additions, a low-density electron droplet inside the dot indeed splits up into smaller fragments. This abrupt disintegration creates a sharp *boundary* between periodic and “paired” parts of the addition spectra, with paired electrons entering into spatially distinct regions within a dot. We also measure the remnant residual interaction between the fragments. Surprisingly, it displays a nearly complete independence from the strength of the applied field for fields larger than required for the localization transition. While no theory exists explaining the observed transition or the pairing phenomenon, recent numerical simulations display results similar to some of our data [66].

5.1 How to Model a Disorder Potential

The fabrication procedure for the samples used in this experiment is outlined in section 2.2.4. A schematic of the experimental setup is shown on Figure 5-1. The dot is arranged between two plates of a tunnel capacitor, which is formed by the $n+$ contact layer and the top gate. Electrons may tunnel back and forth between the dot and the capacitor bottom plate ($n+$ layer) as indicated in Figure 5-1. To create a barrier within a dot, we pattern a top gate in the shape of a dumbbell.

This shape of the gate produces two small vertical dots laterally separated by a small distance (Figure 5-1). The top gate controls the electron density of the entire system. This geometry results in a double potential well with two valleys separated by a saddle. By changing the top gate bias V_g , we gradually fill the double dot system with electrons. At first electrons accumulate in two independent electron puddles, one localized in each dot. The puddles grow laterally with increasing electron number and eventually couple to each other. The coupling mixes states of one dot with those of the other, and electrons start traversing the saddle point. When the two puddles finally merge into a single large dot, the electron wave functions spread over the entire area of the resulting large dot.

By varying lithographic dimensions, we control the height of the saddle and therefore the individual dot electron density at which merging occurs. We examine a number of samples to investigate a broad range of such densities: from two dots, each containing a few localized electrons, up to densities $n = 2.5 - 3.5 \times 10^{11} \text{cm}^{-2}$ in each dot. Remarkably, as we will show below, the magnetic field strongly affects the merging *only* of low-density ($n \approx 1 - 2 \times 10^{11} \text{cm}^{-2}$) electron puddles.

The measurements are carried out using the on-chip bridge circuit described in Chapter 2. To register electron additions, we monitor the ac capacitive response to a small ($< 80 \mu\text{V}$) ac excitation applied between the top gate and the contact layer, while sweeping the dc top gate bias V_g . At V_g values corresponding to the electron additions, an electron oscillates between the dot and the contact increasing the measured ac capacitance [29, 30]. Since one top gate covers both individual

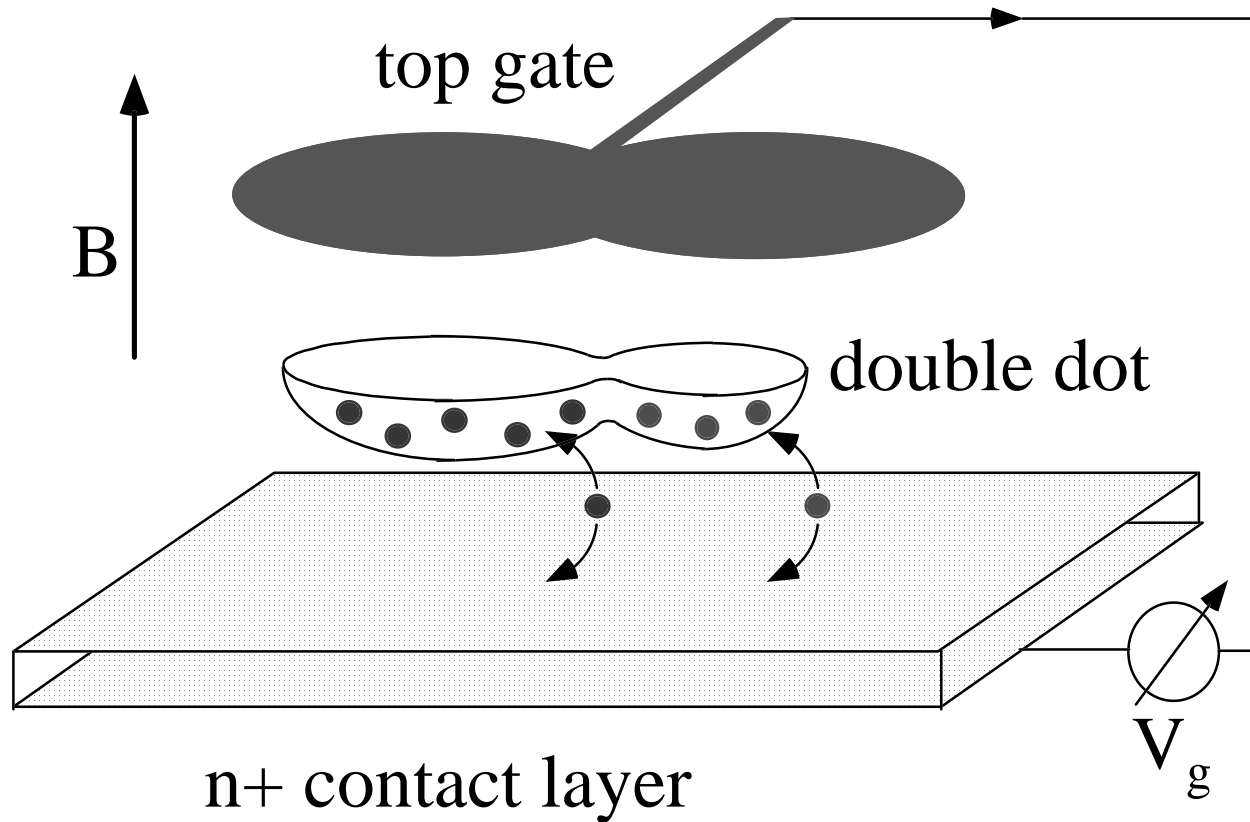


Figure 5-1: Schematic of our double dot samples. The dots potential profile contains two minima separated by a barrier. A single top gate controls the electron densities of the entire double dot system.

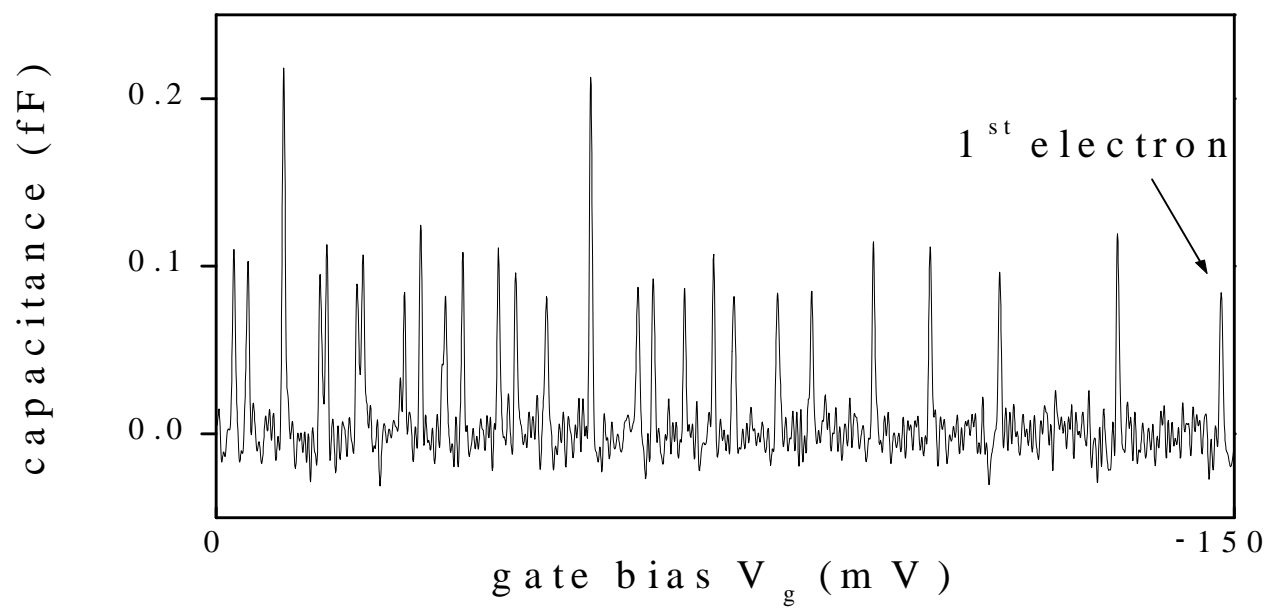


Figure 5-2: Experimentally measured capacitance trace as a function of the top gate bias. Each peak corresponds to an electron addition to the double dot system. Two peaks of double height actually occur because of simultaneous but independent additions to each dot.

dots, an electron addition to either of the dots results in a peak in our capacitance measurements. The resulting capacitance trace is shown on Figure 5-2. Each peak corresponds to the addition of one electron to the quantum dot. Two peaks of double height actually occur because of simultaneous but independent additions to each dot [34].

To distinguish electrons added to one dot from those added to the other, we follow the evolution of the addition spectrum with the perpendicular magnetic field. The general behavior of the electron addition spectrum for a single dot in a magnetic field is well known both for the case of few-electron droplets [31, 12, 28] and for many-electron dots in the Quantum Hall regime [54, 82, 83]. Addition energies oscillate with the field as electrons shift between different angular momentum states. The exact pattern of those oscillations depends sensitively on the details of the confinement potential, and serves as a “signature” of a particular dot. Although in our samples the two dots are made to be nominally identical, the particular shapes of the confinement potential of the two dots are slightly different due to disorder and imperfections in the lithography process. Addition energies for the two dots thus depend differently on the perpendicularly applied magnetic field, permitting us to associate each electron addition with a particular dot.

Also, the analysis of the addition spectrum in the magnetic field allows us to characterize the confinement potential of the system. In particular, we confirm that the confinement potential consists of just *two* minima, as it was designed.

5.2 Addition spectrum of a small symmetric dot

Prior to presenting the real data from our complex double dot system, we describe the addition spectra of each of its two components: individual small dots. In small dots containing just a few electrons, both electron-electron interactions and quantum confinement effects are comparable to the charging energy. Therefore, the spacings between the Coulomb oscillation peaks become irregular [12, 13]. It turns out that the addition spectra for a small dot in a perpendicular magnetic field can be well

described within the constant interaction model for single particle states based on the Darwin-Fock spectrum. The constant interaction model was first offered [53, 54] to connect the addition spectra of quantum dots and well-known single particle spectra for simple confining geometries. Here we present this simplest model for addition spectra of a small symmetric dot, highlight the underlying physical principles, and compare it to our data.

5.2.1 Constant Interaction Model for Single Particle States

The Coulomb blockade peak position in the gate bias V_g , when converted to the dot's energy scale, reflects the electrochemical potential of the dot:

$$\mu_{dot}(N) = U(N) - U(N - 1), \quad (5.1)$$

where $U(N)$ is the total ground state energy for N electrons on the dot. This is, by definition, the minimum energy for adding the N th electron to the dot. Calculations of $U(N)$ and, therefore, $\mu_{dot}(N)$ for several electrons are difficult, especially in a potential that is not exactly known.

However, a reasonable estimate for $U(N)$ can be obtained with the help of two simplifying assumptions. First, we assume that the quantum levels can be calculated independently of the number of electrons on the dot. Second, we parametrize the Coulomb repulsion among electrons in the dot, and between electrons in the dot and those in the nearby environment by a capacitance C . We further assume that C is independent of the number of electrons on the dot. In other words, we think that electrons simply fill single particle states additionally separated by a *constant* charging energy $\Delta E_c = e^2/C$. Then, the addition energy - the separation between the two nearest Coulomb blockade peaks - is given by the following expression:

$$\mu_{dot}(N + 1) - \mu_{dot}(N) = (E_{N+1} - E_N) + e^2/C, \quad (5.2)$$

where E_{N+1} and E_N are sequential single particle states.

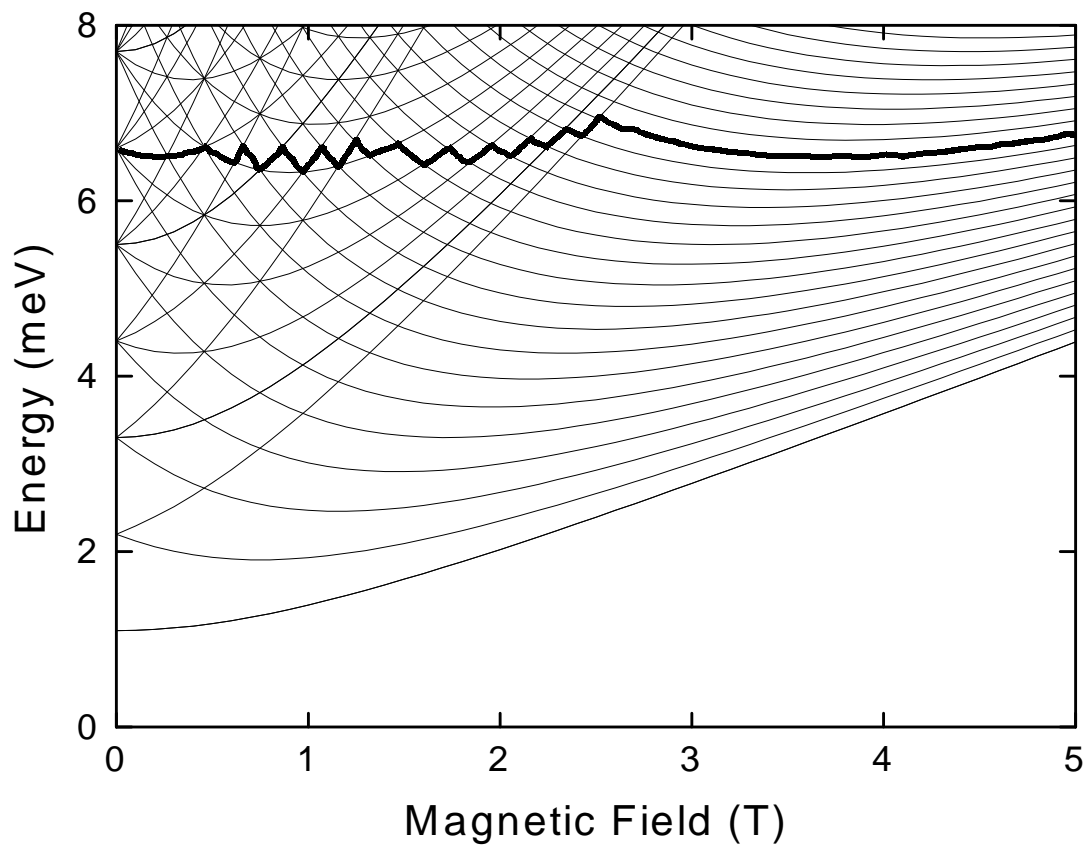


Figure 5-3: The eigenstates E_{nl} of the Schroedinger equation for a two dimensional parabolic potential in the presence of a perpendicular magnetic field, known as Darwin-Fock states (see Equation 5.4). Thick line marks the 35th state.

Single particle states are calculated easily only for a bare confinement potential of the simplest symmetric shapes. In real systems, electrons present in the dot modify the bare confinement potential significantly due to screening. The resulting potential has a flattened bottom in the regions of nonzero electron densities [55]. For this case, more rigorous selfconsistent calculations are required to determine the single particle states [82, 38]. However, for low electron occupancy, these states can still be justifiably derived just from the potential of an empty dot.

5.2.2 Single Particle States in Magnetic Field: Darwin-Fock spectrum

For a circularly symmetric two dimensional confinement potential the quantum numbers for the single particle states are conveniently described by the radial quantum number $n = 0, 1, 2, \dots$ and the angular momentum quantum number $l = 0, \pm 1, \pm 2, \dots$. For a harmonic confinement potential $V(r) = 1/2m\omega_0 r^2$, the noninteracting Schroedinger equation has the following analytic solution for the eigenenergies E_{nl} :

$$E_{nl} = (2n + |l| + 1)\hbar\omega_0 \quad (5.3)$$

It follows from equation 5.3 that the E_{nl} form degenerate sets of states, which are separated by $\hbar\omega_0$ from each other.

The Schroedinger equation for a two dimensional parabolic potential in the presence of a perpendicular magnetic field was first solved in 1928. The eigenenergies are known as Darwin-Fock states [84, 85]:

$$E_{nl} = (2n + |l| + 1)\hbar\sqrt{\frac{1}{4}\omega_c^2 + \omega_0^2} - \frac{1}{2}l\hbar\omega_c, \quad (5.4)$$

where $\hbar\omega_c = \hbar eB/m_*c$ is the cyclotron energy. Figure 5-3 shows the evolution of E_{nl} with the magnetic field calculated for $\hbar\omega_0 = 1.1meV$. Spin is neglected so each state is twofold degenerate. The degeneracies at $B = 0$ are lifted in the presence of a magnetic field. Single particles energies with positive or negative angular momentum

l shift to lower or higher energy, respectively.

Consider a dot which contains N electrons occupying the first N states. An $(N+1)$ th electron entering the dot always chooses the lowest available state. For a different field range, a different eigenstate becomes the lowest available E_{N+1} . As an example, the evolution of 35th state is illustrated in Figure 5-3 (thick line). According to equation 5.2, the resulting addition energies *oscillate* with the field as electrons shift between different angular momentum states.

Comparison of the very details of these oscillation to Darwin-Fock spectrum allows us to characterize the confinement potential of the dot. But before we turn to the data, we would like to describe the consequences of the spin degeneracy of the Darwin-Fock states.

5.2.3 Even-Odd Asymmetry in Coulomb Blockade Spectra

The possible spin degeneracy of single particle states gives rise to several important consequences that go under the name of “even-odd asymmetry” in Coulomb blockade oscillations. When each single particle state accommodates two electrons with opposite spins, the energies for adding the N th even and the $(N+1)$ th odd electron are different:

$$\mu_{dot}(N) - \mu_{dot}(N - 1) = e^2/C \quad \text{for adding even } N \quad (5.5)$$

$$\mu_{dot}(N + 1) - \mu_{dot}(N) = (E_{(N/2)+1} - E_{N/2}) + e^2/C \quad \text{for adding odd } (N + 1) \quad (5.6)$$

An even N th electron is added to the same quantum state $E_{N/2}$ as the previous odd electron occupies. According to our model, only the Coulomb repulsion contributes to the addition energy. On other hand, the lowest available state for the next (again odd numbered) $(N+1)$ th electron is $E_{(N/2)+1}$, which lies higher in energy. Thus, the addition energy for the odd electrons are greater by: $\Delta\epsilon = E_{(N/2)+1} - E_{N/2}$.

The above considerations remain valid as long as the single particle spacing $\Delta\epsilon$ is comparable to, or larger than the electron interaction energy $E_c = e^2/C$. Also,

variation in dot capacitance C with electron number and the resulting changes in the charging energy $E_c = e^2/C$ should be smaller than $\Delta\epsilon$. In general, the relation $\Delta\epsilon \geq E_c$ holds better for smaller dots: the Coulomb energy $E_c = e^2/C$ scales inversely with the dot's size, while the quantum level spacing $\Delta\epsilon$ scales inversely with the square of the dot's size. The magnitude of the changes in dot capacitance depend on the experimental geometry and varies from one experimental setup to another.

The first result of even-odd asymmetry is that two consecutive peaks are closely spaced if they correspond to the same spatial state, whereas a pair of peaks that correspond to different spatial states are spaced more widely. And indeed, even-odd asymmetry in the peak spacing has recently been reported [86, 87] in transport studies of very small lateral dots. Larger dots display no even-odd spacing correlation (or bimodal structure in the spacing distribution) neither at small [88, 89] nor at large values of magnetic field [54, 82]. The ultimate appearance of even-odd asymmetry in small dots is the recently observed Kondo effect: a formation of a Kondo singlet state from the electron localized in the dot and electrons in a reservoir. It occurs only when the number of electrons in the dot is odd, so that one spatial state is only singly occupied [15, 16].

The second, and more general result is that the dependence of the addition energy on some external parameter, such as the magnetic field, differs for even and odd electrons. This holds even if large changes in dot capacitance destroy the asymmetry in the peak spacings. The magnetic field does not significantly modify the average density distribution and, consequently, the Coulomb contribution to the addition energy $E_c = e^2/C$ [82, 38]. However, single particle states in two-dimensional dots are strongly affected by the presence of the perpendicularly applied field (see section 5.2.2) and therefore, $\Delta\epsilon = E_{(N/2)+1} - E_{N/2}$ changes considerably. This leads to the field dependent addition energy for odd electrons ($\Delta\epsilon + e^2/C$), while that for even electrons (e^2/C) does not depend on the applied field.

The following argument helps to visualize our point. Generally addition energies “wiggle” in the field. Section 5.2.2 connects these oscillation with shifts of the spatial electron wavefunction between different angular momentum states. Consecutive odd

and even Coulomb blockade peaks, which are originated from additions to the same spatial state, show similar behavior in the magnetic field: they oscillate in phase, maintaining the constant separation (or field independent addition energy). This behavior was predicted [90] and observed in small vertical dots studied by Tarucha's group [28, 50, 51]. The spectra of our smallest dots exhibit similar features as we will describe below.

Note that because of the small effective mass in GaAs, spin effects in a magnetic field, such as Zeeman splitting, are an order of magnitude smaller than changes in spatial energies. Thus we neglect spin effects in our model and assume each spatial state to be two-fold degenerate. This assumption is valid in the field range considered here.

5.2.4 Our Data from a Small Dot

To summarize, addition spectra for small dots in a perpendicular magnetic field can be well described within the constant interaction model for single particle states based on the Darwin-Fock spectrum. The model predicts two main features of the spectra: oscillatory behavior of addition energies in the field and odd-even pairs.

Figure 5-4 show an example of the magnetic field evolution of four consecutive peaks for one of our small dots. Electron additions are numbered in Figure 5-4. "Wiggles" originating from the crossing of different angular momentum states are clearly seen on the picture. While the separation between traces 5 and 6 is field independent, the spacing between traces 6 and 7 depends strongly on the magnetic field. It is evident that addition traces 5 and 6 oscillate as a pair. The next two: traces 7 and 8 are also paired. Each of these pairs corresponds to filling the one spatial state.

We observe the behavior shown on Figure 5-4 in *all* of our dots with lithographic diameter smaller than $350 \mu m$. The fact that a simple model derived for a *parabolic* potential describes our data extremely well signifies that the potential in our small dot is rather smooth. In other words, it is not affected by disorder and it consist of a *single* smooth minimum. As we described in Chapter 3, the spectrum changes dramatically

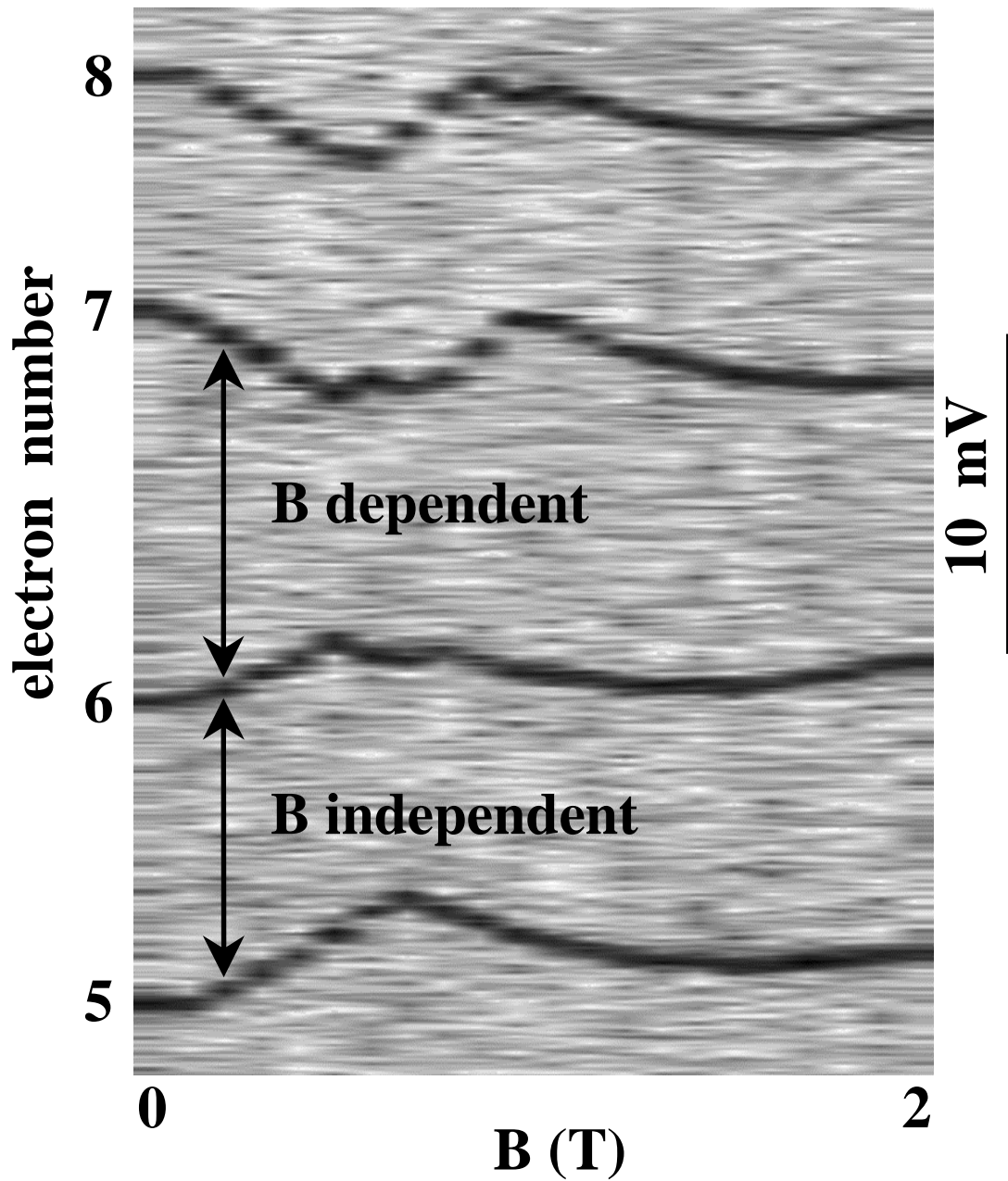


Figure 5-4: Magnetic field evolution of four consecutive peaks for one of our small dots. Electron additions are numbered. “Wiggles” originating from the crossing of different angular momentum states are clearly seen on the picture. While the separation between traces 5 and 6 is field independent, the spacing between traces 6 and 7 depends strongly on the magnetic field. Addition traces 5 and 6 (7 and 8) oscillate as a pair. Each of these pairs corresponds to filling the one spatial state.

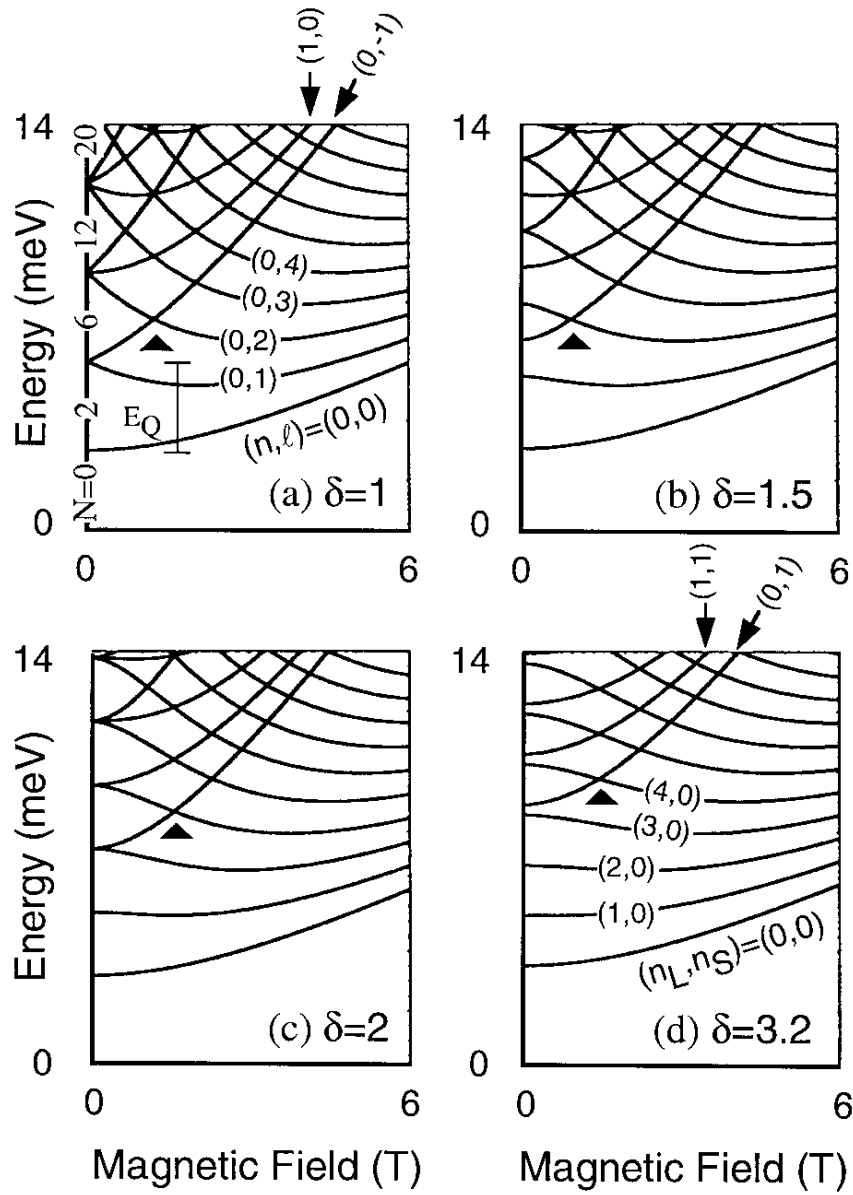


Figure 5-5: Magnetic field dependence of the first ten single-particle energy level for a circular dot with $\delta = 1$, (a), and for elliptical dots with $\delta = 1.5, 2, 3, 2$, (b) to (d). For a circular dot with $\delta = 1$ and the $\delta = 3.2$ ellipse, the quantum numbers (n, l) and (n_x, n_y) are given. The spectrum for a circular dot is in fact the Darwin-Fock spectrum. For elliptical dots the degeneracies of single particle states at zero field are removed, and the up-moving states are shifted towards higher energies. Figure is adopted from reference [50]

for larger dots [29, 32]. We believe that in our larger dots the confinement potential has a more complicated shape and may in fact consist of several local minima.

Careful examination of the spectra allows us to quantify the dot's confinement potential: we estimate its strength and ellipticity. Equation 5.4 for $n = 0$ and $l = 0$ gives us the energy of the first electronic state: $E_{00} = \hbar\sqrt{\frac{1}{4}\omega_c^2 + \omega_0^2}$, where $\hbar\omega_c = \hbar eB/m_*c$ is the cyclotron energy. For every dot we fit the first addition trace to this expression. We find that in our samples, $1.8 \text{ meV} < \hbar\omega_0 < 2.4 \text{ meV}$.

Addition spectra of elliptically deformed dots have been studied both theoretically [90] and experimentally [50]. Modifications in the spectra due to deformations are very subtle and the formalism introduced above can be applied to an elliptical dot as well. The sequence of the single particle spectra on Figure 5-5 adopted from reference [50] illustrates progressive changes in the single particle spectra as confinement potential $V(x, y) = 1/2m(\omega_x x^2 + \omega_y y^2)$ becomes more asymmetric. The asymmetry is characterized by the parameter $\delta = \omega_x/\omega_y$. For a circular dot with $\delta = 1$ and the $\delta = 3.2$ ellipse, the quantum numbers (n, l) and (n_x, n_y) are given. First, the degeneracies of single particle states at zero field are removed. Second, the up-moving states shift towards higher energies.

Consequently, while the first addition trace that shifts up with magnetic field for a circular dot corresponds to addition of the fifth electron, in the $\delta = 3.2$ ellipse only the 9th addition trace belongs to the up-moving traces. Using this approach, we found that our dots are in fact elliptical with a parameter $\delta = \omega_x/\omega_y$ that ranges $1 < \delta < 3$. The parameter ω_0 , with which we used to describe the confinement strength is the geometrical mean of ω_x and ω_y : $\omega_0^2 = \omega_x\omega_y$

5.2.5 Limitations of the Model

Finally we need to mention the limits to the applicability of the simple model. It works well for strong confinement and a small number of electrons in the dot, but for higher electron occupancies new features in the spectra develop, which can not be accounted for within the framework of the single particle picture presented above.

The general oscillatory behavior of the spectra for larger electron numbers is

consistent with the single particle model except for the notable absence of spin degeneracy in this high-density regime. This absence was first reported by McEuen *et al.* in [54, 82] and studied in detail (albeit in small fields) by Marcus' group [89]. The disappearance of the spin degeneracy with increasing density is an unanswered question in the quantum dot community and is a subject of ongoing investigation in our group.

Several modifications to the Darwin-Fock spectra due to direct Coulomb and exchange interactions were studied experimentally and modelled by Tarucha's group [51, 28, 50]. Ultimately, any description of the addition spectra of real dots must go beyond a system of noninteracting electrons confined by a two-dimensional harmonic oscillator.

5.2.6 Conclusions

In this section we have shown that we intuitively understand the basics of the addition spectra of our smallest dots. By employing a simple model, we can characterize the confinement potential. Now, we possess all the tools needed to study how electrons fill an artificial disorder potential: a potential profile of two small dots laterally separated by a small distance.

5.3 Double Dot System

5.3.1 Two Potential Minima: Two Electron Puddles

A capacitance trace from our double dot system is shown on Figure 2. Each peak corresponds to the addition of one electron to the quantum dot. Since one top gate covers both individual dots, an electron addition to either of the dots results in a peak in our capacitance measurements. In other words, two dots are connected in parallel. Two peaks of double height actually occur because of simultaneous but independent additions to each dot. To distinguish electrons added to one dot from those added to the other, we follow the evolution of the addition spectrum with the perpendicular

magnetic field.

Figure 5-6 shows the capacitance traces taken at different values of the magnetic field and plotted together as a grayscale panel. Black denotes high capacitance. Each successive trace corresponds to the energy for adding an electron to the double dot system. The first addition trace (marked by a star) exhibits behavior typical of the lowest electronic state in the parabolic potential $E_{00} = \hbar\sqrt{\frac{1}{4}\omega_c^2 + \omega_0^2}$. The five traces that follow the first one develop into an easily recognized Darwin-Fock family. The seventh addition to the dot (marked by a star), however, does not fit into the sequence. In fact, it looks similar to the very first addition trace. We interpret this trace as the first electron addition to the second dot. Careful examination of the spectra reveals many traces (all of them are marked by full circles on the Figure 5-6) that do not belong to the first Darwin-Fock family. But they themselves form another Darwin-Fock set. Thus, the entire spectrum shown appear as a superposition of two sets of traces. Each set looks like the typical spectrum of a single small dot (see section 5.2). Because such separation of the spectrum is possible, we conclude that our system consists of just *two* smooth potential wells, each accomodating *one* electron droplet.

Incidental alignment of the ground states of the two droplets for some particular values of the gate bias and the magnetic field may cause simultaneous but independent electron additions to each individual dot. Indeed, multiple level crossings (some marked by empty triangles on Figure 5-6) can be seen on the plot. At each crossing point, the peak in the capacitance signal has double height, indicating an independent addition of two electrons to the two-dot system. The exact coincidence of the peaks suggests that capacitive coupling between two droplets is negligible.

The two observed Darwin-Fock patterns are similar, but not identical. This happens because the exact pattern of these oscillations depends sensitively on the details of the confinement potential. The particular shapes of the confinement potential of the two dots are slightly different due to disorder and imperfections in the lithography process. This leads to slightly different oscillation pattern in the spectra and allows us to associate each electron addition with a particular dot.

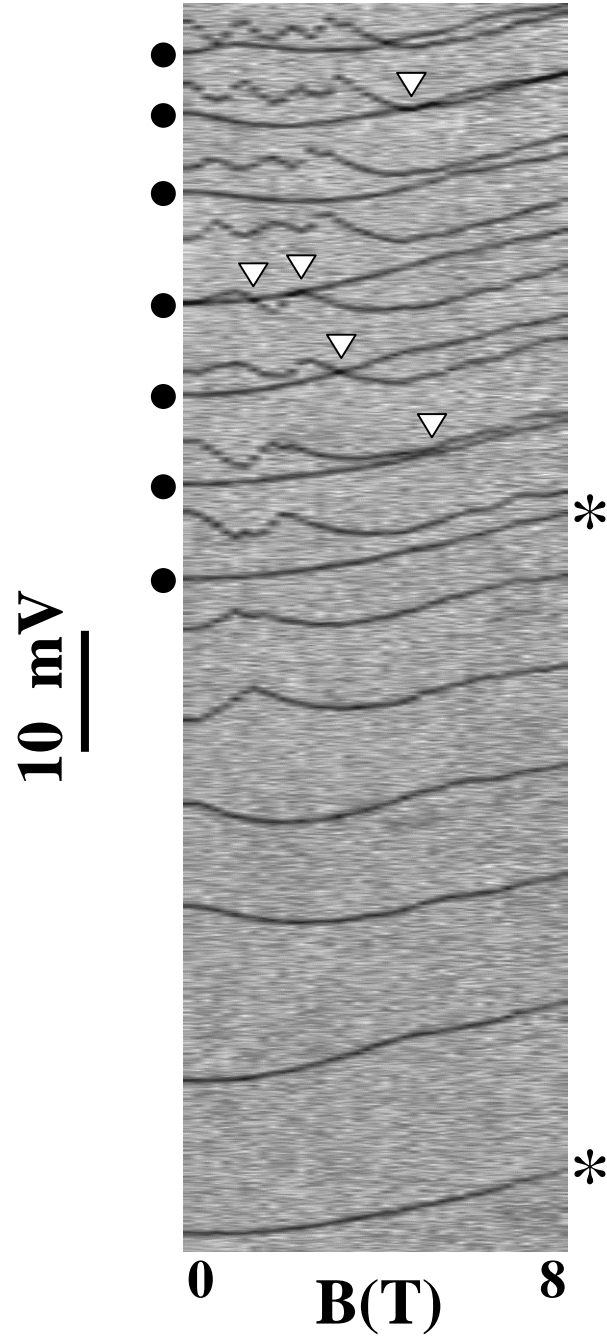


Figure 5-6: Figure shows the capacitance traces taken at different values of the magnetic field and plotted together as a grayscale panel. Black denotes high capacitance. Each successive trace corresponds to the energy for adding an electron to the double dot system. The entire spectrum shown appear as a superposition of two Darwin-Fock families of traces (traces belonging to one of the two are marked by full circles. Level crossings are marked by empty triangles. Stars denote first electron addition to each of the two dots.

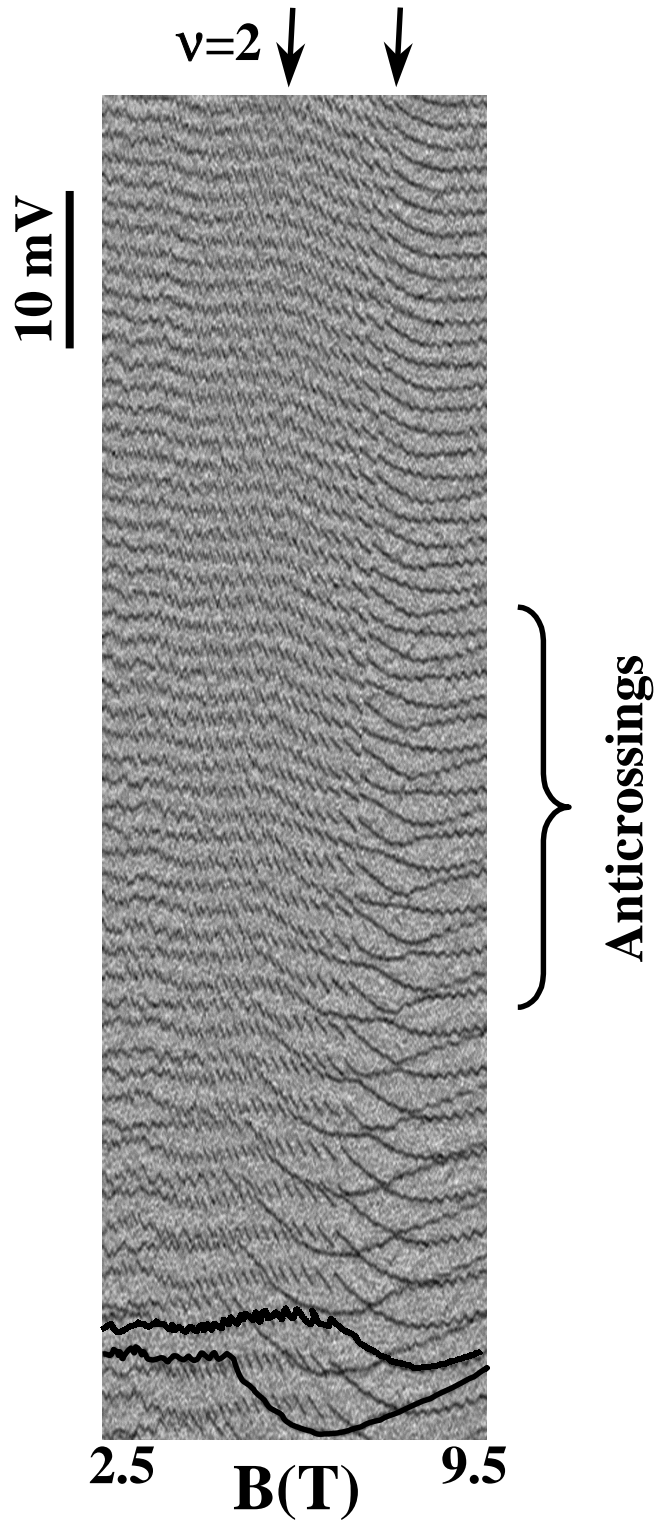


Figure 5-7: The range of the addition spectrum, in which the initially separate dots display the interaction is shown on the grayscale panel. At the bottom of the panel the addition traces can again be separated into two sets. One trace of each of the two families is highlighted on the figure. On top of the panel there is only single ladder of the periodic traces. Two arrows indicate on positions of the $\nu = 2$ maxima for the two dots.

5.3.2 High-Density Electron Puddles Merge

By changing the top gate bias V_g , we gradually fill the double dot system with electrons. Analysis of Figure 5-6 determines that at first electrons accumulate in two independent electron puddles, one localized in each dot. As the puddles grow laterally with increasing electron number they eventually couple to each other. The range of the addition spectrum, in which the initially separate dots display the interaction is shown on the grayscale panel in Figure 5-7. The panel is built similarly to Figure 6 from the separate capacitance traces as a function of the top gate voltage.

At the bottom of the panel the addition traces can again be separated into two sets. One trace of each of the two families is highlighted on the figure. The spectrum consists of two non-interacting ladders of oscillating traces with nearly perfect periodicity of the traces within each ladder. The traces from different sets do not display any detectable splitting while crossing one another. On the contrary, on top of the panel there is only single ladder of the periodic traces. This indicates that the two initially separate electron puddles have merged into a single one and the electron wavefunctions are spread over the entire area of the resulting large dot.

The transition from two completely independent to a single puddle occurs over a range of $V_g \approx 25 \text{ mV}$. The bias range at which the transition occurs does not depend on the applied field. As the coupling mixes states of one dot with those of the other, and electrons start traversing the barrier between the two wells. In this regime, when the ground states of individual dots are aligned with each other, a finite tunnel coupling splits the two aligned levels [70, 71, 72, 73]. Note the regular change in the values of the splitting at the anti-crossings without any prominent fluctuations.

As we discussed in Chapter 3, the magnetic field at which all electrons fall into the lowest Landau level, $\nu=2$, can be readily identified by the position of a prominent maximum in all of the traces [31, 52]. The gate voltage position of the capacitance peak reflects the chemical potential of the dot. As in two-dimensional systems the chemical potential of the dot peaks just as the higher Landau levels depopulate completely. Two arrows indicate on positions of these maxima for two dots. Jumps in

the traces at higher magnetic fields, where both spin levels of the lowest Landau level are filled, are usually interpreted as single electron spin-flips [54, 12].

This general oscillatory behavior is consistent with the single particle model presented in section 5.2 except for a notable absence of spin degeneracy in the high-density regime, which we mentioned earlier.

The position of $\nu = 2$ in the magnetic field provides an estimate of the dot density. In a dot with a flat-bottom potential, the electron density of the dot is related to the Landau level filling fraction ν by $n = \nu(eB/hc)$. We find that for the gate biases V_g just below merging (at the bottom of the panel), the two electron puddles have densities $n_1 = 2.4 \times 10^{11} \text{cm}^{-2}$ and $n_2 = 3.2 \times 10^{11} \text{cm}^{-2}$, correspondingly. As we mentioned in a previous section 5.3.1, our dots have slightly different potentials, which leads to the difference in the exact values of the electron density.

Figure 5-7 illustrates our ability to distinguish between electron localization in either of the potential wells and those delocalized over the entire sample. We neither expect nor observe any unusual behavior for this sample. Because the barrier is high, electrons spill over it at the gate biases V_g that correspond to the high density in individual dots: $n = 2.5 - 3.5 \times 10^{11} \text{cm}^{-2}$. This density range translates into $r_s \approx 1$. Therefore, for these densities the dots are essentially metallic: electron interactions are weak. We did not detect any unusual behavior in our single dots at this density range.

5.3.3 Low-Density Electron Puddles Merge and Break up

To investigate the merging of two low-density electron droplets we examine a different sample with a lower barrier between the two potential wells. In sharp contrast to the previous case, as we will show below, magnetic field strongly affects the merging of low-density ($n \approx 1 - 2 \times 10^{11} \text{cm}^{-2}$) electron puddles.

A grayscale panel on Figure 5-8 presents the addition spectrum for a different sample with a lower barrier. The panel is built from the separate capacitance traces taken at different values of the magnetic field. Black denotes high capacitance. Each successive black trace corresponds to the energy for adding an electron to the double

dot system. The first electron enters the system at the gate bias $V_g = -290 \text{ mV}$. The figure does not show the low-density part of the spectrum ($-290 \text{ mV} < V_g < -140 \text{ mV}$). But it appears as a simple superposition of two different Dawrin-Fock families of traces, which is similar to the spectrum shown in section 5.3.1. Because such separation of the spectrum is possible, we conclude that up to $V_g = -140 \text{ mV}$ our system consists of two independent electron droplets. At much higher densities ($V_g > -45 \text{ mV}$) there is only one periodic Coulomb ladder, indicating that the initially separate electron droplets have merged into a single one.

The transition between the two limits occurs over gate biases $-140 \text{ mV} < V_g < -45 \text{ mV}$, depending on the strength of the applied magnetic field. At zero field, the merging occurs in an interval $\Delta V_g = 25 \text{ mV}$ wide centered around $V_g = -125 \text{ mV}$. The gate bias $V_g = -125 \text{ mV}$ corresponds to electron densities in each individual dot of $1.2 \times 10^{11} \text{ cm}^{-2}$ and $1.7 \times 10^{11} \text{ cm}^{-2}$ respectively. Each dot contains about 30 electrons. This density range is lower than that considered in section 5.3.2 and matches the density range at which we observe the paired electron additions in large individual dots. For higher densities and at zero field there is one combined dot under the gate. However, a magnetic field greater than $4T$ dramatically affects the spectrum.

There exists a clearly visible sharp boundary, which separates the spectrum in two parts. It is marked by a line on Figure 5-8. To the left of the boundary (the low field side), all electron addition traces show a similar evolution with magnetic field; electrons appear to enter one combined dot and the Coulomb blockade produces a nearly periodic addition spectrum. To the right of the boundary (the high field side), the periodicity of the spectrum is broken, and many anomalous, closely spaced electron additions are seen. With increasing magnetic field, the boundary between the two regimes extends up to densities of $1.7 \times 10^{11} \text{ cm}^{-2}$ and $2.2 \times 10^{11} \text{ cm}^{-2}$, in each dot respectively (over 60 total electron additions to the two-dot system). An increase in density of each dot along the boundary can be approximated by the linear relation $\Delta n \propto 0.1 \times B(T) \times 10^{11} \text{ cm}^{-2}$ for both of the two individual dots. This linear relation holds for all of our samples. Surprisingly this boundary follows the same

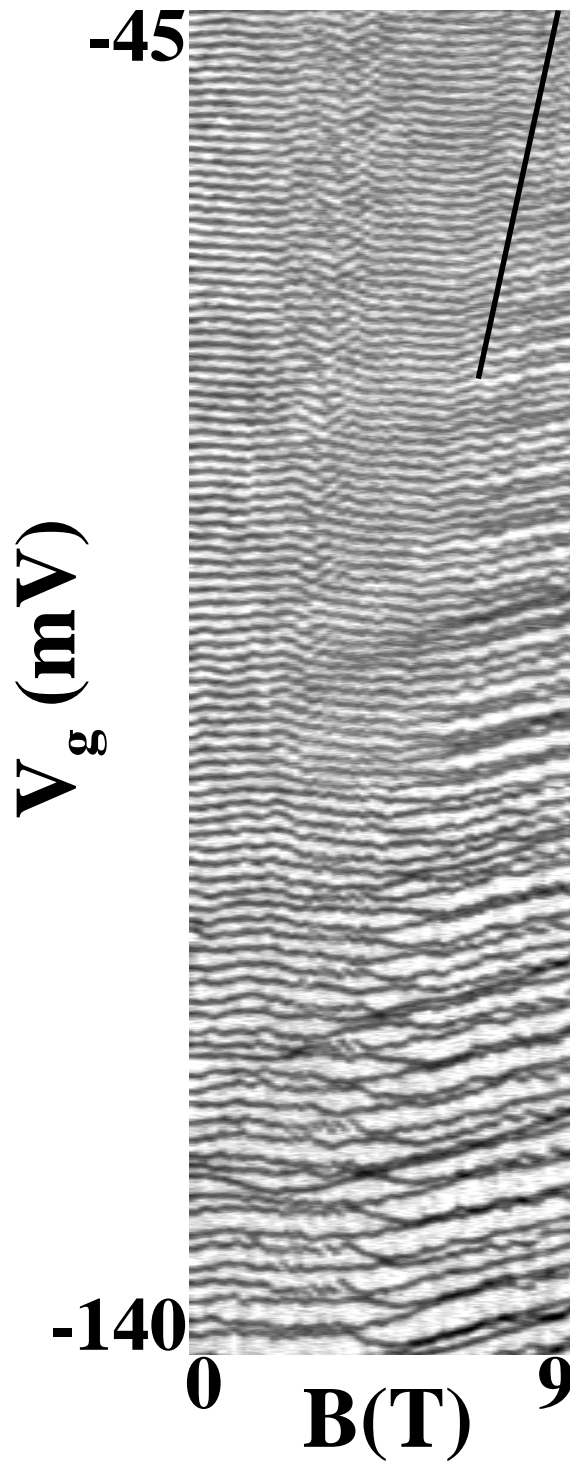


Figure 5-8: The the addition spectrum, for a new sample with a lower barrier. A magnetic field greater than $4T$ dramatically affects the spectrum. There exists a clearly visible sharp boundary, which separates the spectrum in two parts. The boundary is marked by a line. To the left of the boundary (the low field side), all electron addition traces show a similar evolution with magnetic field; electrons appear to enter one combined dot and the Coulomb blockade produces a nearly periodic addition spectrum. To the right of the boundary (the high field side), the periodicity of the spectrum is broken, and many anomalous, closely spaced electron additions are seen.

linear density-field relation as the one seen in individual dots of larger sizes [32] (see Chapter 3).

To understand the origin of this boundary we expand the addition spectrum to the right of the boundary. Figure 5-9 shows this part of the spectrum taken with better resolution and at lower temperatures. A line indicates the position of the boundary. Again, all traces oscillate with magnetic field. But here the origin of the oscillations is different from that of the low-field case considered above. For magnetic fields higher than $4T$, electrons within each dot fill only the lowest orbital Landau level, but with both spin-up and spin-down electrons. With increasing magnetic field, the electron orbits shrink and the Coulomb repulsion causes the redistribution of electrons between the two spin-split branches of the lowest orbital Landau level. This produces oscillations in the single electron traces known as “spin flips” [82, 83, 11].

The most noticeable feature of the Figure 5-9 is the existence of two different oscillation patterns. Two traces, each representing its own pattern, are marked by R and B , correspondingly. In fact, the entire spectrum can be separated into two nearly periodic Coulomb blockade sets, which differ by their “spin flip” patterns. Further on, we will refer to these sets of addition traces as the “R” set and the “B” set. A schematic of the spectra shown on Figure 5-10 illustrates our point. Since addition traces within each set are widely separated by Coulomb blockade and spaced nearly periodically, any two traces that appear close to each other belong to *different* sets. The existence of two patterns characteristic of the individual dots indicates that, to the right of the boundary, there exist two separate dots, despite the fact that for zero field two dots are merged into one. We conclude that the boundary separates two regimes in $V_g - B$ space. In one regime, electron wavefunctions are spread over the entire area of the double dot and in the other each electron dwells in one of two individual dots.

In the latter regime, the two dots are not completely independent. Though the magnetic field breaks one combined electron dot into two separate ones, a residual coupling remains. The barrier between the two dots is small, and interdot tunneling remains possible [91, 92, 93, 94, 95]. When ground states of individual dots are aligned

with each other, a finite tunnel coupling splits two aligned levels [70, 71, 72, 73]. Such alignment creates the equivalent of a molecular hybrid state. An example of such splitting are the two hybridized traces marked by a top circle in Figure 5-9. The two hybridized traces cannot be solely associated with either of the two spin-flip patterns but rather exhibit features belonging to both of them.

The hybridization shown is not a rare occurrence. Each pair of closely spaced traces mixes into a hybrid. Three hybrids that appear on Figure 5-9 are marked by circles. Since “R” traces as well as “B” traces appear nearly periodically in gate voltage, the occurrence of these pairs is determined by the ratio of two Coulomb blockade periods ($\Delta V_g^R/\Delta V_g^B$). For the gate bias range shown on Figure 5-9 the two periods differ somewhat. Approximately, the ratio is: $\Delta V_g^R/\Delta V_g^B = 4/3$. We believe that the difference reflects the difference in the individual dot’s areas. The capacitance of a dot to the gate C_g in our geometry is proportional to the dot’s area, and therefore, the spacing between Coulomb blockade peaks is inversely proportional to the dot’s area: $\Delta V_g = e/C_{gate} \propto e/Area$. For higher gate biases the peak spacing for both dots decreases, because dots grow in size and the ratio changes. The ratio of individual dot areas differs from sample to sample, resulting in different patterns of the hybrid formation.

There are two spurious traces in the spectrum (marked by empty triangles). The traces do not oscillate in the field, and therefore, are not associated with electron additions to either of the dots. We see similar traces on some (but not all) of our samples that have a low barrier between two dots and, hence, exhibit the boundary. These traces always arise in the gate bias range that corresponds to the merging of the two electron puddles and disappear for high electron densities. We associate them with electron additions to a local potential minimum in our samples. The origin of this minimum is not clear, but the presence (or absence) of the “extra” addition traces does not seem to affect the behavior of the other electrons in either dot. We thus exclude them from our discussion.

We now focus our discussion on a pair of hybrid states. A part of the addition spectrum around a pair of hybrid states (the topmost hybrids on Figure 5-9) is shown

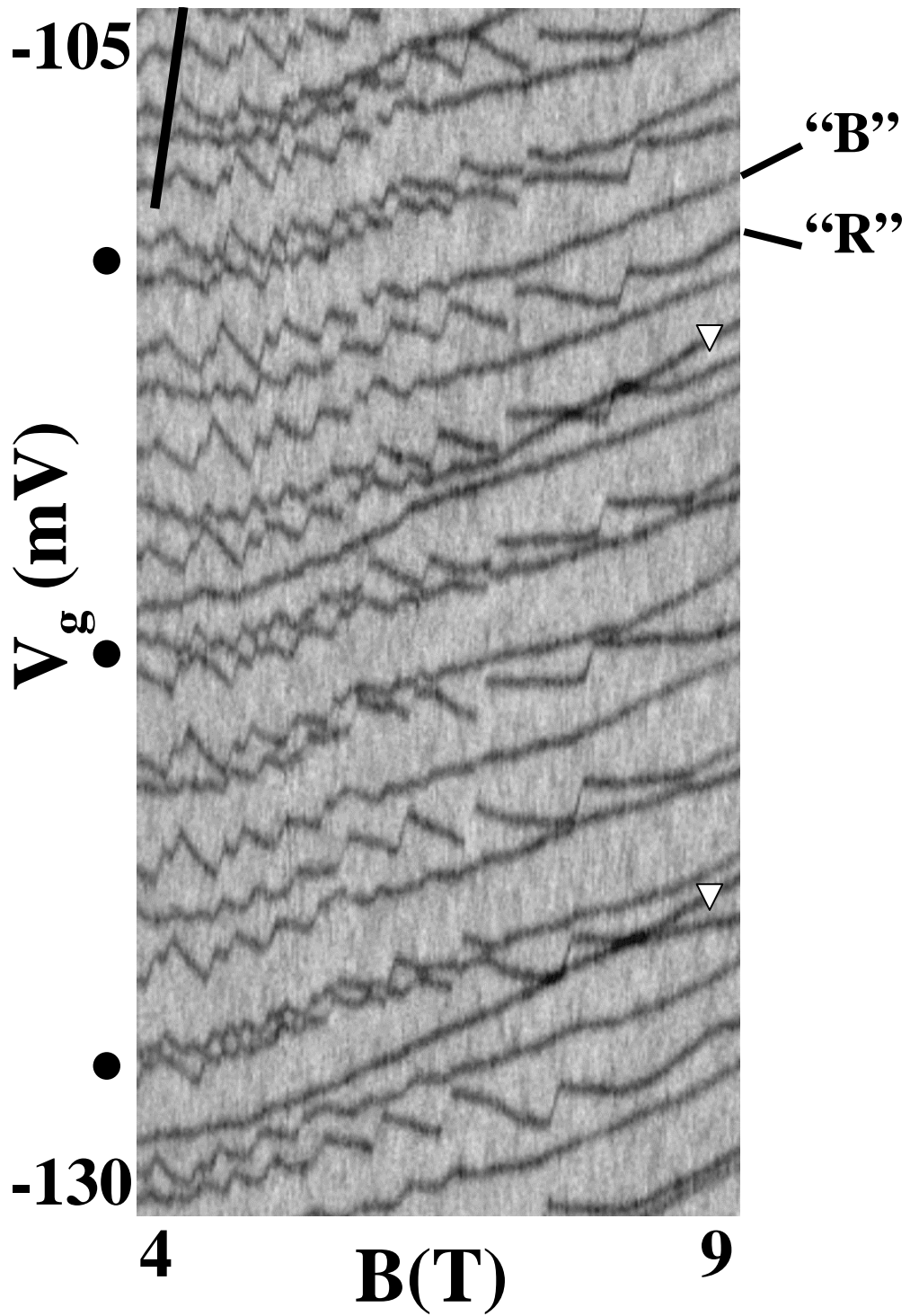


Figure 5-9: A part of the spectrum expanded to the right of the boundary (marked by a line). Two traces, each representing its own oscillation pattern are marked by R and B . Full circles mark three pairs of hybrid states. Two spurious traces are marked by empty triangles.

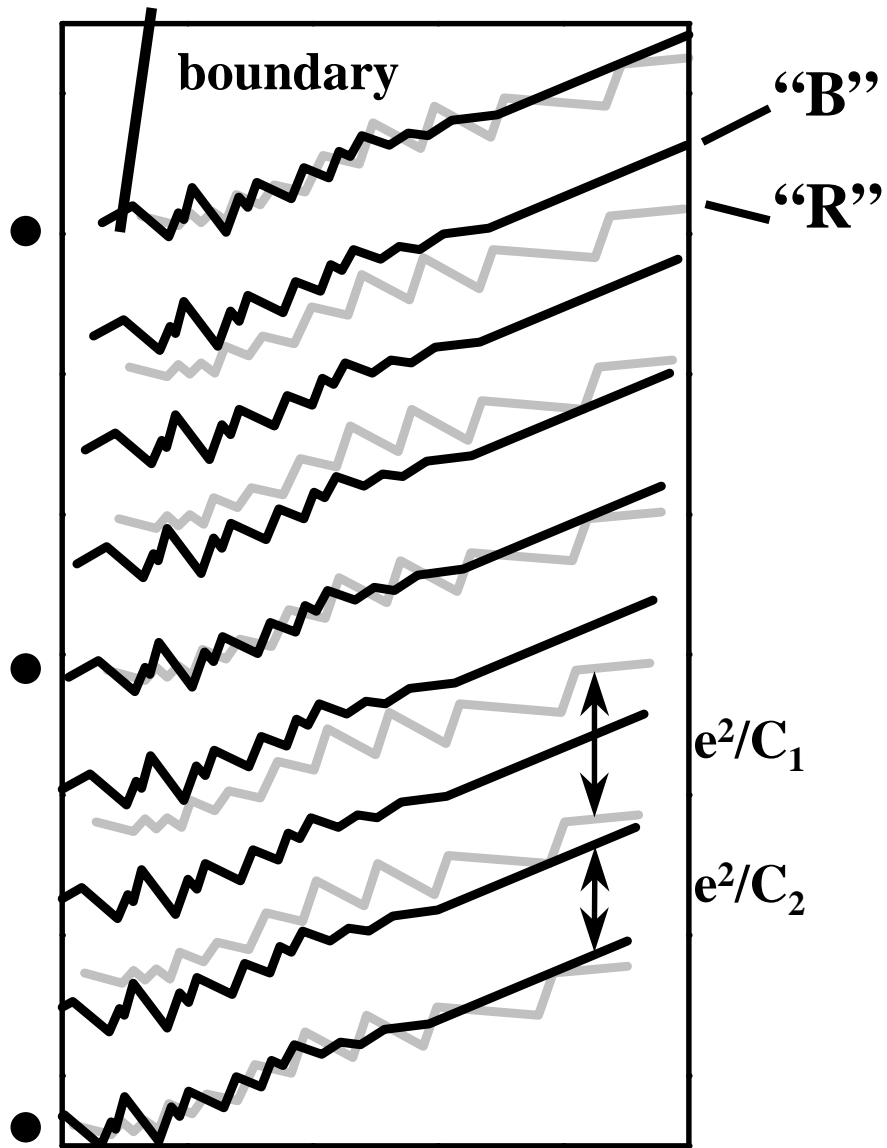


Figure 5-10: Schematic representation of the spectrum shown on Figure 5-9.

in Figure 5-11A. Six subsequent addition traces, marked by empty circles, from bottom to top are $R1$, $B1$, $H1$, $H2$, $B3$, $R3$. While traces $(R1, R3)$ and $(B1, B3)$ correspond to electron additions to one dot or the other, each trace of the pair $(H1, H2)$ is shared between both dots.

We estimate the coupling strength between two dots by describing the spectra using single particle states. We reconstruct the two hybridized states $H1$ and $H2$ from the neighboring “one-dot states” $R1$, $B1$, $B3$, $R3$ in the following way. First, we assume that in the absence of a residual interaction the spectrum would be as presented in Figure 5-11B. In place of the hybrid states $H1$, $H2$ there are two unperturbed independent states from the two dots: $R2$ and $B2$. The following argument allows us to create $R2$ ($B2$). The periodicity within each (R and B) set of traces predetermines the gate bias at which the “R” trace (“B” trace) appears. Neighboring traces within each family look alike and can almost be obtained from one another by a simple shift in the $V_g - B$ plane. Thus for imaginary unperturbed states $R2$ and $B2$ we take $E_2^R = (E_1^R + E_3^R)/2$ and $E_2^B = (E_1^B + E_3^B)/2$. Second, we assume that tunneling between $R2$ and $B2$ produces an off-diagonal matrix element U , resulting in the following Hamiltonian for this two-level system:

$$\begin{bmatrix} E_2^B & U \\ U^* & E_2^R \end{bmatrix} \quad (5.7)$$

Then diagonalization of the Hamiltonian 5.7 splits E_2^R and E_2^B into a pair of hybrid states:

$$E_{1,2}^H = \frac{(E_2^R + E_2^B)}{2} \pm \sqrt{\frac{(E_2^R - E_2^B)^2}{4} + U^2} \quad (5.8)$$

Using U as the only fitting parameter we fit $E_{1,2}^H$ to our data. The value of U that produces the best fit provides the estimate for the coupling strength between two dots.

Surprisingly for such a simplistic model we obtain practically perfect fits to our data (Figure 5-11C). Unexpectedly, the residual coupling strength U ($U \approx 0.1 \times (e^2/C_{dot})$ for the case shown) displays nearly complete independence of the strength

of the applied field for fields larger than required for the localization transition.

The results of similar fitting for different densities are summarized in Figure 5-12. For a given density (the gate voltage V_g) the magnetic field abruptly breaks up one combined dot in two fragments. For higher densities, a larger field is required for such a transition. For the fields larger than required for the transition some residual tunnel coupling between the two fragment remains. Though constant in field, this coupling increases with density, and becomes comparable to $E_c = e^2/C_{dot}$ at densities of around $2 \times 10^{11} cm^{-2}$. The boundary ceases to exist at these densities. In fact, as we described in section 5.3.2 the boundary is altogether absent in samples for which the individual dot densities at the merging point are higher than $2.3 \times 10^{11} cm^{-2}$, i.e. the magnetic field has no effect on the merging of two high-density dots.

5.4 Summary

This Chapter presents yet another method of studying localization in a small low-density electron puddle placed in a disorder potential. Using Single Electron Capacitance Spectroscopy, we study electron additions in quantum dots with a “disorder” potential prepared artificially. We intentionally create a dot with a potential profile containing two smooth minima separated by a barrier. Through analysis of the addition spectra in a magnetic field, we distinguish between electrons localized in either potential well or delocalized over the entire dot.

Our studies conclusively demonstrate that under precisely the same conditions for observation of the paired electron additions, a low-density electron droplet inside the dot indeed splits up into smaller fragments. This abrupt disintegration creates a sharp *boundary* between periodic and “paired” parts of the addition spectra, with paired electrons entering into spatially distinct regions within a dot. The boundary essentially separates two phases: in one, electrons are delocalized over the entire sample, and in the other, electrons are confined in local disorder minima. We believe that a similar scenario takes place in large single dots (described in Chapter 3), in which real disorder is present [32]. In that case the boundary is presumably related

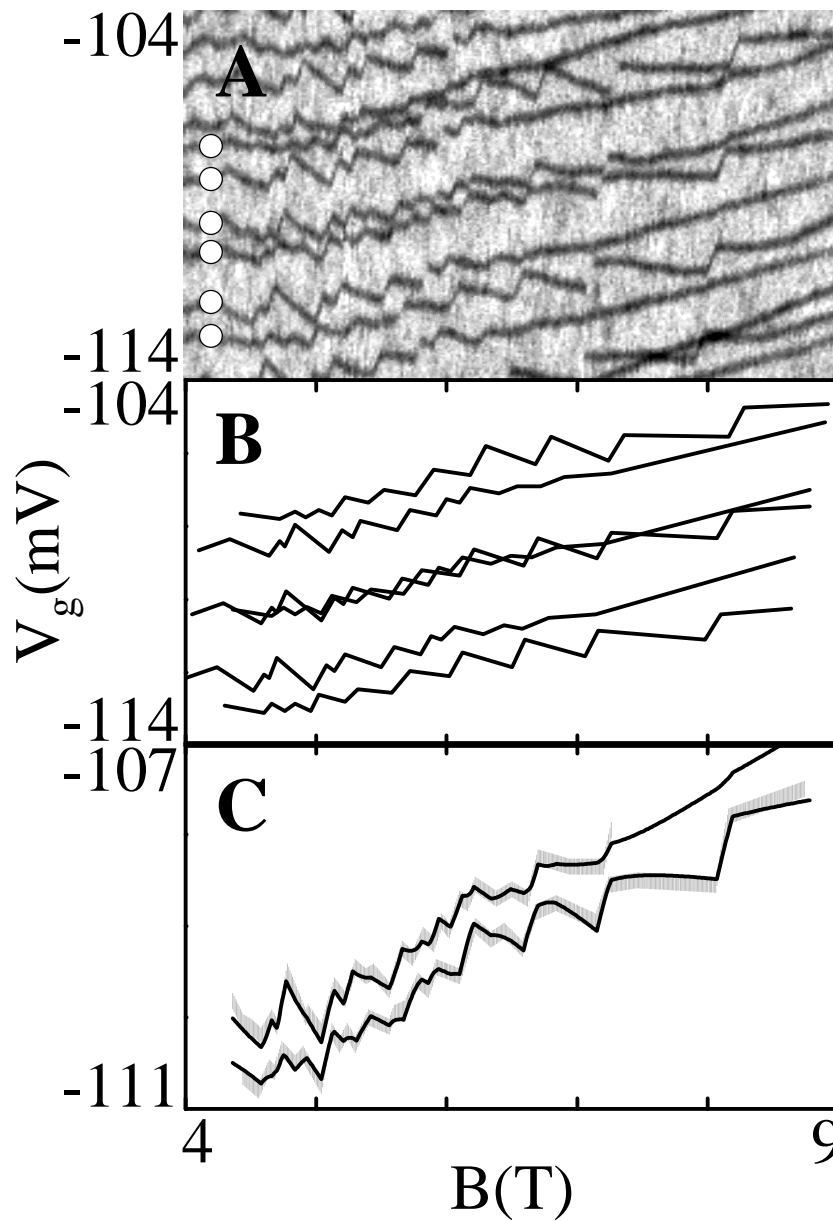


Figure 5-11: **A.** An addition spectrum expanded to the right of the boundary. Six subsequent addition marked by empty circles are $R1$, $B1$, $H1$, $H2$, $B3$, $R3$ (bottom to top). $R1, R3$ and $B1, B3$ represent two oscillation patterns. Hybridized traces $H1$, $H2$ do not belong to any of the patterns. **B.** The hypothetical spectrum in absence of the interaction between two dots. Hybrid states $H1$, $H2$ are replaced by two unperturbed independent states from two dots: $R2$, $B2$. **C.** Reconstruction of the hybrid states. The data ($H1$, $H2$) are shown in gray, black are fits.

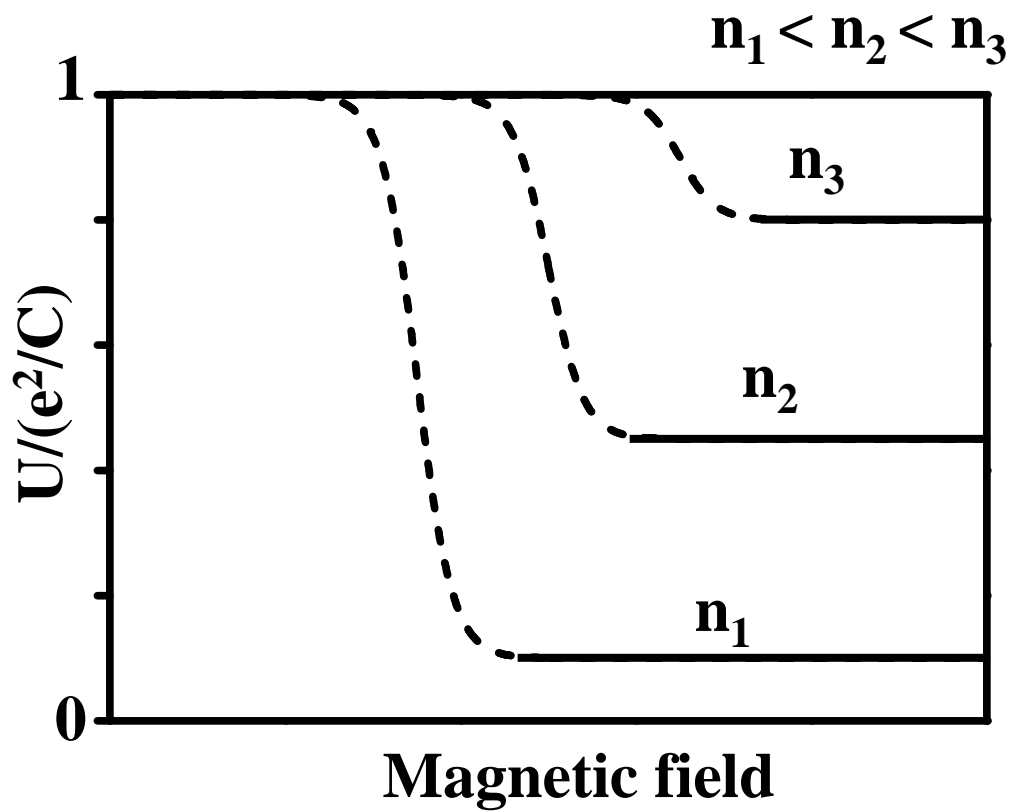


Figure 5-12: Schematic field dependence of the tunneling matrix element U for different densities ($n_1 < n_2 < n_3$). Solid lines denote regions where residual coupling is extracted as described in the text.

to a break up of the larger droplet into a central core and a localized periphery.

We also measure the remnant residual interaction between the fragments. Surprisingly, it displays a nearly complete independence on the strength of the applied field for fields larger than required for the localization transition.

The physical mechanism of such separation or of the pairing phenomena has yet to be established. However, a recent paper [96] shows that a two-phase coexistence of high density liquid and a low-density gas might be energetically favorable in the interacting two-dimensional system placed in a disorder potential. Also numerical calculations by Canali [66] (see section 3.4) support our finding that two electrons in the pair enter into spatially separated regions of the dot.

Chapter 6

Summary and Directions for Future Research

For half a century physicists have worked to understand localization of strongly interacting electrons in a disorder potential. Either electron interactions or disorder can produce localization [21, 22]. Though their interplay in two-dimensional systems has been a subject of intense experimental and theoretical studies [17, 26, 27, 3, 4], no theory exists fully describing the effects of both disorder and strong interactions.

Quantum dots provide a convenient system for studying electron localization on a microscopic scale. However, the traditional transport techniques for studying lateral quantum dots [11] sense primarily delocalized electronic states. A possible exception is transport studies in vertical structures, but these do not permit variation of electron density [28, 13], a critically important parameter that changes the effective strength of electron interactions. We study electron additions in vertical quantum dots using Single Electron Capacitance Spectroscopy (SECS) [29]. It has demonstrated the capability of probing both *localized* and delocalized states of electrons. Furthermore, this method allows us to study two-dimensional dots of various sizes and over a broad range of electron densities.

In our experiments, we measure the energies required to add successive electrons to an initially vacant quantum dot. Our dots are made of standard GaAs/AlGaAs heterostructures. At low temperatures, a dot that is poorly coupled to its surround-

ing must contain an integer number of electrons. A nearby gate electrode can draw electrons into the dot one at a time. We follow how each entering electron overcomes (with the help of the increasing gate voltage) the mutual repulsion of those electrons already present in the dot: this is accomplished by registering a sequence of the gate voltages, at which the additions occur. Contrary to the belief that it would take more energy to add each successive electron to a quantum dot as the electrons would repel each other, our SECS measurements have revealed an astonishing phenomenon: for the low-density regime, electron additions can occur in pairs. Under certain conditions, not one but two electrons join the assemblage at the same gate voltage. It costs no energy to add a second electron in the pair once the first one has been added. These paired electron additions indicate that an unidentified mechanism cancels the repulsion between two electrons. We hypothesized that the pairing occurs for densities below the localization-delocalization transition within a dot, and two electrons in the pair are added to spatially isolated regions within a dot.

This thesis describes two experiments we have produced to study this transition in a controlled fashion. In one experiment, we added an additional side gate to distinguish electrons residing at the edge of the dot from electrons in the center [33]. In another, we created a dot with a potential profile that contains two minima separated by a barrier [34]. Our studies have conclusively demonstrated that under exactly the same conditions as we observe the paired electron additions [29, 32], a low-density electron droplet inside the dot does indeed split up into smaller fragments, with each residing in its local disorder minima. Two electrons in the pair are actually added to spatially distinct regions within a dot. While there exists no strict theory explaining all observed details of this very sudden disintegration, several recent numerical calculations are in support of our data [96, 66]. Below we will discuss possible direction for our future research.

6.1 Further Study of Localization

The results presented in the Chapters 4 and 5 demonstrate that in our dots we observe fragmentation of low-density electron droplets into several electron puddles. The mechanism of this separation has yet to be established. Meanwhile there exists a number of challenging experimental tasks.

The simplest idea (and the hardest to implement) that comes to mind is to combine the two experimental techniques: to create a double dot system with a pincher gate. For now we adjust a barrier between two dots by probing enormous amount of different samples. A pincher gate around the double dot would allow to us change the barrier between two dots *in situ* on a single sample. This would produce a variable “disorder” potential. Recall, that we observe the sharp boundary between localized and delocalized regimes only in the low barrier samples, and the samples with a high barrier does not exhibit the boundary. For an adjustable barrier between the two dots we would be able to study disappearance of the boundary with increasing barrier heights.

Another possibility is to adjust the natural disorder rather than the artificial one. We have already discussed the source of disorder in section 2.2.4. In our structures the dot is arranged between two plates of a tunnel capacitor. The lower (tunnel) barrier allows electron to tunnel from a reservoir, and the top (blocking) barrier is not transparent to tunneling. A δ doping Si layer in the middle of the top blocking barrier to provide the quantum well with electrons. The positive charges of donor atoms, which released their electrons, attract the electrons and binds them to the quantum well. However, this positive charge is not uniform. The donor atoms within the layer are spaced randomly, and only fraction (about 30%) of them are ionized. Therefore, there are multiple local minima in plane of the quantum well underneath positively charged donor atoms. Consider replacement of the δ donor layer in the insulating top AlGaAs barrier by a heavily doped AlGaAs layer of finite width. This replacement would not change the profile of the conduction band and electrons are still be attracted to the quantum well. However, the disorder potential due to the

randomly distributed donors would be screened by electron gas in the heavily doped layer. In the δ doping structure we observe delocalization only above critical density $n_0 = 1 \times 10^{11} \text{ cm}^{-2}$. It would be interesting to check if this density remains the same for cleaner samples.

It is also interesting to change the lower tunnel barrier in our sample. In our current structures the barrier is transparent for entire range of our experimental frequencies. A less transparent barrier would permit studies of the tunneling rates. On other hand in strong applied field (both in parallel and perpendicular arrangements) we observe a strong decay in the tunneling rate. A more transparent barrier would enable us to make experiments strong, particularly, in parallel field. This way we can separate orbital and spin effects in our dots.

Finally, we could study statistics of the peak spacing in our largest dots. Section 3.4 mentions some theoretical efforts in this area [65]. We can test the prediction of the theory in the low-density regime not accessible by other experimental technique.

6.2 Spectroscopy of Excited States and Study of Tunneling Rates

Single Electron Capacitance Spectroscopy directly probes only the ground states in our dot. By combining it with another method developed in our lab: Time Domain Capacitance Spectroscopy [60], we can develop a powerful probe of both ground and excited states. TDCS essentially measures real time capacitance response to a sharp pulse applied between low-dimensional system and a reservoir. As electrons tunnel from the reservoir onto the system in response to the initial pulse, they induced a charge on a nearby gate electrode. The charge on this electrode is measured in real time.

Consider an application of a sharp pulse to a dot. If the height of the pulse is just about the charging energy, then one electron is added to the dot. The tunneling rate of this event can be measured directly by TDCS. For increasing magnitude of

the initial pulse more channels (due to the dot's excited states) will be available for tunneling and, hence, the tunneling rate is reduced. By measuring the rate versus the magnitude of the pulse we can map the excitation spectrum of the dot.

6.3 Spin in Small Dots

Many exciting research topics originate from studies of small quantum dots. This section presents our preliminary data taken on small dots. The previous chapters of this thesis were devoted to the localization transition, which occurs in our large dots with decreasing electron densities. Different processes take place in small dots. In small dots containing just a few electrons, both the electron-electron interaction energy and the quantum confinement energy are comparable to the charging energy. Because of the strong confinement small dots exhibit atom-like features for low electron occupancy: electrons fill two-fold degenerate orbital states in pairs of spin up and spin down. The Coulomb interactions, however, modify this simple picture significantly.

6.3.1 How and Why Coulomb Interactions Could Modify Darwin-Fock Spectrum

As we described in section 5.2, addition spectra for a small dot in a perpendicular magnetic field can be described within the constant interaction model for single particle states based on the Darwin-Fock spectrum. The double spin degeneracy of single particle states gives rise to several important consequences that go under the name of “even-odd asymmetry” in Coulomb blockade oscillations. In particular, the dependence of the addition energy on magnetic field differs for even and odd electrons.

The following argument helps to visualize our point. Generally addition energies “wobble” in the field. Section 5.2.2 connects these oscillations with shifts of the spatial electron wavefunction between different angular momentum states. Consecutive odd and even Coulomb blockade peaks, corresponding to spin up and spin down additions to the same spatial state, show similar behavior in magnetic field: they “wobble” in

phase, maintaining the constant separation (or field independent addition energy). On other hand, the spacing between an even and a following odd peaks (addition energy) varies drastically as magnetic field changes, because these electrons occupy different spatial state.

This behavior was predicted [90] and observed in several experiments [31, 12, 28, 50, 51] in small dots containing just a few electrons. But for higher electron occupancies new features in the spectra develop, which can not be accounted for within the framework of the single particle picture presented above. The general oscillatory behavior of the spectra for larger electron numbers is consistent with the single particle model except for the notable absence of spin degeneracy in this high-density regime. This absence was first reported by McEuen *et al.* in [54, 82] and studied in detail (albeit in small fields) by Marcus' group [89]. It is not clear whether under these conditions consecutive electrons enter the dot with parallel spins. So far the disappearance of the spin degeneracy with increasing density has not been understood, but strong Coulomb interactions must play a role here.

Halperin argued [97] that symmetry properties combined with Coulomb repulsion may induce spin flips in the ground state. Consider two spatial states E_1 and E_2 . Two electrons with spin up and spin down fill E_1 first, and then the next two fill E_2 in a similar fashion. However, because of the smaller overlap the two wavefunctions, the Coulomb energy between two electrons occupying these states is smaller when one electron fills E_1 and the other fills E_2 . Therefore, placing the second electron on E_2 saves the Coulomb energy though it costs the difference in confinement energies $E_2 - E_1$. If the cost is smaller than the gain then one spin up electron occupies E_1 while the next one fills E_2 with the same spin direction. The exchange part of the Coulomb energy only enhances the effect and ensures the alignment of the two spins. In fact, Oreg, Byczuk and Halperin proposed a model explaining a mechanism for internal spin-flip transitions in the armchair carbon nanotube [98] based on this consideration.

In quantum dots, several modifications to the Darwin-Fock spectra due to direct Coulomb and exchange interactions were studied experimentally and modelled by

Tarucha's group [51, 28, 50]. Basically, their experiments focus on certain degeneracy points between two spatial levels E_1 and E_2 in a dot. Away from the degeneracy point two electrons with spin up and spin down fill E_1 first, and then the next two fill E_2 in a similar fashion. Near the degeneracy point, the gain due to Coulomb repulsion is larger than the cost in the confinement energy $E_2 - E_1$, and two spin up electrons occupy E_1 and E_2 . Note that because of the small effective mass in GaAs, spin effects in a magnetic field, such as Zeeman splitting, are an order of magnitude smaller than changes in spatial energies and can be neglected.

6.3.2 Beyond Darwin-Fock: Data

The spectra of our smallest dots exhibit similar features as we will describe below. Our data suggests that not only we observe spin-flips of a second electron added to *any* fourfold degeneracy point, but also we are able to follow the restoration of the spin filling. After the first two electrons occupy E_1 and E_2 with their spin up, the next two electrons fill the same states with their spin down. Even though the spin-flip occurs when the second electron enters the dot, it is immediately compensated by the third electron addition. These processes produce a series of downward and upward cusps, which gradually wash away the even-odd asymmetry as the electron occupancy increases.

The capacitance traces taken at different values of the magnetic field are plotted together on the greyscale panel in Figure 6-1A. Black denotes high capacitance. Each successive trace corresponds to the energy for adding an electron to the small dot. Altogether 23 addition traces are shown. The lowest trace shown represents the first electron added. The overall spectrum can be described qualitatively within the constant interaction model for Darwin-Fock states, as is typical for individual small circular dots [12, 13, 28]. Addition energies oscillate with magnetic field. Pairs of consecutive odd and even Coulomb blockade peaks, corresponding to spin up and spin down additions to the same spatial state, show similar behavior in magnetic field. These pairs are marked by brackets. However, more careful inspection of the data shows features that the simple model does not explain. For the fields higher

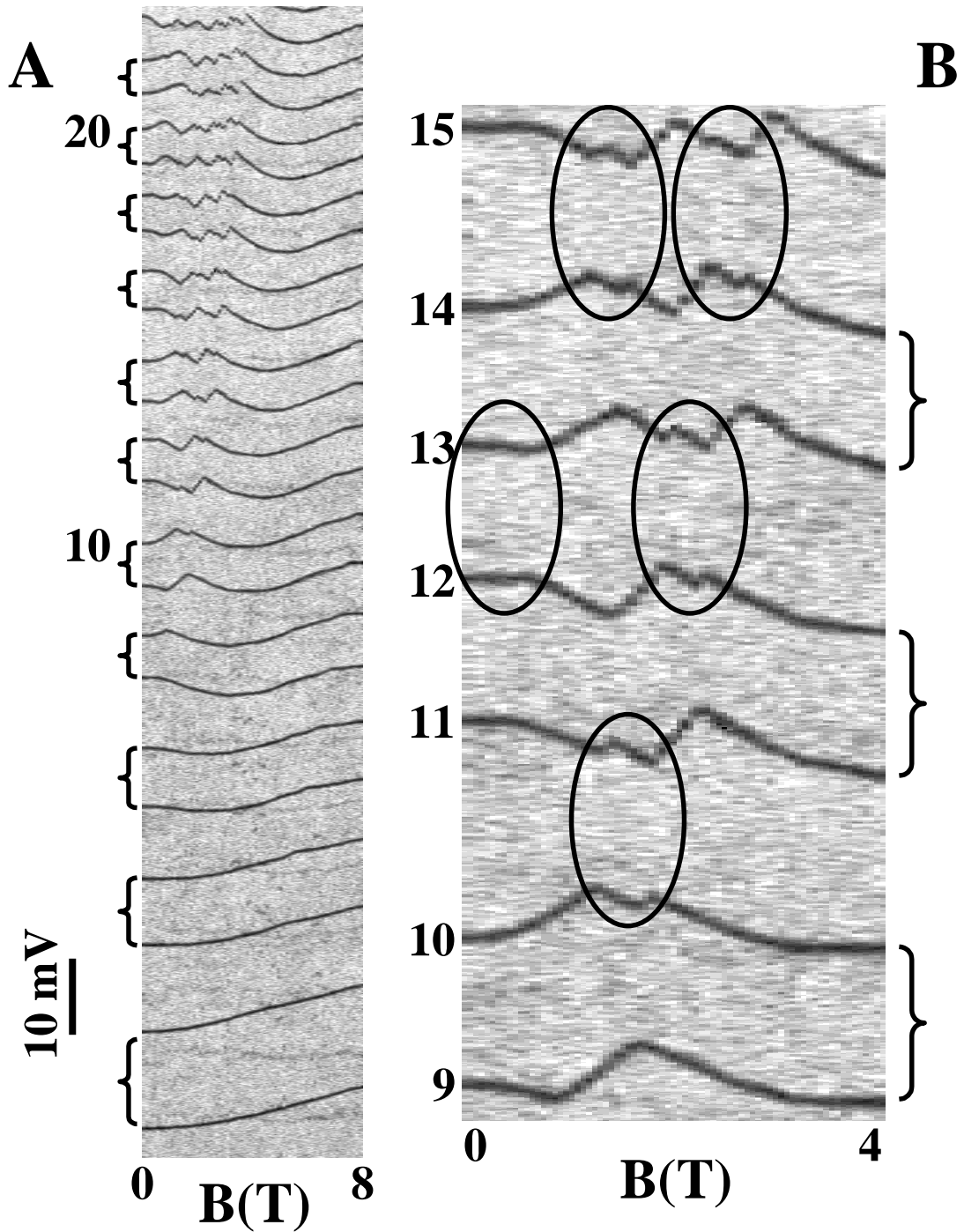


Figure 6-1: A. Magnetic field evolution of first 23 consecutive peaks for one of our small dots. 10th and 20th electron additions are numbered. Vertical bar show the gate voltage scale (10 mV). Addition traces “wiggle” in the field. Traces that wiggle as a pair are marked by brackets. B. An expansion into a part of the spectrum shown in A. Numbers on the left counts the traces. Brackets mark even-odd pairs. Downward and upward cusps are highlighted by empty ovals.

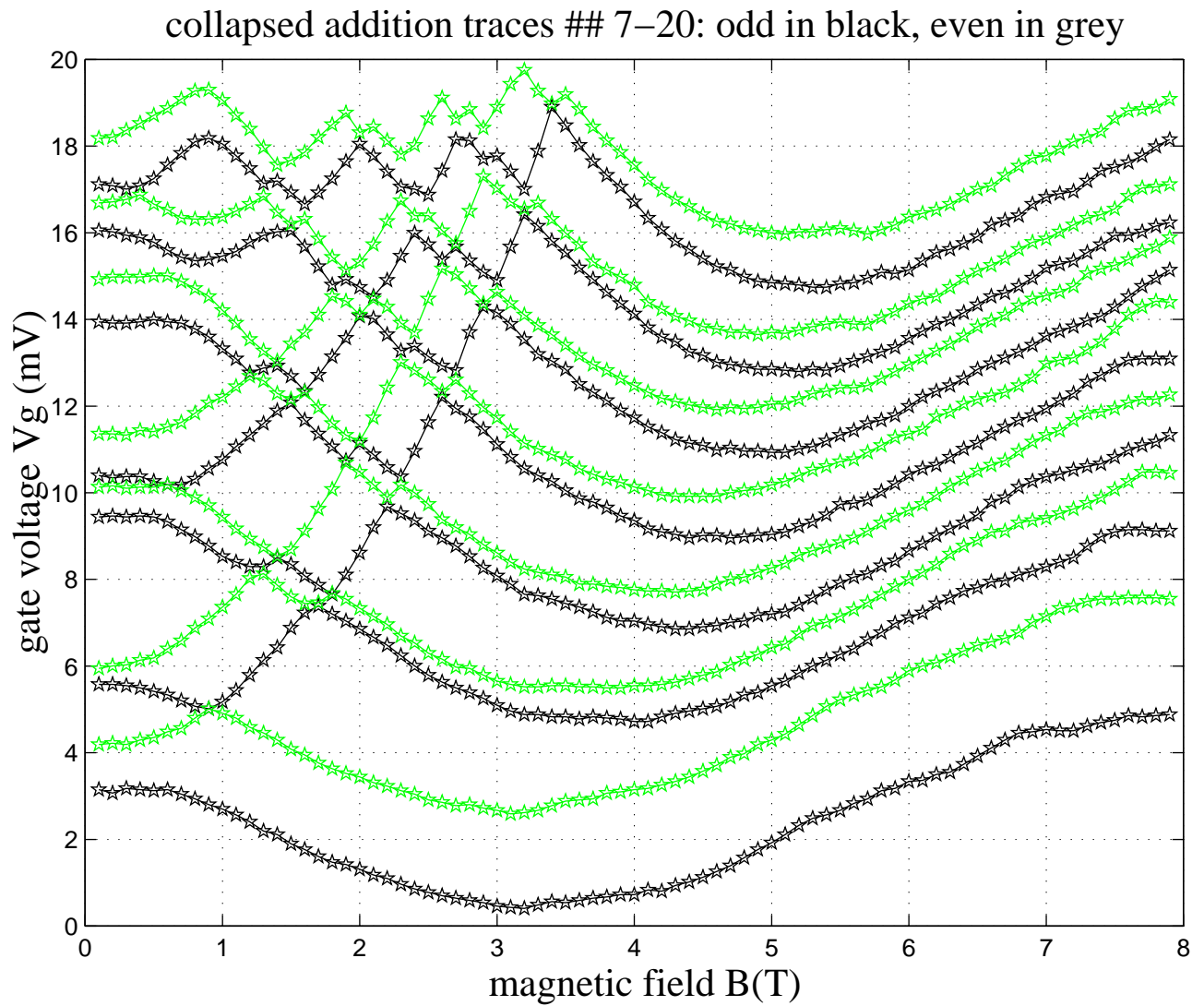


Figure 6-2: Collapsed addition traces from 7th to 20th from figure 6-1A. Note a perfect match between upward and downward cusps.

than $\approx 1T$ the 8th trace nicely pairs with 7th trace. But for smaller values of the field $B \leq 1T$ it does not replicate the 7th trace, but instead has downward slope. Note that 9th trace in this field range has slope opposite to that of 8th trace. This is not the sole deviation from the simplest Darwin-Fock spectrum.

Figure 6-1B expands a part of the addition spectrum between 9th and 15th electrons. Brackets again mark even-odd pairs. Consider the 10th addition trace around $B = 1.5T$. Around this field it does not follow the 9th trace. Instead it has a downward cusp. Surprisingly, the 11th trace has an upward cusp at this field. In naive picture, the 11th and 10th electron additions are associated with different spatial state and are not related. By examining figure 6-1B carefully, we find many pairs of cusps (highlighted by empty ovals) that belong to “unrelated” addition traces. To test how well upward cusps match downward cusps we collapse the spectrum, by shifting addition traces in the gate voltage. A totally unexpected result of this subtraction is shown on Figure 6-2. The plot shows a very ordered pattern. The cusps perfectly match each other.

We believe that this pattern arises due to mechanism outlined in section 6.3.1. The understanding of the very details of our data is a subject of our intensive studies.

Appendix A

Fabrication Recipes

This appendix contains our fabrication process. We adopted the following logic for the list below. When a fabrication step is listed for the first time, we add few important comments. For consecutive entries we keep the description short. The physical principles behind every step are presented in Chapter 2. Here we limit ourself to the very technical issues. For some step only approximate numbers are given. This is because certain conditions fluctuate a lot from one day to the other. The general rule for these steps: calibration is required to be performed on dummy samples before the real sample is processed.

The exposure in sections A.2, A.4, A.4, A.5 are performed using optical lithography on chips 6×11 mm. Each chip contains 18 mesas. The processes in sections A.6, A.7, A.8 are done by E-beam lithography on small chips, each containing only one mesa.

A.1 Sample Cleaning

While performing the boiling and ultrasonic bath we place a paper filter on the bottom on the glass beaker prior to placing our sample inside. This prevents brittle GaAs samples from hitting against the walls of the glass beaker.

1. Boil in 1,1,1 Trichloroethane (TCA) for 2 min. This step mainly removes grease from the surface. We perform this step only after receipt from the grower.

2. Clean in ultrasonic bath in acetone for 2 min.
3. Clean in ultrasonic bath in methanol for 2 min.
4. Blow dry with N_2 before methanol dries by itself.
5. After cleaning the surface needs to be covered with a resist as soon as possible.

The cleaning of the samples is extremely important for the success of all processing steps. We perform the following procedure before every lithographical step of our fabrication process. If the visible residues are left on the surface, some or all steps needs to be repeated and time interval may be increased.

A.2 Mesa Definition

1. Clean sample: see section A.1.
2. Spin Shipley positive resist 1813 at 4000 rpm for 40s.
3. Soft bake in $90^\circ C$ oven for 30 min. The resulting thickness of the photoresist is about $1\mu m$. For features with dimensions less than $3\mu m$ a thinner Shipley 1805 resist may be used. This resist produces thickness of about $0.3\mu m$.
4. Align the sample with the mask and expose.
5. Develop in MF-319 developer. The exposure and development times needs to be calibrated at the beginning of the day. Generally exposure time is around 10s, and successive development is about 1 min.
6. Rinse in DI water for 1 minite.
7. Blow dry with N_2 .
8. Etch mesa in (1 : 8 : 1000) $H_2SO_4/H_2O_2/H_2O$ solution. The etch rate is about 45nm/min, but needs to be calibrated before every important step. This solution saturates quickly and needs to be replaces often if many samples are

being processed. The rates for (1:8:500) and (1:8:250) are larger by a factor of 2 and 4, correspondingly

9. Rinse in Di water for 1 min.
10. Strip the photoresist by soaking in acetone. Use ultrasonic bath if needed.

A.3 Ohmic Contacts: Positive Resist

1. Clean sample: see section A.1.
2. Spin Shipley positive resist 1813 at 4000 rpm for 40s.
3. Soft bake in $90^{\circ}C$ oven for 25 min.
4. Align the sample with the mask and expose.
5. Soak in Chlorobenzene for 4 min. You may see the exposed pattern at this step.
6. Soft bake in $90^{\circ}C$ oven for 5 min.
7. Develop in MF-319
8. Rinse in DI water for 1 min.
9. Blow dry with N_2 .
10. Clean in UV ozone oven for 30 s. This step cleans the surface of the resist's residue but also damages the resist profile
11. Load the sample in evaporator after a quick etch of 10 s in $H_2SO_4/H_2O_2/H_2O$ (1:8:1000).
12. Evaporate metallic layers according to the following sequence: nickel 5 nm, germanium 35 nm, gold 70 nm.

13. Lift off by soaking in acetone. If the unwanted metal does not come off easily, use ultrasonic bath or spray with acetone. If nothing helps, place the sample in boiling NMP (1-methyl-pyrrolidone). *Important:* do not let the sample dry before the lift-off is completed. Upon the completion of the lift-off step the sample must be clean.
14. Clean in ultrasonic bath in methanol for 2 min.
15. Blow dry with N_2 .
16. Anneal the contacts at $435^\circ C$ for 0.5 min. The parameters for the Eurotherm strip heater that was used for the ohmic contacts are:

$$\begin{aligned}
 Pr1 : 400 & \quad Pr2 : 600 & \quad Pr3 : 100 & \quad Pr4 : 800 \\
 Pl1 : 200 & \quad Pl2 : 420 & \quad Pl3 : 435 & \quad Pl4 : 0 \\
 Pd1 : 0.5 & \quad Pd2 : 0 & \quad Pd3 : 0.5 & \quad Pd4 : End
 \end{aligned}$$

17. Check the contact resistance after annealing on the probe station. Contacts with resistance of $1.8 - 2.4 K\Omega m$ (for two contacts in series) does not freeze out at He temperatures.

A.4 Ohmic Contacts: Negative Resist

The latest series of samples we processed with negative photoresist. We found that negative resist provide large degree of undercut and facilitates the lift-off procedure greatly. Below we list only the steps that differ from previous section

1. Clean sample: see section A.1.
2. Spin NR8-1000 at 3000 rpm for 40s.
3. Bake on $130^\circ C$ hot plate for 1 min. The resulting thickness of the photoresist is about $1\mu m$.

4. Align the sample with the mask and expose. Again, the exposure and development times needs to be calibrated at the beginning of the day. Generally exposure time and development times are larger for this resist: 20s, 2 min correpondingly.
5. Develop in RD-2.
6. Rinse in DI water for 1 min.
7. Blow dry with N_2 .
8. Clean the sample in plasma asher for 1 min. The negative resist provide much better undercut, that is not destroyed by 1 min in our plasma asher. The ashing rate is about 160 nm/min.

For the following steps: evaporation, lift-off, annealing see section A.3.

A.5 Lead Deposition

This lithographical step is analogous to ones described in sections A.3 and A.4 up to loading the sample into evaporator:

1. Evaporate metallic layers according to the following sequence: chromium 5 nm, gold 120 nm.
2. Lift off. Upon the completion of the lift-off step the sample must be clean.
3. Clean in ultrasonic bath in methanol for 2 min.
4. Blow dry with N_2 .

A.6 Dot Formation

1. Clean sample: see section A.1.
2. Spin MMA(8.5)MAA (6% in Ethyl Lactate) at 2700 rpm for 40s.

3. Bake in $130^{\circ}C$ oven for 30 min. The resulting thickness is about 200nm.
4. Spin 950PMMA (1% in Chloronezene) at 4000 rpm for 40s.
5. Bake in $170^{\circ}C$ oven for 30 min. The resulting thickness is about 50nm.
6. Cleave the large chip.
7. Write the pattern on the E-beam machine. Parameters used: Accelerating Voltage = 20 kV ; Probe current = 20 pA ; Area dose = 220 $\mu C/cm^2$; Line dose = 1.6 nC/cm .
8. Develop in MIBK:IPA 2:3 for 1 min.
9. Rinse in IPA for 30s.
10. Blow dry with N_2 .
11. Ozone cleaning 20s.
12. Evaporate metallic layers according to the following sequence: chromium 5 nm, gold 35 nm.
13. Lift-off.
14. Clean in ultrasonic bath in methanol for 2 min.
15. Blow dry with N_2 .
16. Ozone cleaning for 20 min.
17. Dry etch or wet etch to remove GaAs cap layer (30nm).

A.7 Side Gate Deposition

1. Clean sample: see section A.1.
2. Spin MMA(8.5)MAA (6% in Ethyl Lactate) at 2700 rpm for 40s.

3. Bake in $130^{\circ}C$ oven for 30 min. The resulting thickness is about 200nm.
4. Spin 950PMMA (2% in Chloronezene) at 4000 rpm for 40s.
5. Bake in $170^{\circ}C$ oven for 30 min. The resulting thickness is about 100nm.
6. Write the pattern on the E-beam machine. Parameters used: Accelerating Voltage = 20 kV; Probe current = 20 pA; Area dose = $200 \mu C/cm^2$.
7. Develop in MIBK:IPA 2:3 for 30s.
8. Develop in PGMEA:EA 1:4 for 30s (45s may facilitate the following lift-off).
9. Rinse in IPA for 30s.
10. Plasma Asher for 3s.
11. Evaporate metallic layers according to the following sequence: chromium 4 nm, gold 5 nm.
12. Lift-off.
13. Clean in ultrasonic bath in methanol for 2 min.
14. Blow dry with N_2 .

A.8 Patches Deposition

1. Clean sample: see section A.1.
2. Spin MMA(8.5)MAA (6% in Ethyl Lactate) at 2700 rpm for 40s.
3. Bake in $130^{\circ}C$ oven for 30 min. The resulting thickness is about 200nm.
4. Spin 950PMMA (2% in Chloronezene) at 4000 rpm for 40s.
5. Bake in $170^{\circ}C$ oven for 30 min. The resulting thickness is about 100nm.

6. Write the pattern on the E-beam machine. Parameters used: Accelerating Voltage = 20 kV; Probe current = 20 pA; Area dose = 200 $\mu\text{C}/\text{cm}^2$ for feature less than $2\mu\text{m}$; Area dose = 180 $\mu\text{C}/\text{cm}^2$ for feature larger than $2\mu\text{m}$.
7. Develop in MIBK:IPA 2:3 for 30s.
8. Develop in PGMEA:EA 1:4 for 30s.
9. Rinse in IPA for 30s.
10. Plasma Asher for 3s.
11. Evaporate metallic layers at two angles according to the following sequence: set the stage angle to -10° and evaporate chromium 5 nm; set the stage angle to $+10^\circ$ and evaporate chromium 5 nm followed by gold 15 nm; set the stage angle to -10° and evaporate gold 15 nm. 10 turns on our sample stage corresponds to 10° .
12. Lift-off.
13. Clean in ultrasonic bath in methanol for 2 min.
14. Blow dry with N_2 .

Appendix B

JEOL 6400 Scanning-Electron Microscope: getting the best lithographical resolution

We perform the electron-beam lithography in a JEOL 6400 Scanning Electron Microscope. The following beam parameters are used:

1. Accelerating voltage: 20 *kV*. Higher voltage reduces additional exposure due to backscattering. On other hand, they might introduce defects into the sample and , therefore, reduce the sample quality.
2. Probe current: 20 *pA*. Smaller probe current would increase the resolution, but the poor signal-to-noise ratio makes the focusing virtually impossible.
3. Aperture setting: 4. Smallest aperture is necessary for the small probe current.
4. Working distance: 6 *mm*. Getting the sample as close as possible to the gun increases the resolution.
5. Magnification: 1000. Although all the patterns are written with a *MAG* = 1000, we change the magnification many times during the set-up and optimization of the beam.

Before writing, the microscope beam must be properly aligned, focused, corrected for astigmatism, etc. This is performed on a resolution standard, placed in the microscope chamber next to the sample on the same chip holder. The resolution standard is made of a thin film of gold on a graphite substrate. The gold consists of balls of diameters ranging from 50nm to 100nm and can easily be used for focusing at a magnification of 300000, the maximum magnification of the machine. The following pages outlines our setup, the beam optimization and actual writing procedures.

I Sample mounting.

- 1 Mount a sample so that mesa is perpendicular to the rod.
- 2 Press the red button to pump out the lock.
- 3 Align the stage: $X = 25.0$, $Y = 29.0$, $Z_{coarse} = 39$, $tilt = 0$, $rotation = 0$, Z_{fine} is counterclockwise all the way.
- 4 Check that ACC VOLT is off. Open the valve, push the sample to the stage, unscrew the rod, take it off, close the valve, check that pressure starts going down (Penning 1002).
- 5 Press the red button to vent the lock, take the rod out.
- 6 $Z_{coarse} = 8$ or 15 (the exact value might differ for different X, Y, and the sample mount).

II Setting up the probe current.

- 1 Press the BREAK key to enable the screen, press PF2 to enable the EOS menu.
- 2 Scan speed FAST.
- 3 Magnification < 1000 .
- 4 Coarse focus $Z_{coarse} = 2$ mm.
- 5 Press D-MAG button.
- 6 Press the MODE button until you get a horizontal line.

- 7 Press key INS key, type "ACC 20", turn ACC VOLT on.
- 8 Set CL coarse = 13 (EOS 1st menu) by turning the probe current knob.
- 9 Contrast=255, turn the Brightness knob up until the line starts to rise.
- 10 Turn the filament current up to 240 mA (2-3 min)
- 11 Maximize the current by changing the GUN ALIGNMENT, make several iterations: XY; tilt; XY; tilt. Gun alignment knobs are to the left from the filament knob.
- 12 Check that decreasing CL coarse will increase the probe current.
- 13 PCD on, by changing CL fine (+ and - keys in EOS 1st menu) set up the exact current value (say, 0.020nA).

Comments: When PCD is on and Keithley reads the probe current, white switch AEM must be turned down. When maximizing the probe current look at the Keithley and the height of the line on the left screen (latter can be only done with PCD off.)

III Focusing the microscope.

- 1 Get picture on the left screen by pressing the PIC button.
- 2 Find something to focus on, magnification ≈ 10000 , do it step by step increasing the magnification while moving from the edge.
- 3 WOBLER on, change the aperture until picture is stable, WOBLER off.
- 4 Focus on something ($MAG \approx 40000$), correct for astigmatism to get sharper image, repeat for higher magnification until $MAG = 300000$.
- 5 Repeat steps 3 and 4.
- 6 Set scan position and shift to zero
- 7 Set the probe current again (see **II-13**)

Comments: When doing steps 3c,3d,3e change place on the sample constantly. If you can not see anything turn PMT link off (EOS, 3rd menu). For fine positioning use + and - on the keyboard (EOS, 2nd menu).

IV Connecting the computer.

- 1 Switch the monitor on.
- 2 Connect “beam” BNC cable and plug the blue box.

V Aligning the sample.

- 1 Find the sample ($MAG \approx 5000$), adjust the height using Z_{fine} (to the left from the X knob, clockwise to rise), adjust focus.
- 2 Scan rotation on, align the scan coordinates with the sample coordinates.
- 3 Change the stage coordinates (X, Y) slightly, by adjusting the stage rotation knob (to the right from the X knob) align the sample with the scan. Scan rotation needs to be constantly adjusted during this procedure. Finally, X stage movement should move the image on the left screen vertically, Y - horizontally.
- 4 Find the centerline, focus on the centerline in the “line” MODE - make the step as sharp as possible. ($MAG \approx 20000$)
- 5 WARNING! This step should be done very fast! Make sure that scan movement light off (left side of the keyboard), switch to the PIC, find the alignment mark in the middle of the mesa, put it in the middle of the screen; switch to the “line” MODE, by adjusting the X scan position, focus on the step for different magnification until you get to the highest, PCD on; set position and image shift to zero (EOS, 2nd menu).

VI Writing.

- 1 Press PIC button
- 2 Set brightness to zero (EOS, 1st menu).
- 3 $MAG = 1000$
- 4 Flip the blue box switch on top of the microscope (pull a bit to flip).
- 5 Switch Beam Blanker to external

- 6 Check the current (Keithley), adjust if necessary
- 7 Start the program: cd user, pg runfile
- 8 PCD off, hit the SPACEBAR.
- 9 Turn the brightness up to see the writing.

VII Subsequent writing.

- 1 Change the stage position
- 2 MAG = 20000
- 3 Flip the blue box switch on top of the microscope (pull a bit to flip).
- 4 Beam blanker off.
- 5 Turn up the brightness (EOS, 1st menu)
- 6 Repeat starting from step V-4.

VIII Switching off

- 1 Stage back into initial position.
- 2 Filament off (few seconds)
- 3 ACC VOLT off.
- 4 MAG = 300000
- 5 Flip the blue box switch on top of the microscope (pull a bit to flip).
- 6 Beam blanker OFF
- 7 Scan speed SLOW
- 8 Monitor off, press PF1 and the BREAK key to switch microscope monitor off.
- 9 Take the sample out (see I) .

Bibliography

- [1] K. von Klitzing, G. Dorda, and M. Pepper. New method for high-accuracy determination of the fine-structure constant based on quantized Hall resistance. *Physical Review Letters*, 45:494, 1980.
- [2] D. C. Tsui, H. L. Stormer, and A. C. Gossard. Two-dimensional magnetotransport in the extreme quantum limit. *Physical Review Letters*, 48:1559, 1982.
- [3] S.V. Kravchenko, G.V. Kravchenko, J.E. Furneaux, V.M. Pudalov, and M. D'Iorio. Possible metal-insulator transition at $B = 0$ in two dimensions. *Physical Review B*, 50:8039, 1994.
- [4] D. Popovic, A.B. Fowler, and S. Washburn. Metal-insulator transition in two dimensions: Effects of disorder and magnetic field. *Physical Review Letters*, 79:1543, 1997.
- [5] Y. Hanein, U. Meirav, D.Shahar, C.C.Li, D. C. Tsui, and Hadas Shtrikman. The metalliclike conductivity of a two-dimensional hole system. *Physical Review Letters*, 80:1288, 1998.
- [6] M.Y. Simmons, A.R.Hamilton, M.Pepper, E.H. Linfield, P. D. Rose, D. A. Ritchie, A.K.Savchenko, and R.G.Griffiths. Metal-insulator transition at $B = 0$ in a dilute two-dimensional GaAs-AlGaAs hole gas. *Physical Review Letters*, 80:1292, 1998.
- [7] Y.Imry. In G.Grinstein and G.Mazenko, editors, *Directions in Condensed Matter Physics*. World Scientific, Singapore, 1986.

- [8] R. Landauer. *IBM J.Res.Dev.*, 1:222, 1957.
- [9] M.P.A. Fisher and L.I. Glazman. Transport in a one-dimensional Luttinger liquid. In L.L. Sohn, L.P. Kouwenhoven, and G. Schoen, editors, *Mesoscopic Electron Transport*, volume 345 of *NATO ASI Series*. Kluwer Academic Publishers, Dordrecht, 1997.
- [10] M.Bockrath, D.H. Cobden, J.Lu, A.G. Rinzler, R.E. Smalley, L.Balents, and P.L. McEuen. Luttinger liquid behavior in carbon nanotubes. *Nature*, 397:598, 1999.
- [11] M. A. Kastner. Artificial atoms. *Physics Today*, 46:24, 1993.
- [12] R. C. Ashoori. Electrons in artificial atoms. *Nature*, 379:413, 1996.
- [13] L.P. Kouwenhoven, C.M. Marcus, P.L. McEuen, S. Tarucha, R.M. Westervelt, and N.S. Windgreen. Electron transport in quantum dots. In L.L. Sohn, L.P. Kouwenhoven, and G. Schoen, editors, *Mesoscopic Electron Transport*, volume 345 of *NATO ASI Series*. Kluwer Academic Publishers, Dordrecht, 1997.
- [14] In Hermann Grabert and Michel H. Devoret, editors, *Single Charge Tunneling: Coulomb blockade Phenomena in Nanostructures*, volume 294 of *NATO ASI Series*. Plenum Press, New York, 1992.
- [15] D. Goldhaber-Gordon, H. Shtrikman, D. Mahalu, D. Abusch-Magder, U. Meirav, and M. A. Kastner. Kondo effect in a single-electron transistor. *Nature*, 391:156, 1998.
- [16] S.M. Cronenwett, T.H. Oosterkamp, and L.P.Kouwenhoven. A tunable kondo effect in quantum dots. *Science*, 281:540, 1998.
- [17] B. L. Altshuler and A. G. Aronov. Electron-electron interaction in disordered conductors. In A. L. Efros and M. Pollak, editors, *Electron-Electron Interactions In Disordered Systems*. Elsevier Science Publishers, 1985.

- [18] C.W.J. Beenakker and H. van Houten. Quantum transport in semiconductor nanostructures. In H. Ehrenreich and D. Turnbull, editors, *Solid State Physics*, volume 44. Academic Press, 1991.
- [19] In L.L. Sohn, L.P. Kouwenhoven, and G. Schoen, editors, *Mesoscopic Electron Transport*, volume 345 of *NATO ASI Series*. Kluwer Academic Publishers, Dordrecht, 1997.
- [20] R. Dingle, H. L. Stormer, A. C. Gossard, and W. Wiegman. Electron mobilities in modulation-doped semiconductor heterojunction superlattices. *Applied Physics Letters*, 7:665, 1978.
- [21] N.F. Mott. The basis of the electron theory of metals, with special reference to the transition metals. *Proc. Phys. Soc. London, A* 62:416, 1949.
- [22] P. W. Anderson. Absence of diffusion in certain random lattices. *Physical Review*, 109:1492, 1958.
- [23] J.T. Edwards and D.J. Thouless. Numerical studies of localization in disordered systems. *J. Phys. C*, 5:807, 1972.
- [24] D.J. Thouless. Electrons in disordered systems and the theory of localization. *Phys. Rep.*, 13:93, 1974.
- [25] E. Abrahams, P.W. Anderson, D.C. Licciardello, and T.V. Ramakrishnan. Scaling theory of localization: absence of quantum diffusion in two dimensions. *Physical Review Letters*, 42:673, 1979.
- [26] D. Belitz and T.R. Kirkpatrick. The Anderson-Mott transition. *Review of Modern Physics*, 66:261, 1994.
- [27] P.A. Lee and T.V. Ramakrishnan. Disordered electronic systems. *Review of Modern Physics*, 57:287, 1985.

- [28] S. Tarucha, D.G. Austing, T. Honda, R.J. van der Hage, and L.P. Kouwenhoven. Shell filling and spin effects in a few electron quantum dot. *Physical Review Letters*, 77:3613, 1996.
- [29] R. C. Ashoori, H.L. Stormer, J.S. Weiner, L.N. Pfeiffer, S.J. Pearton, K.W. Baldwin, and K.W. West. Single-electron capacitance spectroscopy of discrete quantum levels. *Physical Review Letters*, 68:3088, 1992.
- [30] R. C. Ashoori, H.L. Stormer, J.S. Weiner, L.N. Pfeiffer, S.J. Pearton, K.W. Baldwin, and K.W. West. Single-electron capacitance spectroscopy of a few electron box. *Physica B*, 189:117, 1993.
- [31] R. C. Ashoori, H.L. Stormer, J.S. Weiner, L.N. Pfeiffer, K.W. Baldwin, and K.W. West. N-electron ground state energies of a quantum dot in magnetic field. *Physical Review Letters*, 71:613, 1993.
- [32] N.B. Zhitenev, R. C. Ashoori, L.N. Pfeiffer, and K.W. West. Periodic and aperiodic bunching in addition spectra of quantum dots. *Physical Review Letters*, 79:2203, 1997.
- [33] N.B. Zhitenev, M. Brodsky, R. C. Ashoori, L.N. Pfeiffer, and K.W. West. Localization-delocalization transition in quantum dots. *Science*, 285:715, 1999.
- [34] M. Brodsky, N.B. Zhitenev, R. C. Ashoori, L.N. Pfeiffer, and K.W. West. Localization in artificial disorder: Two coupled quantum dots. *Physical Review Letters*, 85:2356, 2000.
- [35] L.I. Glazman and K.A. Matveev. Removal of coulomb blockade of one-electron tunneling by quantum fluctuation. *Sov. Phys. JETP*, 71:1031, 1990.
- [36] K.A. Matveev. Quantum fluctuation of metallic particle charge under coulomb blockade conditions. *Sov. Phys. JETP*, 72:892, 1991.
- [37] D.J. Thouless. Maximum metallic resistance in thin wires. *Physical Review Letters*, 39:1167, 1977.

- [38] E. B. Foxman. *Single Electron Charging and Quantum Effects in Semiconductor Nanostructures*. PhD thesis, Massachusetts Institute of Technology, 1993.
- [39] R. C. Ashoori, N.B. Zhitenev, L.N. Pfeiffer, and K.W. West. Paired additions of electrons into quantum dots: How and why does localization destroy Coulomb blockade to produce pairing. *Physica E*, 3:15, 1998.
- [40] M. Brodsky, N.B. Zhitenev, R. C. Ashoori, L.N. Pfeiffer, and K.W. West. Delocalization in a double quantum dot system. *Physica E*, 6:680, 2000.
- [41] Ralph Williams. *Modern GaAs Processing Methods*. Artech House, 1990.
- [42] David Berman. *The Aluminum Single-Electron Transistor for Ultrasensitive Electrometry of Semiconductor Quantum-Confined Systems*. PhD thesis, Massachusetts Institute of Technology, 1998.
- [43] R.E. Behringer, P.M. Mankiewich, and R.E. Howard. Fabrication of ultrahigh resolution structures in compound semiconductor heterostructures. *J. Vac. Sci. Technol.*, B5:326, 1987.
- [44] A.Scherer, M.L. Roukes, H.G. Craighead, R.M. Ruthen, E.D. Beebe, and J. Harbison. Ultranarrow conducting channels defined in GaAs-AlGaAs by low-energy ion damage. *Applied Physics Letters*, 51:2133, 1987.
- [45] M.L. Roukes and A.Scherer. Quantum device microfabrication: resolution limits of ion beam patterning. *Applied Physics Letters*, 55:377, 1989.
- [46] M.Boroditsky, I.Gontijo, M.Jackson, R.Vrijen, E.Yablonovitch, T.Krauss, C.-C.Cheng, A.Scherer, R.Bhat, and M.Krames. Surface recombination measurements on III-V candidate materials for nano-structure light-emitting diodes. *Journal of Applied Physics*, 87:3497, 2000.
- [47] Mikhail Boroditsky. *Modification of spontaneous emission in photonic crystals*. PhD thesis, University of California, Los Angeles, 1999.

- [48] P.T. Coleridge. Correlation lengths for scattering potentials in two- dimensional electron gases. *Semicond. Sci. Technol.*, 12:22, 1997.
- [49] R. C. Ashoori. *The Density of States in the Two-Dimensional Electron Gas and Quantum Dots*. PhD thesis, Cornell University, 1991.
- [50] D.G. Austing, S. Sasaki, S. Tarucha, S.M. Reimann, M. Koskinen, and M. Man- ninen. Ellipsoidal deformation of vertical quantum dots. *Physical Review B*, 60:11514, 1999.
- [51] S. Tarucha, D.G. Austing, Y.Tokura, W.G. van der Wiel, and L.P. Kouwenhoven. Direct coulomb and exchange interaction in artificial atoms. *Physical Review Letters*, 84:2485, 2000.
- [52] R. C. Ashoori, H.L. Stormer, J.S. Weiner, L.N. Pfeiffer, S.J. Pearton, K.W. Baldwin, and K.W. West. Energy levels of an artificial atom probed with single- electron capacitance spectroscopy. *Surface Science*, 305:558, 1994.
- [53] R. H. Silsbee and R. C. Ashoori. Comment on “Zeeman bifurcation of quantum- dot spectra”. *Physical Review Letters*, 64:1991, 1990.
- [54] P.L. McEuen, E.B. Foxman, U. Meirav, M.A. Kastner, Y. Meir, N.S. Wingreen, and S.J. Wind. Transport spectroscopy of a coulomb island in the quantum hall regime. *Physical Review Letters*, 66:1926, 1991.
- [55] A. Kumar, S. E. Laux, and F. Stern. Electron states in a GaAs quantum dot in a magnetic field. *Physical Review B*, 42:5166, 1990.
- [56] R. C. Ashoori, J.A. Lebens, N.P.Bigelow, and R.H.Silsbee. Equilibrium tunneling from the two-dimensional electron gas in GaAs: Evidence for a magnetic-field- induced energy gap. *Physical Review Letters*, 64:681, 1990.
- [57] R. C. Ashoori, J.A. Lebens, N.P.Bigelow, and R.H.Silsbee. Energy gaps of the two-dimensional electron gas explored with equilibrium tunneling spectroscopy. *Physical Review B*, 48:4616, 1993.

- [58] J.P.Eisenstein, L.N.Pfeiffer, and K.W. West. Coulomb barrier to tunneling between parallel two-dimensional electron system. *Physical Review Letters*, 69:3804, 1992.
- [59] H. B. Chan, P. I. Glicofridis, R. C. Ashoori, and M. L. Melloch. Universal linear density of states for tunneling into the two-dimensional electron gas in a magnetic field. *Physical Review Letters*, 79:2867, 1997.
- [60] H. B. Chan. *Tunneling Spectroscopy of the Two-Dimensional Electron Gas*. PhD thesis, Massachusetts Institute of Technology, 1999.
- [61] Y.Wan, G.Ortiz, and P.Phillips. Pair tunneling in semiconductor quantum dots. *Physical Review Letters*, 75:2879, 1995.
- [62] M.E. Raikh and L.I. Glazman. Two-electron state in a disordered 2D island: Pairing caused by the coulomb repulsion. *Physical Review Letters*, 77:1354, 1996.
- [63] A.A. Koulakov and B.I. Shklovskii. Charging spectrum and configurations of a Wigner crystal island. *Physical Review B*, 57:2352, 1998.
- [64] D.L.Miller. Inhomogeneous states in quantum dots. *cond-mat/9808103*, 1998.
- [65] Y.Avishai, D.Berend, and R.Berkovits. Fluctuation of conductance-peak spacing in large semiconductor quantum dots. *Physical Review B*, 59:10707, 1999.
- [66] C.M.Canali. Disorder and interaction-induced pairing in the addition spectra of quantum dots. *Physical Review Letters*, 84:3934, 2000.
- [67] L.S. Levitov. Private Communication.
- [68] V.M. Bedanov and F.M.Peeters. Ordering and phase transitions of charged particles in a classical finite two-dimensional system. *Physical Review B*, 49:2667, 1994.
- [69] A. V. Khaetskii, V. I. Fal'ko, and G. E. W. Bauer. Electrostatics of inter-Landau-level diodes. *Physical Review B*, 50:4571, 1994.

- [70] K.A.Matveev, L.I.Glazman, and H.U.Baranger. Tunneling spectroscopy of quantum charge fluctuations in the Coulomb blockade. *Physical Review B*, 53:1034, 1996.
- [71] K.A.Matveev, L.I.Glazman, and H.U.Baranger. Coulomb blockade of tunneling through a double quantum dot. *Physical Review B*, 54:5637, 1996.
- [72] J.M.Golden and B.I.Halperin. Relation between barrier conductance and Coulomb blockade peak splitting for tunnel-coupled quantum dots. *Physical Review B*, 53:3893, 1996.
- [73] J.M.Golden and B.I.Halperin. Higher-order results for the relation between channel conductance and the Coulomb blockade for two tunnel-coupled quantum dots. *Physical Review B*, 54:16757, 1996.
- [74] E.P.Wigner. On the interaction of electrons in metals. *Physical Review*, 46:1002, 1934.
- [75] B.Tanatar and D.M.Coperley. Ground state of the two-dimensional electron gas. *Physical Review B*, 39:5005, 1989.
- [76] S.T.Chui and K.Esfarjani. A mechanism for quantum melting in two dimensions. *Europhysics Letters*, 14:361, 1991.
- [77] S.T.Chui and B.Tanatar. Impurity effect on the two-dimensional-electron fluid-solid transition in zero field. *Physical Review Letters*, 74:458, 1994.
- [78] A.G. Eguiluz, A.A. Maradudin, and R.J. Elliott. Two-dimensional Wigner lattice in a magnetic field and in the presence of a random array of pinning centers. *Physical Review B*, 27:4933, 1983.
- [79] R.Egger, W. Hausler, C.H. Mak, and H.Grabert. Crossover from Fermi liquid to Wigner molecule behaviour in quantum dots. *Physical Review Letters*, 82:3320, 1999.

- [80] R.Egger, W. Hausler, C.H. Mak, and H.Grabert. Erratum: Crossover from Fermi liquid to Wigner molecule behaviour in quantum dots. *Physical Review Letters*, 83:462, 1999.
- [81] J.P.Eisenstein, L.N.Pfeiffer, and K.W. West. Negative compressibility of interacting two-dimensional electron and quasiparticle gases. *Physical Review Letters*, 68:674, 1992.
- [82] P.L. McEuen, E.B. Foxman, J. Kinaret, U. Meirav, M.A. Kastner, N.S. Wingreen, and S.J. Wind. Self-consistent addition spectrum of a coulomb island in the quantum hall regime. *Physical Review B*, 45:11419, 1992.
- [83] O. Klein, C. de C. Chamon, D. Tang, D.M. Abusch-Magder, U. Meirav, X.-G. Wen, M. A. Kastner, and S.J. Wind. Exchange effects in an artificial atom at high magnetic fields. *Physical Review Letters*, 74:785, 1995.
- [84] C.G.Darwin. *Proc. Cambridge Philos. Soc.*, 27:86, 1930.
- [85] V.Fock. *Z.Phys.*, 47:446, 1928.
- [86] D.J. Goldhaber-Gordon. *The Kondo Effect in a Single-Electron Transistor*. PhD thesis, Massachusetts Institute of Technology, 1999.
- [87] A.M.Chang. Private Communication.
- [88] S. R. Patel, S. M. Cronenwett, D. R. Stewart, A. G. Huibers, C. M. Marcus, C. I. Duruoz, J. S. Harris, K. Campman, and A. C. Gossard. Statistics of peak spacing fluctuations. *Physical Review Letters*, 80:4522, 1998.
- [89] D. R. Stewart, D. Sprinzak, C. M. Marcus, C. I. Duruoz, and J. S. Harris Jr. Correlations between ground and excited state spectra of a quantum dot. *Science*, 278:1784, 1997.
- [90] A.V. Madhav and T. Chakraborty. Electronic properties of anisotropic quantum dots in a magnetic fields. *Physical Review B*, 49:8163, 1994.

- [91] F.R.Waugh, M.J. Berry, D.J. Mar, R.M.Westervelt, K.L.Campman, and A.C.Gossard. Single electron charging in double and triple quantum dots with tunable coupling. *Physical Review Letters*, 75:705, 1995.
- [92] F.R.Waugh, M.J. Berry, C.H.Crouch, C.Livermore, D.J. Mar, R.M.Westervelt, K.L.Campman, and A.C.Gossard. Measuring interaction between tunnel-coupled quantum dots. *Physical Review B*, 274:1332, 1996.
- [93] C.Livermore, C.H.Crouch, R.M.Westervelt, K.L.Campman, and A.C.Gossard. The coulomb blockade in coupled quantum dots. *Science*, 274:1332, 1996.
- [94] A. S. Adourian, C. Livermore, R. M. Westervelt, K.L.Campman, and A.C.Gossard. Evolution of coulomb blockade spectra in parallel coupled quantum dots. *Applied Physics Letters*, 75:424, 1999.
- [95] C.H.Crouch, C. Livermore, R. M. Westervelt, K.L.Campman, and A.C.Gossard. Evolution of coulomb gap in tunnel-coupled quantum dots. *Applied Physics Letters*, 71:817, 1997.
- [96] Juhren Shi, Song He, and X.C.Xie. Droplet state in an interacting two-dimensional electron system. *Physical Review B*, 60, 1999.
- [97] B.I. Halperin. Private Communication.
- [98] Y. Oreg, K.Byczuk, and B.I. Halperin. Spin configurations of a carbon nanotube in a nonuniform external potential. *Physical Review Letters*, 85:365, 2000.